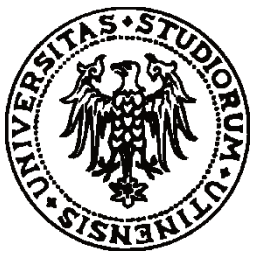

UNIVERSITÀ DEGLI STUDI DI UDINE

Corso di Dottorato di Ricerca in Scienze dell'Ingegneria Energetica e Ambientale

Ciclo XXIX

Dipartimento Politecnico di Ingegneria e Architettura

A revisitation of transient CO_2 methanation over Rh/CeO_2 and Rh/CeO_2-ZrO_2 based catalysts

Supervisore

Prof. Alessandro Trovarelli

Dottoranda

Monica Julieth Valencia Botero

Agosto 2017

Acknowledgments

I want to thank my Advisor, Professor Alessandro Trovarelli, for his teachings, advices and suggestions. Also, I wish to highlight the role of Professor Carla de Leintenburg along this journey, since her support was the mainstay of experimental work. Besides, Doctor Sara Colussi deserves a special mention, as her help during writting activities was unvaluable. Undoubtly, this thesis would not be successfully finished without them. I also acknowledge the support from my colleagues of our research group. I really appreciate all of your collaboration during my PhD time.

On the other hand, I want to thank to Professor Jordi Llorca from Energy Technique Institute of the Polytechnic University of Catalonia (Barcelona, Spain) because of his support with the HR-TEM measurements.

Abstract

The aim of this thesis was the study of CO_2 activation over Rh/CeO_2 and Rh/CeO_2-ZrO_2 catalysts. Rh/CeO_2 catalysts are particularly interesting since a high activity peak during transient state have been obtained at conditions such that other Me/Redox systems do not (Me: noble metal, Redox: Redox support). Accordingly, this work had two main specific objectives: The first was to study the effect of pretreatment conditions on the transient activity of catalysts with reduction degrees higher than polycrystalline ceria, such as nanoshaped ceria and ceria-zirconia based catalysts. The second was to determinate if the high activity during transient state is related to the reducibility degree of ceria-based catalysts, i.e. the role of oxygen vacancies on CO_2 activation. To reach the objectives rhodium over several supports (namely ceria nanocubes, ceria nanorods, polycrystalline ceria, ceria-zirconia mixes and zirconia) were prepared, characterized and tested. The results indicated that samples with higher reduction degrees were not only more active ones during transient state, but also this effect was longer on the time, i.e. it tooks more time to reach the steady state. These findings agree with the proposal of the oxygen vacancies performing a key role during CO_2 activation.

Keywords: CO_2 activation, oxygen vacancies, CO_2 methanation, Rh/CeO_2, Rh/CeO_2-ZrO_2.

Contents

List of figures

List of tables

Acronyms

BET	Brunauer-Emmett-Teller surface area
CCS	Carbon capture and Sequestration
CCU	Carbon capture and Utilization
FID	Flame Ionization Detector
HRTEM	High-Resolution Transmission Electron Microscopy
HTR	High Temperature Reduction
IEA	International Energy Agency
LTR	Low Temperature Reduction
Me	Noble Metal
MTR	Medium Temperature Reduction
OSC	Oxygen Storage Capacity
RWGS	Reverse Water Gas Shift
SSA	Steady State Activity
TA	Transient Activity
TCD	Thermal Conductivity Detector
TGA	Thermogravimetric analysis
TPR	Temperature Programmed Reduction
TWC	Three-Way Catalysts
WGS	Water Gas Shift
XRD	X-ray diffraction

Chapter 1. Introduction

1.1 Overview of CO_2 emissions and carbon capture

With the increasing of CO_2 emissions, global warming is accelerated because of the ‘‘greenhouse effect’’, accompanied by abnormal climate changes [1, 2]. In the 2015 Paris Climate Conference, the global agreement for the reduction of CO_2 emissions was strengthened [3]. Despite the efforts that politics have made in recent years, the world’s climate threshold of 400 ppm of CO_2 has been reached permanently on September 2016 as observed in the NOAA Observatory of Mauna Loa [4] leading the average world temperature to increase by 1,5 °C with respect the values recorded pior to the industrial revolution. Although most of the anthropogenic emitted CO_2 comes mainly from the combustion of fossil fuels, up to now their use as major energy source appears inevitable because of their large availability and affordability. Moreover, it would be impossible to force the energy demand limitation of developed as well as emerging countries populations [5]. So, in the recent years, the advancement towards the so called low-carbon economy has been strongly encouraged by many countries, including the European Union that has indicated CO_2 and greenhouse gases emissions reduction as a priority within the Horizon 2020 framework program [6] funding many research projects in this field.

There are two main philosophies in reducing CO_2 emissions: carbon dioxide capture and sequestration (CCS), or carbon dioxide capture and reuse. The former approach is based on traditional technologies such as absorption, adsorption, and membranes separation, and it has been already developed at industrial scale. On the other hand, the combined capture and utilization of carbon dioxide (CCU) that allows to cut costs is still far from this stage apart from few applications

[7]. On the other hand up to now the combined capture and utilization of carbon dioxide (CCU) is still far from this stage apart from few applications [8]. The reasons for the technological gap between CCS and CCU are related mostly to the "inert" nature of carbon dioxide, that needs a high energy input to become reactive. CO_2 reacts readily with medium to strong nucleophiles such as water, amines, or carbanions, but the high transformation kinetic barrier to C-H and C-C bond formations and the thermodynamic restrictions make hard to follow the synthetic path.

CCS technologies are expensive and with uncertain impact on the environmental for what concerns, the storage of large amount of CO_2 on caves, oceans, or underground layers. Therefore, many international organizations (i.e. International Energy Agency (IEA), EU) support programs aimed to reuse instead of storing CO_2. The current industrial demand of CO_2 is relatively low. As a reactant, CO_2 is mainly used in urea synthesis, but its use as a technological fluid should not be neglected. Its industrial demand is around 232 Mt per year. Only few of this amount is obtained through a CO_2 recovering [8]. By taking into account this later aspect, and that CO_2 can be a renewable, widely available, low-cost and low-toxicity C1 feedstock, there are many advantages to conceive processes at low carbon footprint via a CCU approach. Economical and environmental efforts could match especially if the number of localized sources of concentrated and sometimes pressurized gas streams already available will be exploited. Coal-fired power plants frequently amount to tens of millions of tons of CO_2 per plant per year. Refining and petrochemical processes, and a number of processes such as iron, steel, and cement industries can provide large volumes of quite concentrated streams of CO_2 generated in specific sites at sustainable price and in quantities that are more than sufficient for even large-scale synthetic purposes [9-11].

The CO_2 emissions from actually coal-fired power plants frequently amount to tens of millions of tons of CO_2 per plant per year. Refining and petrochemical processes, and a number of processes such as iron, steel, and cement industries can provide large volumes of quite concentrated streams of CO_2 generated at individual sites. In this perspective, economical and environmental efforts could match.

Despite the fact that CO_2 is a renewable, widely available, low-cost and low-toxicity C1 feedstock, current industrial demand is relatively low. The CO_2 industrial demand is around 232 Mt per year; as a reactant, CO_2 is mainly used in urea synthesis, but its use as a technological fluid should not be neglected. Unfortunately, few of the currently using CO_2 derived from its recovering [8].

Carbon dioxide conversion promoted by heterogeneous catalysis plays a great interest and has attracted extensive research work due to its environmental and industrial application. However, the effective transformation of CO_2 is still difficult due to its high thermodynamic stability, which requires high temperatures with an energy-intensive process. For this reason, the rational design and preparation of efficient heterogeneous catalysts with high performance and stability are of vital importance in realizing CO_2 activation.

A massive CO_2 reutilization as a feedstock needs the development of new processes. In this perspective many applications have been studied and can be grouped into three major areas divided on the basis of the reduction level of the carbon dioxide: CO_2 addition with the incorporation into a new molecule without formal reduction of the oxidation state of carbon; a partial or fully CO_2 reduction with H_2 (see Figure 1.1) obtaining multipurpose products, from the lightly reduced formic acid, passing through aldehyde and methanol, to the deeply reduced methane. Regarding the reduction processes, the technologies with the highest readiness level are focused on the productions of synthetic fuels or their precursors through the reverse water gas shift (RWGS), CO_2 reforming of methane (Dry reforming, DR), Fisher–Tropsch synthesis and the full hydrogenation of CO_2 to methane.

In all these approaches the effective transformation of CO_2 is difficult due to its high thermodynamic stability, which requires high temperatures with an energy-intensive process. Carbon dioxide conversion promoted by catalysts consequently plays a great interest and has attracted extensive research work for the rational design and preparation of efficient catalysts with high performance and stability. The selectivity of homogeneous and heterogeneous catalysts towards many processes is currently tested in a number of large-scale demonstration projects or

they have already been implemented on an industrial scale as in the production of urea, salicylic acid and carbonates.

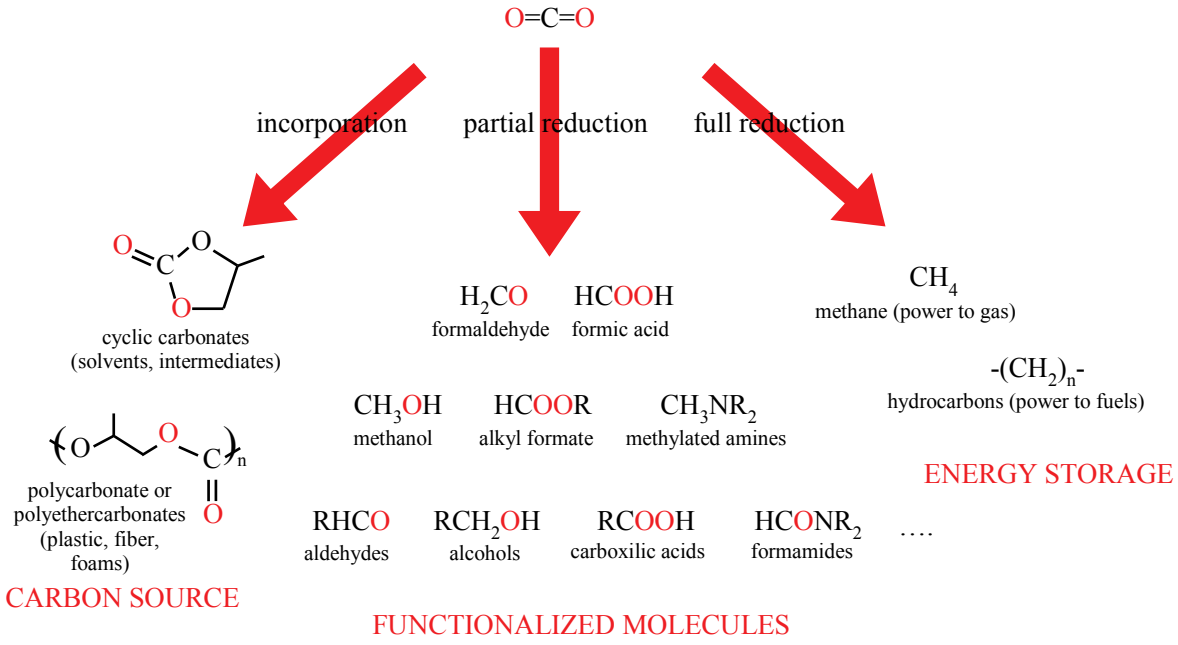

Figure 1.1 Research lines for the utilization of CO_2 in production of chemicals or energy storage. Incorporation of CO_2 without a formal reduction, partial reduction with bond formation in a large synthetic diversity ant complete reduction to saturated hydrocarbons.

Moreover, the high energy requirement (in terms of heat, electrons and hydrogen) for the conversion of CO_2 into a saturated hydrocarbon suggests the development of technologies (electrolyser and fuel cell systems) capable of buffering the power fluctuations of the grid when primary renewable resources such as sun and wind, which have an intermittent character, are used [11-13].

CO_2 hydrogenation to methane had been a keystone of the development of heterogeneous metal catalysis, applied in the large-scale manufacture of substitute natural gas from the products of coal gasification and up to now continues to be used in combination with the methanation of carbon monoxide for the purification of synthesis gas in the ammonia production process. Nowadays, this reaction is investigated with the perspective of different applications: from H_2 storage recycling CO_2 from emissions to futuristic application. In this hypothesis, bringing terrene hydrogen, it would

be possible convert the carbon dioxide present in great amount in Mars' atmosphere into methane and water for fuel and astronaut life-support systems [14].

1.2 CO_2 methanation

The Sabatier reaction, i.e. the CO_2 hydrogenation to methane, was discovered at the beginning of 20th century, nowadays, in a low carbon economy perspective, this process provides at the same time a method to store H_2 by using the existing infrastructure for the storage, transport, and utilization of natural gas and a route to recycle CO_2 from emissions to give a useful fuel with potential commercial applications and environmental benefits [15]. This promising application justifies increasing industrial interest in this field and fundamental and applied academic efforts to clarify the role of catalysts to promote CO_2 hydrogenation.

Although the CO_2 methanation is thermodynamically favorable, it is always difficult because of significant kinetic barriers of the reduction that involves an eight-electron process [16, 17]. This means that the reaction has to be operated at high temperature with an energy-waste process also through a catalytic process.

$$CO_2 + 4H_2 \leftrightarrow CH_4 + 2H_2O \qquad \text{(Eq. 1.1)}$$

ΔH_{298K} = -252.9 kJ/mol, ΔG_{298K} = -130.8 kJ/mol

The reaction requires a bifunctional catalyst, where the role of metal is the activation of hydrogen, whereas the support favours the carbon dioxide coordination and activation. Many catalytic systems based on noble metals (i.e. Ru, Rh or Pd) supported on various oxides (i.e. SiO_2, TiO_2, Al_2O_3, ZrO_2, and CeO_2) have been investigated as catalysts for this reaction, however supported nickel catalysts remain the most widely studied materials [18]. Although the methanation of CO_2 seems to be a

simple reaction, its mechanism appears to be difficult to establish. The nature of the intermediate of the methane formation process is still under debate. One mechanism proposed for CO_2 methanation involves the direct hydrogenation of CO_2 to methane without forming CO as intermediate (Cu/ZrO_2 [19]). The other, more probable, involves the conversion of CO_2 to CO prior to methanation (see Figure 1.2). The subsequent reaction follows the same mechanism as for CO methanation (Ni/SiO_2: [20, 21]; Ni{100}: [22, 23]).

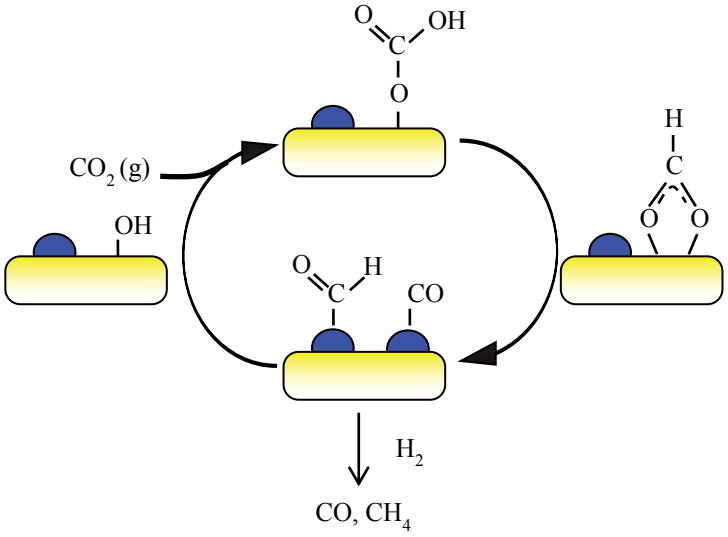

Figure 1.2 Proposed mechanism for CO_2 hydrogenation
The CO_2 hydrogenation is performed over Metal (blue) on support (yellow) (Ru/TiO_2: [23-25]; Pd/TiO_2: [26]; Pd/Al_2O_3 [27]; Rh/Al_2O_3: [28]. The reaction needs the vicinity of support "carbonate" species and hydrogen adsorbed and activated over metal.

It is worthy noting that, even for CO methanation, there is still no consensus on the kinetics and mechanism. It is still under debate the role of hydrogen carbonate and formate species identified during the reaction on the surface as well as the role of the support material for the stabilization of the active metal or the identification of active sites [28-30]. In this reaction, the nature of support plays a crucial role in the type of interaction between metal and support. Several researchers mentioned that an electronic interaction occurred between supports and active species discussing the role of an enhanced electron transfer with basic oxides from the support to the supported metals [31-33]. Thus the electron donation from the metals into an antibonding π-orbital of the CO adsorbed on the metals can be increased. Then the bond of the metals and carbon can be

strengthened and consequently the C-O bond weakened. Moreover, it has been proposed that CO_2 conversion to CO should take place at the metal–support interface because most of CO_2 adsorbs not on the active metal but on the support material while the dissociative H_2 adsorption take place on the metal [23-25, 34-38].

Among the supports, there is a great interest in catalytic properties of reducible oxides. It has been observed that small metal nanoparticles when loaded on the reducible supports (e.g., TiO_2, CeO_2) significantly enhance their methanation performance owing to a strong metal–support interactions [37, 39-43]. Moreover in Ni-supported on USY zeolites, it was shown that methanation has been promoted through the addition into the zeolite matrix of CeO_2 which provides additional adsorption/activation sites leading to higher CO_2 concentration on the surface [44]. The presence of Ce modifies the surface population and seems to change the CO_2 hydrogenation mechanism following a pathway that passes from carbonates to formates as reaction intermediates. The presence of Ce modifies the surface population and seems to change the CO_2 hydrogenation mechanism following a pathway that passes from carbonates to formates as reaction intermediates.

In addition to the CO_2 adsorption capability of Ce, it has to be considered a further contribute of reducible supports to the catalytic activity. These materials generate oxygen vacancies that participate to the activation of inert CO_2 such as in the Rh or Ni/CeO_2 and Rh/TiO_2 systems. The presence of vacancies on these supports, creates an additional driving force to facilitate the breakeage of carbon-oxygen bonds which is considered to be a rate-determining step of CO_2 methanation [37, 43, 45] **and it candidates Ceria as a catalyst component to activate carbon dioxide.**

1.3 CeO_2 and CeO_2-based materials

To enhance the comprehension of active support role, this thesis strives to clarify the nature of

reaction sites and the role of the pretreatment temperature in the activation of CO_2 molecules on Rh/CeO_2 based catalysts. Ceria is widely used as a support and its redox properties are considered to play a key role in determining the catalytic behavior in many reactions acting as an oxygen buffer by storing and releasing O_2 due to the cerium redox couple. Consequently, the interest on these supports is related to their ability to easily change the oxidation state from Ce^{4+} of CeO_2 to Ce^{3+} of Ce_2O_3 through a series of nonstoichiometric CeO_{2-x} oxides that in the composition range of $0<x<0.5$ maintains the fluorite structure, creating oxygen vacancies (Vo).

$$CeO_2 + xH_2 \leftrightarrow CeO_{2-x} + xH_2O + xV_0 \qquad \text{(Eq. 1.2)}$$

This face-centered cubic structure (f.c.c., space group $Fm\bar{3}m$, a=0.541134 nm, JCPDS 34-394) shows cubic closed-packed array of metal atoms with all tetrahedral holes filled by oxygen atoms (See Figure 1.3). Cerium oxide can form different phases depending on temperature and oxygen partial pressure. Temperatures above 685 °C and low oxygen pressure induce formation of α phase, oxygen deficient non stoichiometric oxides with disordered fluorite related structure [46, 47]. After thermal treatment, α phase evolves into several fluorite related phases (Ce_nO_{2n-2m}) with ordered oxygen vacancies [48, 49] such as the β phase (Ce_6O_{11} [50]), $Ce_{11}O_{20}$ (δ) or Ce_7O_{12} phases [51]. At high temperature, the increase of oxygen vacancy number brings, through the formation of a non stoichiometric body-centered cubic structure (σ, space group $Ia\bar{3}$), to Ce_2O_3 that can show a C-type structure. All these oxides **show very close to f.c.c. structures** and can easily exchange oxygen. The reversibility and fast removal/uptake of oxygen occurs through continuous formation and filling of oxygen vacancies while maintaining the structural integrity of the fluorite ceria lattice. This *oxygen storage capacity* (OSC) is one of the major advantages profited by many important reactions studied on Ce based catalysts. Over the last few years, noble metals or transition metal

oxides supported on CeO_2 have been tested in several redox processes: Selective CO oxidation in hydrogen rich streams [52, 53], VOC catalytic combustion (Toluene: [54]; CH_4: [55, 56]), diesel engines (Soot: [57-59]), selective dehydrogenations [60], Water Gas Shift (WGS) [61], hydrocarbon dry [62], and steam reforming [63, 64], as well as ethanol steam reforming [65]. However, the success of ceria is strictly connected to its role in the Three Way Catalysts [66].

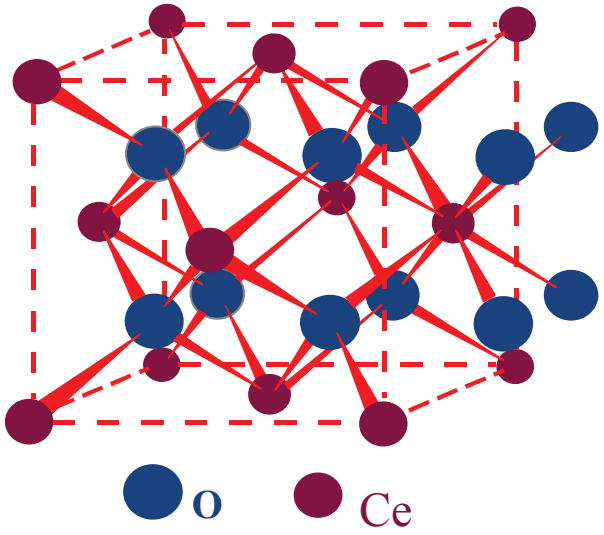

Figure 1.3 Fluoritic CeO_2 structure

The CeO_2 ability of oxygen exchange as well the stabilization of metal dispersion and the promotion of side reaction through interfacial metal/ceria contact sites [67] has been exploited in TWCs converters that operates under dynamic conditions, because of composition, temperature and flow rate of exhaust gases. The oscillatory conditions of air/fuel ratio in the frequency range of 0.1 to 1 Hz depending on driving conditions, require materials with the ability to store oxygen when it exceeds the stoichiometric ratio (lean condition), and release in oxygen deficient feed (rich conditions) [68, 69]. The simultaneous oxidation of CO and HCs and the reduction of NOx is performed by the oxygen buffering/storage capacity of CeO_2 [70-72]. Unfortunately in TWCs reaction conditions, the use of pure ceria is limited by its poor thermal stability. CeO_2 deactivates in its OSC when the exhaust temperature exceed 1123 K due to sintering of ceria particles and at high

temperature, surface area drops at very low values, thus affecting low temperature redox activity [73, 74]. The solution has been identified into Ceria-Zirconia mixed oxides that show high OSC and thermal stability. Recently, the same limit of OSC deactivation under drastic conditions has been evidenced into an application that involves CO_2: The thermal splitting of H_2O and CO_2 for green fuel generation (see Figure 1.4). This approach bypasses the large amounts of hydrogen request in the methanation route exploting the ceria reducibility.

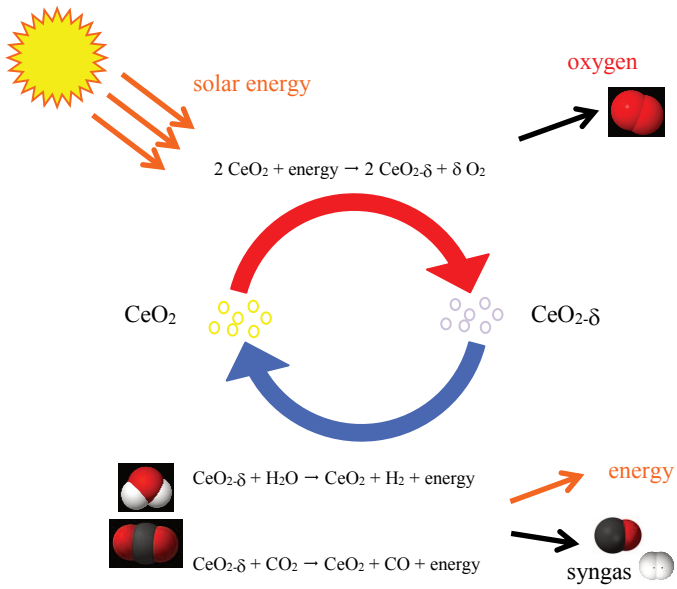

Figure 1.4 Solar-driven thermochemical cycle for syngas production

The feasibility of a solar-driven thermochemical cycle for dissociating H_2O and CO_2 using nonstoichiometric ceria has been demonstrated in a two steps cycle [75-77] with an energy conversion efficiency of about two orders of magnitude greater than the photocatalytic approaches.

$$High - T_{red}: CeO_2 \rightarrow CeO_{2-\delta} + \frac{\delta}{2} O_2 \qquad (Eq.\,1.3)$$

$$Low - T_{ox}\ with\ H_2O: CeO_{2-\delta} + \delta H_2O \rightarrow CeO_2 + \delta H_2 \qquad (Eq.\,1.4)$$

$$Low - T_{ox}\ with\ CO_2: CeO_{2-\delta} + \delta CO_2 \rightarrow CeO_2 + \delta CO \qquad (Eq.\,1.5)$$

Into a concentrated solar radiation reactor, Ceria reduction is performed in inert atmosphere at high temperature (>1500 °C), whereas syngas production (and reoxidation of partially reduced Ceria) is performed at lower temperature (<1000 °C) flowing CO_2 and H_2O. Despite to the importance of oxygen vacancies in CO_2 activation, material stability is an essential criterion for a viable thermochemical process in order to guarantee the long life efficiency. This critical point opens interesting perspectives for the application to the process of ceria-based catalysts that are able to maintain high surface area (and OSC) under drastic conditions.

1.3.1 Ce-Zr catalysts

The research for the solution of early TWCs thermal stability problems has led to the development of materials with enhanced performance durability and thermal stability through the partial substitution of Ce^{4+} with smaller ions of Zr^{4+} in the fluorite lattice [67]. Doping CeO_2 lattice by substitution of with Zr brings to the formation of solid solutions that are currently the components of the new generation of TWCs [78, 79]. Crystal structure, phase stability and oxide ion diffusion of Ceria-Zirconia solid solution (CZ) depend on composition, temperature as well as synthesis method and grain size. Nevertheless the unit cell dimensions (or cell volume for tetragonal phases) of $Ce_xZr_{1-x}O_2$, stressed by the presence of a smaller Zr^{4+} ion (0.084 nm) with respect to Ce^{4+} (0.097 nm), usually decrease linearly with the cerium content in CZ samples following the Vegard's rule (i.e., a linear lattice parameter dependence on the solute concentration) [80]. Ceria–zirconia mixed oxides can show three stable phases (monoclinic, tetragonal and cubic) and two metastable tetragonal phases (t′ and t″) that are highly efficient oxygen exchangers [81-84] (See figure 1.5).
The origin of the enhanced reducibility and improved OSC of these materials may be due to several reasons including the presence of structural defects and local compound formation or partially

reduced phases (i.e. pyrochlore $Ce_2Zr_2O_7$), and the amount of surface oxygen that increases with surface area thermal stability [85-88]. On the other hand, the incorporation of low-valent over-sized dopants (Ce^{3+}) in the ZrO_2 structure generates oxygen vacancies in the lattice reducing the stress due to adopting a eight-fold coordination, typical of flourite structure, instead of the more favorable (for the small Zr^{4+}) seven fold one (typical of the monoclinic ZrO_2) [89]. This greatly affects the reducibility and greatly improves the OSC of materials that exhibit better performance in fluoritic $Ce_xZr_{(1-x)}O_2$ oxides with $0.6<x<0.8$ [90-92].

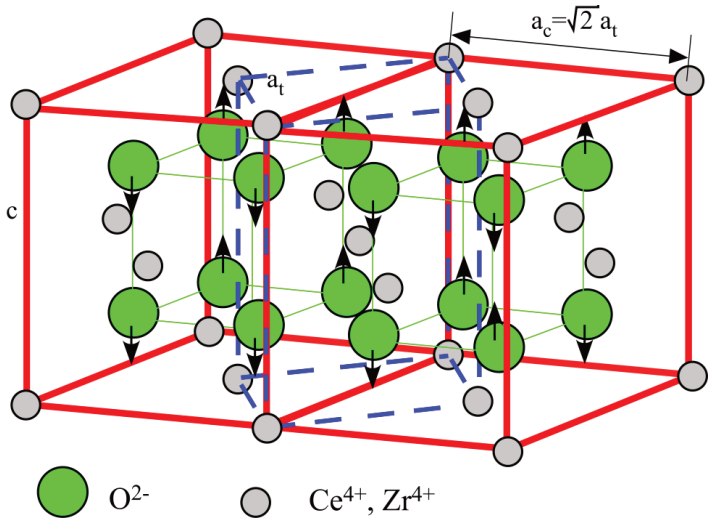

Figure 1.5 Relationship between pseudocubic fluorite and tetragonal crystal structure of Ceria-Zirconia
(Green circles: O^{2-}, grey circles: Ce^{4+} or Zr^{4+}, solid red lines indicate the cubic fluorite cell, dashed blue lines the tetragonal one. The arrows indicate the oxygen displacement from the regular cubic fluorite). Adapted from [93].

Moreover, at least at 400 °C, the storage of oxygen in pure CeO_2 can be restricted to the surface, while for $Ce_{0.63}Zr_{0.37}O_2$ sample subsurface oxygen is involved in the redox process [90]. In a different paper, the presence of a supported noble metal (Rh, Pt) had been observed to emphasize the reduction of the CZ materials even at low temperature reduction in comparison with the CeO_2 sample in parallel with an increased catalytic activity in the NO-CO reaction [94]. A direct relation between the increase of the bulk reduction degree and better performances in oxygen mobility had

been attributed to the structural distortion induced by the presence of smaller Zr^{4+} ion into the solid solutions (See figure 1.5). This leads to higher oxygen diffusion coefficients that in CZ have been calculated to be two orders of magnitude larger than in Ceria samples [95] with a correlated enhanced activity in CO oxidation performed in transient conditions. Very high CO_2 conversion achieved on Very high CO_2 conversion achieved on $Ni/Ce_{0,72}Zr_{0,28}O_2$ was attributed not only to the CZ ability to highly dispers nickel but also to its higher redox properties due to Ni^{2+} incorporation into the support lattice [96].

Finally, the induced higher mobility of oxygen ions has stimulated a great amount of academic work that highlighted the utility of ceria based catalyst and found a real applications in several fields: from Diesel soot combustion, to water gas shift reaction, or NOx storage and reduction [58, 97-99].

1.3.2 Nanoshaped ceria

A different approach is suggested by literature studies, to increase the oxygen mobility of ceria, i.e. by playing on the shape of its nanocrystals [100]. The catalytic reactivity of ceria appears sensitive not only to the size but also to the shape of the nanocrystals as a consequence of well-defined facet exposed. This correlation has been explored as a result of recent synthetic routes toward size/shape-controlled nanostructures in CeO_2 system that made available new materials [101].

The development of shape-controlled synthesis of inorganic nanomaterials received great attention due to their unique shape-dependent properties and nowadays allow experimental studies on real well defined surface catalysts. Various synthetic approaches provide ceria with different shapes as nanorods and nanocubes [102] as well as defined nano-octraedrons [103] or flower-like CeO_2 [104] or, more recently, tailored branched ceria octapods [105].

The hypothesis of a shape dependency activity in ceria real catalysts was first formulated on ceria

powders tested into CO oxidation as a three-way catalyst model reaction [106]. However, previous works evaluated the CeO_2 surface stability with theoretical molecular mechanics methods [107] and assigned the lowest energy to the most compact {111} surface while less energy is required to form oxygen vacancies on {110} and {100} surfaces. The comparison between polycrystalline nanoparticles and single crystalline CeO_2 nanorods evidenced a higher activity for the nanostructured material, in which the well-defined {001} and {110} planes are predominantly exposed, in comparison to the traditional polycrystalline nanoparticles which expose the most thermodynamically stable {111} planes [108-110].

Vacancy formation is strongly influenced by CeO_2 crystal size: Zhou et al. observed that the oxygen vacancy concentration increases two orders of magnitude of magnitude passing from 60 nm compared to 4 nm single crystals [111]. More recently theoretical studies supported the hypothesis that oxygen vacancies are easier to form on {110} and {001} planes where the formation energy of oxygen vacancies is lower compared with CeO_2 {111} planes [112-115]. The experimental CO-OSC scale of values (in terms of exposed crystal planes) measured in nanostructured CeO_2 follows the order of nanocubes ({100} > nanorods ({110} and {100}) >> nanopolyhedra ({111} and {100}) [102]. Morover Fabris et al. observed that oxygen vacancies tend to segregate on the {110} rather than on the {111} surface [116] and Sayle et al. [117] found that {100} is more reactive and important catalytically as compared with either {110} or the {111} in the modeling of CeO_2/YSZ{111} system.

In CO oxidation CeO_2 nanorods with exposed well-defined reactive {001} and {110} planes are more active than polycrystalline ceria with the {111} planes at least in CO oxidation. The facet-dependent catalytic activity on nano-shaped ceria had been described into several theoretical [118] and experimental studies [102, 119, 120]. Catalytic properties of oxide catalysts and their sensitivity to crystal morphologies and exposed surfaces have been observed also in oxidation of toluene to benzaldehyde on ceria nanocubes [121] as well in soot combustion [122].

The face sensitivity of CeO_2 is confirmed by the opposite behavior into acetylene partial

hydrogenation compared to CO oxidation. On the basis of previous observations, where was evidenced that an excessive degree of surface reduction of CeO_2 depresses the partial hydrogenation of alkynes to olefins [123] [hydrogenation and oxidation comparison tests have been performed on well defined nanoshaped Ceria. The inverse structure sensitivity of CeO_2 in ethylene production performance, higher on the {111} facets of the conventional polyhedral nanoparticles rather than {100} ones of nanocubes, has been associated with a easier formation of vacancies and defects sites on CeO_2 {100} which are adverse to acetylene hydrogenation contrary to the opposite trend of CO oxidation [124].

On the basis of these results, several investigations have been performed on metals supported on nanoshaped ceria. Reverse Water Gas Shift (RWGS) has been studied on both nanoshaped ceria, as well Ni/ceria nanocubes highlighting the role of the increase of oxygen vacancies in the nanoshaped support. CO_2 dissociation occurs over the support vacancies rather than on the metal and so it is favoured on a nanostructured support, which is richer in vacancies [125]. The highest catalytic activity and lower methane selectivity of nanoshaped Pt/CeO_2 on the WGS demonstrate that the nanostructured morphology of the ceria support and the exposed crystal planes play a crucial role [126].

The higher WGS activity and the capability of the RhPd to dissociate the C-C bond according to the nanostructure of the support are the basis of the higher hydrogen production in the low temperature ethanol steam reforming reaction on $RhPd/CeO_2$ nanocubes compared to nanorods or conventional oxide [127]. Hsiao et al. [128] reported a better rate of conversion of H_2 in ethanol-reforming reaction on Rh/cubic and rod shaped ceria compared with polycrystalline samples, confirming the effect of the morphology on the activity.

Gold catalysts supported over selected surfaces markedly affect the activity in CO preferential oxidation in a H_2-rich gas (CO-PROX) [129] and in low-temperature CO oxidation [130].

The morphology of the ceria support on Fe/CeO_2 catalyst plays a key role not only on the CO_2 hydrogenation but also on the methane to hydrocarbon selectivity and the olefin to paraffin ratio

[131]. In addition, the activation and conversion at low temperature in CO_2 methanation is facilitated by the presence of oxygen vacancy, accounting for the key role of concentration of oxygen vacancies in the hydrogenation reactions [132].

In conclusion, it is evident that catalytic performances and exposed crystal planes are strictly correlated. Catalyst morphology could be selectively modulated to obtain the reducibility degree in order to direct activity and selectivity in structure sensitive reactions in which formation of surface oxygen vacancies results of paramount importance.

1.3.3 Previous works

The present work is inspired by previous studies focused on Rh/CeO_2, where the influence of catalyst reduction temperature has been analyzed in CO_2 methanation reaction. It was observed that the methane production in transient condition (by pulsing CO_2) is temperature reduction depending: over a high temperature reduced catalyst (HTR: 500 °C), Rh supported over ceria showed a better transient catalytic activity pulsing CO_2 than after low temperature reduction conditions (LTR: 223 °C) [133] (See figure 1.6) This extra activity is destroyed during subsequent pulses and reaches comparable values than after LTR. Remarkably, although no water is detected initially, it is normally detected when the methane production follows down to the conventional value indicating a key role in this behavior. Moreover, the high activity can be reversible.

This effect was observed, but less evident, over platinum metal supported on ceria [45] The mechanism proposed for Rh/CeO_2 [45], highlights that oxygen vacancies, particularly those present in the bulk, are the driving force for CO_2 activation while metal is important in providing active H-species for the hydrogenation reaction. Moreover, the metal H_2 activation promotes the support reduction by means of the hydrogen spillover (migration of H species from metal to support) and it allows to establish a interaction between metal and partially reduced support.

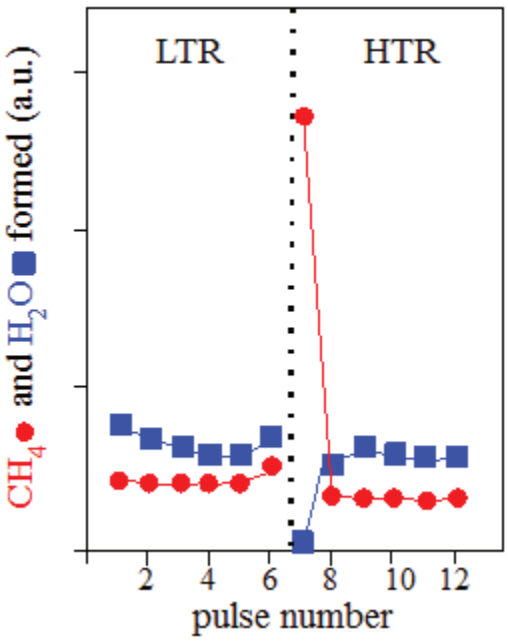

Figure 1.6 CH_4 and H_2O produced after CO_2 pulses over Rh/CeO_2 in H_2 flow after LTR (500 K) and HTR (773 K) reduction.

In transient condition studies [45, 133, 134] on carbon dioxide methanation over NM/CeO_2 carbon dioxide methanation (NM: noble metal), the H_2 treatment temperature does not generate the reduced oxide metal decoration observed in the classic strong metal-support interaction (SMSI) [45, 133, 134]. This effect, observed by Tauster et al. [135] on NM/TiO_2 reduced at 500°C, shows a reversible coverage of the metal by partially reduced oxide associated with H_2 and CO chemisorption suppression. On the contrary in Rh/CeO_2 catalysts a higher temperature reduction (700 °C) is required to induce the metal decoration [136]. A coordinated action between metal and partially reduced ceria is evidenced by the enhanced activity: the role of the support is to coordinate carbon dioxide, while the strong transient enhancement of the activity is attributed to the oxygen vacancies that are able to activate CO_2 but are annihilated by the reaction [134].

Shedding light into the nature of this metal-support interaction in reducible oxide supported catalysts is important since it has a strong influence on the catalytic properties of the system and SMSI is invoked in many different reactions (i.e. CO_2 hydrogenation to methanol over $Pd–Cu/CeO_2$ [137], CO oxidation over core-shell $Au-CeO_2$ nanostructures [138], methane dry reforming on

Ni/CeO_2 [62, 139], CO_2 Reforming of CH_4 on Ni/CeO_2 [140], Pt/CeO_2 for crotonaldehyde hydrogenation [141].

In the catalytic performance of ceria based materials its role as an oxygen vector, and the interaction between metal and partially reduced support that activates C-O bonds are ofter involved. The role of bulk or surface CeO_2 reducibility in CO_2 methanation has been evidenced and discussed by Trovarelli et al. [142] where the reduction of Rh/Ceria is modified by its dispersion over SiO_2 while the higher oxygen mobility and the easier reducibility of Ce^{4+} appear responsible for the higher catalytic activity in $Rh/Ce_{0.8}Zr_{0.2}O_2$ compared with rhodium supported on ceria [143].

Now the development of new materials with enhanced oxygen storage capacity suggests the possibility to deepen the understanding of the CO_2 activation mechanism and allows us to modulate the support reduction with the final goal of obtain "high activity sites" that can be regenerated into milder reaction conditions. To explore the oxygen vacancies role, nanostructured materials have been compared with a polycrystalline ceria. Rhodium over Ceria nanorods and nanocubes catalysts have been synthetized, characterized and tested in CO_2 methanation with steady state, transient and pulse condition after different reduction temperatures. Furthermore the redox behavior of CeO_2 has been modified by doping with different Ce/Zr ratios. The synthetized CeO_2-ZrO_2 mixed oxides, after characterization, catalytic activity has have been analyzed in transient and steady state catalytic activity experiments.

Chapter 2. Experimental methods

The materials used in this work comprised a series of catalysts based on Rh supported on ceria and ceria-zirconia, that are listed in Table 2.1. Ceria and ceria-zirconia supports were synthesized via precipitation and co-precipitation methods and Rh deposition was carried out by incipient wetness impregnation. The catalysts obtained were characterized by means of B.E.T surface area and porosimetry measurements, X-Ray Diffraction analysis (XRD), Temperature Programmed Reduction (TPR), Thermogravimetric Analysis (TGA), Transmission Electron Microscopy (TEM). Catalytic activity tests in CO_2 hydrogenation were performed under transient and steady state conditions by varying both the pretreatment and the reaction parameters.

Table 2.1 List of samples used in this work

Nominal composition	Sample name
1%Rh/CeO_2-cubes	RhCe-C
1%Rh/CeO_2-rods	RhCe-R
1%Rh/CeO_2	RhCZ100
1%Rh/$Ce_{0.1}Zr_{0.9}O_2$	RhCZ10
1%Rh/$Ce_{0.5}Zr_{0.5}O_2$	RhCZ50
1%Rh/$Ce_{0.75}Zr_{0.25}O_2$	RhCZ75
1%Rh/ZrO_2	RhCZ0

2.1 Synthesis methods

Polycrystalline ceria, ceria-zirconia and zirconia supports were synthesized by precipitation/co-precipitation of nitrate precursors in the presence of H_2O_2, according to the procedure reported in the literature [144]. In particular, the desired amounts of a solution of cerium nitrate ($Ce(NO_3)_3 \bullet 6H_2O$) and a 0.4 M solution of zirconyl nitrate ($ZrO(NO_3)_2$) were mixed in a suitable amount of distilled water. A proper amount of 30% w/v solution of hydrogen peroxide (H_2O_2) was

added to the solution of precursors until reaching a molar H_2O_2:(Ce+Zr) ratio of 3. The addition of H_2O_2 guarantees the oxidation of Ce^{3+} precursor into Ce^{+4}, which is more easily hydrolysable, leading to the formation of highly dispersed crystallites of CeO_2. The solution was then stirred for 45 minutes and a 30%w/v solution of ammonium hydroxide (NH_4OH) was used as a precipitating agent, until a pH value of 10.5 was reached. The precipitate was filtered and washed three times with deionized water. The supports so obtained were dried overnight at 120°C and calcined at 500°C for 3 hours in static air. The quantity used for each preparation are detailed in Table 2.2.

Table 2.2 Precursor amounts used in CZ catalyst synthesis

Sample name	$Ce(NO_3)_3$•$6H_2O$ (g)[a]	$ZrO(NO_3)_2$ (ml)[a]	H_2O_2 (ml)[a]
RhCZ0	0.00	20.3	2.8
RhCZ10	0.34	17.5	2.6
RhCZ50	1.47	8.5	2.3
RhCZ75	2.03	3.9	2.1
RhCZ100	2.52	0.0	2.0

[a] *Quantities to prepare 1 g support.*

In order to check the effect of different ceria facets on the catalytic behavior of the samples, also ceria nanocubes and nanorods were synthesized according to a procedure implemented in our research group [122]. For the preparation of 1 g of ceria nanocubes a solution of sodium hydroxide (27.86 g of NaOH dissolved in 101.6 ml of distilled water) was added dropwise into a ceria solution (2.52 g of $Ce(NO_3)_3$•$6H_2O$ dissolved in 14.5 ml of distilled water), under vigorous mixing. Once a precipitate was observed, the resulting suspension was poured in a tightly sealed Teflon-lined cylinder and placed inside a stainless-steel autoclave. The suspension was heated at 180°C and kept at this temperature for 24 hours; then it was cooled and centrifugated three times after washing with an ethanol solution. The supports so obtained were dried overnight at 60°C and calcined at 400°C for 3 hours in static air.

Ceria nanorods were obtained by a similar procedure: 35.54 g of NaOH were dissolved in 94.03 ml of distilled water and slowly mixed with a ceria solution (2.52 g of $Ce(NO_3)_3$•$6H_2O$ dissolved in 18.8 ml of distilled water). The suspension was again poured in the Teflon-lined cylinder and

heated at 140°C for 48 h inside the autoclave. After cooling, centrifugation and washing was carried out as for the ceria nanocubes. The powder was then dried overnight at 60°C and calcined at 400°C for 3 hours.

All Rh-containing catalysts (nominal metal loading 1%) were prepared by incipient wetness impregnation [145], using $RhCl_3$ (Johnson Matthey Chemical Limited) as metal precursor. A proper amount of saturated rhodium solution (26 mg of $RhCl_3 \cdot xH_2O$ containing 38,5%w of $RhCl_3$ dissolved in distilled water) was added dropwise to the support, while mixing with a pestle until complete wetness of the powder was obtained. After impregnation, the samples were dried overnight at 120°C. Then the catalysts were calcined at 550°C for 3 hours in static air, with the exception of 1%Rh/CeO_2-cubes and 1%Rh/CeO_2-rods, which were calcined at 500°C for 3 hours.

2.2 Catalysts characterization

The physical-chemical characterization is carried out with the aim of defining the structural and redox properties of catalysts, which in turn are used to understand the activity trends. In particular, in this work it was important to characterize deeply the catalysts in order to try to correlate their intrinsic properties with their activity for CO_2 methanation, as one of the main objective of the thesis was to investigate the effect of increased (or modified) reducibility on the catalytic performances. Surface area and porosimetry analysis, x-ray diffraction (XRD), temperature programmed reduction (TPR) experiments and thermogravimetric analysis were performed in the Laboratories of the Group of Catalysis for Energy and Environment at the University of Udine. High resolution transmission electron microscopy (HRTEM) analysis was carried out at the Energy Technique Institute of the Polytechnic University of Catalonia (Barcelona).

2.2.1 Surface area measurements and x-ray diffraction analysis

Figure 2.1 shows the Micromeritics TRISTAR 3000 apparatus for Brunauer-Emmett-Teller (BET) surface area measurements and porosimetry analyses. The system consists of two main units: the degassing and the nitrogen adsorption/desorption unit. The degassing is carried out under vacuum at 150°C for 1.5 hour in order to remove moist and other impurities from the catalyst surface. Once degassed, the sample (about 200-300 mg) is transferred inside the adsorption unit, where the adsorption-desorption of nitrogen is carried out at -196°C while recording the relative pressure.

Figure 2.1 Micromeritics TRISTAR 3000 apparatus

The x-ray diffraction spectra of supports and Rh-containing catalysts were collected with a Philips X'Pert Pro diffractometer (see Figure 2.2) equipped with an X'Celerator detector. The operating parameters were: 40 kV, 40 mA, Cu-K_α radiation, step width of 0.02 and counting time of 40 s/step in the range $20° \leq 2\theta \leq 100°$. Phase identification was carried out with Philips X'Pert HighScore software.

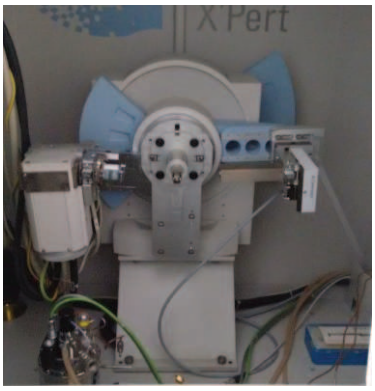

Figure 2.2 Philips X'Pert Pro diffractometer

2.2.2 HRTEM

High resolution transmission electron microscopy is a powerful technique that can provide information about the sample morphology, oxidation state and composition at atomic level. A thin layer of sample is exposed to a high energy electron beam, and the interaction of the electron wave with the crystal structure of the sample gives rise to the HRTEM image. The imaging process is not simple nor straightforward due to the complexity of the dynamic scattering of the electrons, but the images so obtained offer great insights about the shape of catalyst particles, the presence of oxygen vacancies and lattice defects, the mutual position and interaction between the support and metal clusters and their oxidation state. In this work the microstructural characterization by HRTEM has been carried out in a JEOL 2010F instrument equipped with a field emission source (see Figure 2.3) at an accelerating voltage of 200 kV. The point-to-point resolution was 0.19 nm, and the resolution between lines was 0.14 nm, with the magnification calibrated against a Si standard. Prior to analysis, the sample was dispersed in alcohol in an ultrasonic bath, and a drop of the suspension was poured onto a holey carbon-coated grid.

Figure 2.3 HR-TEM instrument

2.2.3 Redox properties

The redox properties of the materials were investigated by means of temperature programmed reduction experiments and thermogravimetric analysis. TPR tests were carried out in a Micromeritics AutoChem II 2920 apparatus shown in figure 2.4. The sample is loaded in an U-shaped quartz reactor placed in a furnace operating between -80°C and 1000°C. Temperatures below zero are achieved by pumping liquid nitrogen into the furnace. The effluent gases are analyzed by a Thermal Conductivity Detector (TCD) and a water trap ensures the complete removal of water before analysis. The instrument can operate both in continuous and in pulse mode. In addition, the device is connected to an OmniStar quadrupole mass spectrometer that allows collecting TCD data and mass spectra simultaneously.

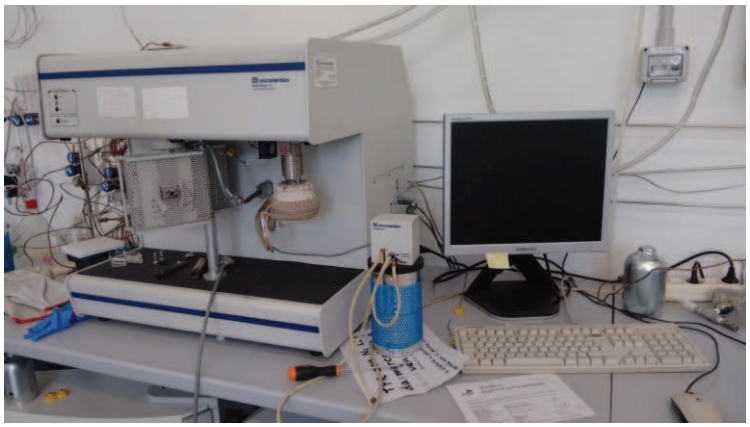

Figure 2.4 Micromeritics AutoChem II 2920 apparatus

Four different kind of experiments were performed in the TPR device:

- ***TPR***: 50 mg of catalyst were treated with 35 ml/min of air at 500°C for 1 hour to clean the catalyst surface. The sample was then cooled until -80°C, and TPR was carried out using 35 ml/min of a 4.5% H_2/N_2 gas mixture with a heating ramp of 10°C/min up to 1000°C.
- ***TPR-O₂***: 50 mg of catalyst were reduced with 30 ml/min of pure H_2 at 223°C (low temperature reduction, LTR) for 2 hours. After this treatment, O_2 consumption was measured by injecting a 2 vol% O_2/He mixture with5 ml pulses every 10 minutes, until no oxygen consumption was detected by TCD (i.e. no change in the area of the peaks was

observed). The system was then cooled and 30 ml/min of He flowed for 1 hour at room temperature. Then, the sample was re-oxidized at 500°C for 1 hour by flowing 35 ml/min of air. After cooling, a second step of reduction was carried out with 30 ml/min of pure H_2 at 500°C (high temperature reduction, HTR) for 2 hours. Again, O_2 consumption was measured by pulsing a 2%O_2/He mixture as after LTR.

- ***TPR-H_2O***: these experiments were carried out without the water trap in order to monitor the production of water from the sample during reduction. In this case the effluent gases were analyzed with the mass spectrometer connected to the TPR instrument. The catalyst (50 mg) was cleaned by flowing 35 ml/min of air at 500°C for 1 hour; the gas was then switched to He and the sample was cooled down to -80°C. Catalyst reduction took place by flowing 35 ml/min of a 4.5% H_2/N_2 gas mixture with a heating ramp of 10°C/min up to 1000°C. It should be highlighted that the goal of this procedure was to observe the hydrogen adsorption/desorption patterns, i.e. to determine if the hydrogen consumption is accompanied by a water production or if the sample can adsorb hydrogen which remains chemisorbed onto the catalyst surface. Adsorbed hydrogen can be estimated as the difference between hydrogen fed to the system and water production.
- ***TPR-isotherm***: the TPR experiment was carried out as before (TPR), but the temperature ramp was held at 223°C for 2 hours, then the sample was cooled and 35 ml/min of He flowed for 1 hour at room temperature. The sample was then re-oxidized at 500°C for 1 hour by flowing 35 ml/min of air and cooled down to -80°C. A second TPR was carried out up to 500°C, where isotherm conditions were kept for 2 hours. These experiments simulated the reduction treatments carried out on the samples in the catalytic setup before methanation reaction.

TGA tests were carried out in a thermogravimetric apparatus TA Instruments Q500 (see Figure 2.5). A vertical thermobalance measures the weight changes due to user selected thermal treatments

inside the furnace. The sample is loaded on a Pt pan which is then automatically suspended on a hook and transferred into the furnace. Two kinds of tests were carried out in this apparatus:

- ***TGA-TPR:*** 40 mg of catalyst were treated with 40 ml/min of air at 500°C for 1 hour to clean the catalyst surface and the system was cooled down to room temperature. Temperature Programmed Reduction was carried out using 40 ml/min of a 4.5% H_2/N_2 gas mixture with a heating ramp of 10°C/min in the temperature range: $50 \leq T(°C) \leq 900$.
- ***TGA-isotherms:*** these experiments repeated the TPR-isotherms carried out in the TPR apparatus. 40 mg of catalyst were treated with 40 ml/min of air at 500°C for 1 hour to clean the catalyst surface. The sample was then cooled down to 50°C and heated again up to 223°C (low temperature reduction, LTR) with 40 ml/min of a 4.5% H_2/N_2 mixture. The sample was held in isotherm conditions for 2 hours. Again, the system was cooled and 40 ml/min of N_2 flowed for 1 hour at room temperature. The sample was then re-oxidized by flowing 40 ml/min of air at 500°C for 1 hour, followed by cooling to room temperature, purging with nitrogen and by a second reducing treatment (40 ml/min 4.5% H_2/N_2) carried out at 500°C (high temperature reduction, HTR) for 2 hours.

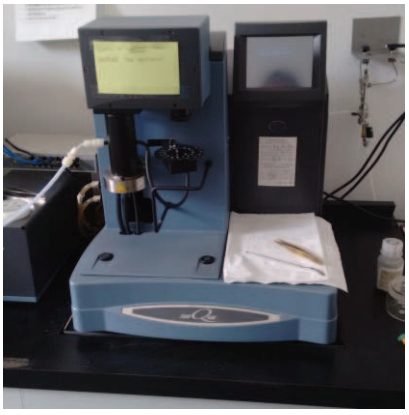

Figure 2.5 Thermogravimetic analyzer Q500

2.4 Catalytic tests

The catalytic tests assessed the transient and steady state methanation activity of Rh-based samples. The methanation catalytic tests were performed under transient and steady state conditions on Rh-based samples. Furthermore, under specific design conditions, they are used to get insights about physical and chemical interactions affecting the catalytic reaction. In this work, catalytic tests were designed specifically to investigate the transient increase of the activity evidenced in CO_2-methanation over Rh-ceria based catalysts. Because of the limitation of the standard steady-state procedures in explaining the outstanding behavior of Rh/CeO_2 catalysts [45], it was necessary to include more complex catalytic tests. These experiments required the design of a specific, versatile setup, which could be used to perform standard steady state and continuous tests, as well as transient experiments that allow to monitor the evolution of methane during the first seconds (or minutes) of test. The equipment allows to investigate the effect of different pretreatments, reaction temperatures and reaction regimens on the CO_2-methanation reaction in order to explain the unexpected behavior of Rh/CeO_2 catalysts. Moreover, a correlation between the methane evolution and the catalytic active sites was expected.

From previous studies, as it was described in the Introduction section, it was known that the production of methane at the very beginning of the experiment was a key issue that discriminates Rh-ceria systems from other metal-support combinations. For this reason, it was fundamental to measure methane as soon as it is produced, not only quantifying it but also minimizing the interferences related to dead volumes, leaks and catalyst deactivation in order to have a direct measure of its rate of production. This could be accomplished only if methane goes directly from the catalytic bed toward the detector as it is produced.

The setup realized for this purpose was based on the pulse-apparatus described in a previous work [142]. A stainless steel reactor (l=25 cm, d_i = 0.1 cm for pulse or 0.5 cm transient/steady state experiments) is inserted into a tubular furnace to control the temperature and connected to a

HP5890 gas chromatograph (GC), equipped with two Poraplot Q columns and two detectors, a TCD and a Flame Ionization Detector (FID). CO and CO_2 are converted to methane inside a methanator in order to detect them into the FID. A system of mass flow controllers regulates the gas feed to the reactor and a set of valves is used to control the feed and to choose the reaction regime, i.e. steady state, pulse or transient (see figure 2.6). V1 valve selects the treatment gas (reduction in pure H_2, outgas in He and oxidation in Air) and V2 switches from steady state or transient to pulse test conditions. V3 loop valve injects CO_2 pulses into flowing H_2 carrier (selected from 1 and 2 valves) into pulse experiments. Valve V4 allows to analyze the reactor effluents, depending to reaction regime: for steady state experiments the reactor outlet goes to V5 (GC built-in sampling valve) that injects the gas into the columns and then to the GC detectors to discriminate the presence of byproducts. In the other position, V4 sends the effluents directly from the reactor to the methanator and FID to analyze pulse or transient outputs. The experimental setup has been modified to send directly the outlet gas to the detector in order to minimize the dead volume. This is particularly useful during transient experiments when an immediate response is needed in order to evaluate the first seconds of methane production. It is important to emphasize that the system presents a critical point: even traces of oxygen depress the transient enhanced activity observed after high temperature reduction hiding the peculiar behavior of Ceria-based catalysts.

2.4.1 CO_2 methanation tests: experimental conditions

Catalytic tests were carried out in two steps: Pretreatment (see Table 2.3) and catalytic activity analysis (see Table 2.4), followed by catalyst reoxidation (500°C in air for 1 hour). The two steps are repeated after reoxidation, usually pretreating the catalyst at a different temperature. Catalyst pretreatment was carried out at low (LT), medium (MT) or high temperature (HT), and before pretreatment a degassing step was carried out (30 min, room temperature, 30 ml/min He).

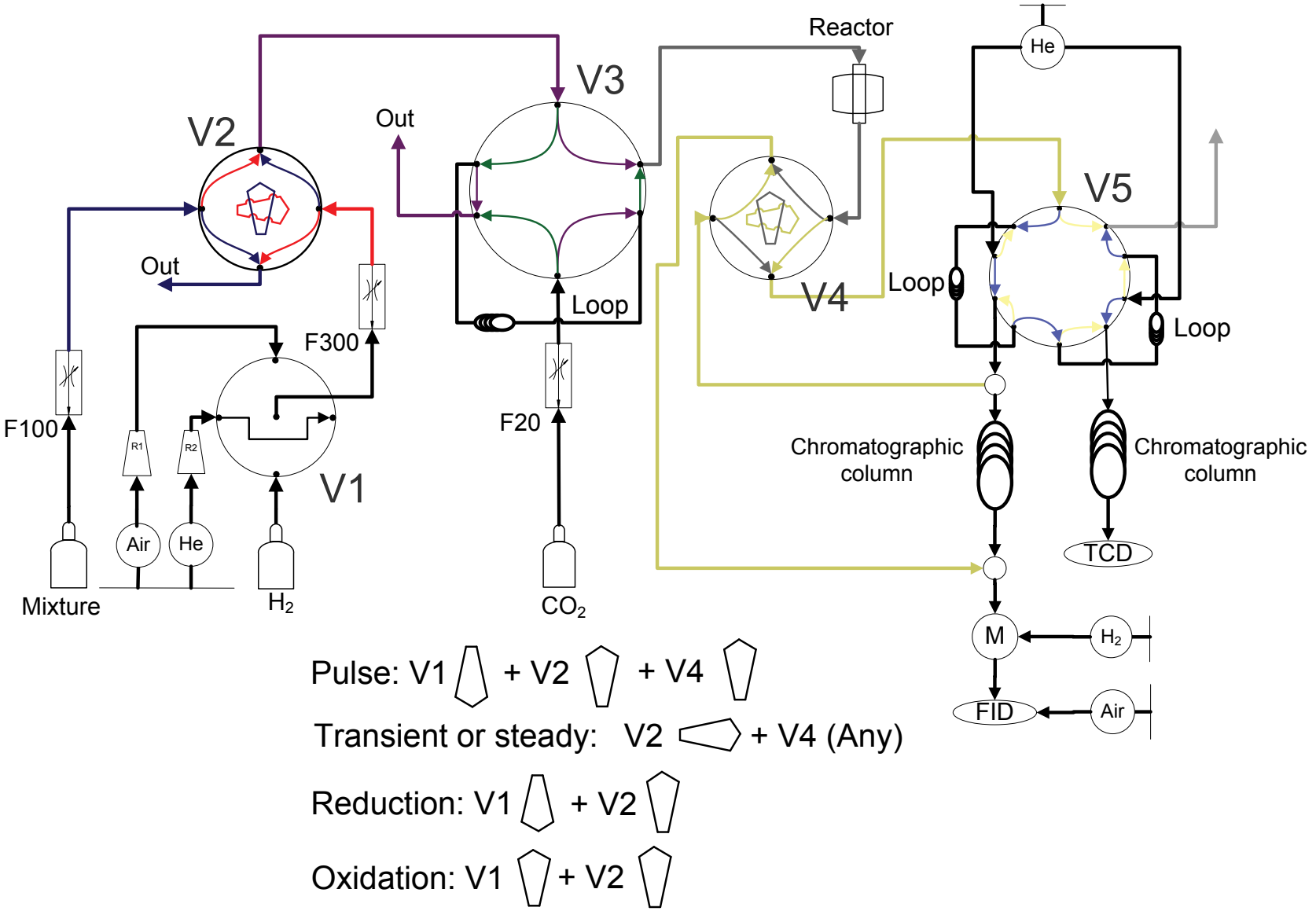

Figure 2.6 Scheme of the custom made experimental setup for CO_2 methanation experiments

Table 2.3 Summary of pretreatment conditions

Name	Type	Gas	Time (h)	Temperature (°C)	Flow (ml/min)
LTR	Reduction	Pure H_2	2	223	30
LTR -4h	Reduction	Pure H_2	4	223	30
LTR-(He)	Reduction	He	2	223	30
LTR-4h-(He)	Reduction	He	4	223	30
MTR	Reduction	Pure H_2	2	350	30
HTR	Reduction	Pure H_2	2	500	30
HTR -4h	Reduction	Pure H_2	4	500	30
HTR -2h-(He)	Reduction	He	2	500	30
HTR-4h-(He)	Reduction	He	4	500	30
Ox	Oxidation	Air	1	500	30
De	Degassing	He	$0.1 \leq t \leq 10$	$20 \leq T \leq 500$	$30 \leq F \leq 100$

The methanation reaction was investigated at atmospheric pressure following two possible schemes:

1) by feeding to the reactor a stoichiometric mixture of CO_2 and H_2 in Helium (2% CO_2, 8% H_2, 90% He) for transient and steady state experiments;

2) by feeding hydrogen and CO_2 pulses.

Table 2.4 summarizes the conditions for all kind of experiments.

Table 2.4 Reaction conditions for different CO_2 methanation experiments

Reaction regimen	Name	Description	Conditions
Pulse	P	CO_2-pulses are injected into the reactor. Between each pulse, pure H_2 flows through the catalytic bed.	- T_{rxn}=223 °C. - Pulse= 20 µL. - m_{cat}=15 mg.
Transient	Tr	A diluted stoichiometric mixture of CO_2/H_2 is sent to the reactor while the temperature is kept constant at a selected value for 1 hour	- $50 \leq T_{rxn}(°C) \leq 400$. - m_{cat}=50 mg. - Feed flow=10 ml/min. - t=60 min
Steady state	SS	A diluted stoichiometric mixture of CO_2/H_2 flows into the reactor. The experiment is carried out until the system reaches the steady state at a selected temperature.	- $50°C \leq T_{rxn} \leq 223°C$. - m_{cat}=50 mg. - Feed flow: 10 ml/min. - t=240 min

Chapter 3. CeO_2-supported catalysts

3.1 Overview

In this chapter the characterization and catalytic behavior of materials based on pure nanoshaped ceria will be described and compared with the behavior of polycrystalline CeO_2 samples prepared by conventional routes. The CeO_2 supports have been prepared and characterized and after loading with Rh, their properties in CO_2 hydrogenation under transient conditions have been studied.

The study of ceria-based materials with controlled morphology is becoming more and more important, due to the unique properties of these systems compared to polycrystalline cerium dioxide [146-148]. In particular, it has been shown that ceria nanocubes and nanorods exhibit a higher reducibility [119], which can lead to higher activity for specific catalytic reactions such as soot [149, 150] and CO oxidation [119, 124], and, more in general, for the reactions requiring a contribution from ceria oxygen vacancies. In addition, interaction with supported metals, can contribute to enhance metal support interaction and develop specific properties which ultimately can lead to increased activity in several reactions [151].

The idea behind this study was then to check whether, by exploiting the enhanced redox properties of nanoshaped ceria, it was possible to improve and/or to stabilize the transient CO_2 methanation activity observed for Rh supported on polycrystalline ceria in our group. This high transient activity was in fact attributed to the presence of active oxygen vacancies on ceria [133]. A similar explanation was also proposed for CO_2 hydrogenation on Rh/TiO_2 catalyst, which upon reduction showed an analogous transient behavior [43]. In principle, the synthesis of ceria nanoshapes exposing preferentially more reactive planes could have helped to reach the goal of increasing the activity of Rh/CeO_2 catalysts. For this purpose, three Rh/CeO_2 samples were prepared (see Table

3.1), characterized and tested for CO_2 methanation. The catalysts consisted on Rh supported on ceria nanocubes, ceria nanorods and polycrystalline ceria, as reported in Chapter 2.

3.2 Characterization

Textural properties are reported in Table 3.1 and they show that the samples have a surface area comprised between 25 and 36 m^2/g. In particular, the surface area of the nanoshaped ceria cubes and rods is higher compared to polycrystalline ceria, as well as their total pore volume and average pore size. The impregnation of rhodium on ceria supports does not alter significantly their textural properties, likely due to the low nominal content of metal.

Table 3.1 Textural properties of CeO_2 and Rh/CeO_2 catalysts[a]

Description	Sample	BET S.A. (m^2/g)	Pore volume (cm^3/g)	Pore size (Å)
Polycrystalline CeO_2	CZ100	25.6	0.10	118
CeO_2 Nanocubes	CeO_2-C	35.5	0.25	180
CeO_2 Nanorods	CeO_2-R	36.2	0.31	294
Rh on polycrystalline CeO_2	RhCZ100	25.5	0.10	114
Rh on CeO_2 nanocubes	RhCe-C	36.2	0.27	176
Rh on CeO_2 nanocubes	RhCe-R	33.0	0.29	286

[a] Measured after drying and calcination at 550°C for 3 hours.

The XRD spectra were recorded for bare supports and supported catalysts (see Figure 3.1). However, no noticeable differences were found between the supports and metal supported samples, all the spectra show only the characteristic peaks of pure ceria that crystallizes in the fluorite cubic phase. There are no diffraction peaks due to the presence of Rh, likely because the metal loading is too low to be detected and/or rhodium is highly dispersed on the support (see also HRTEM analysis).

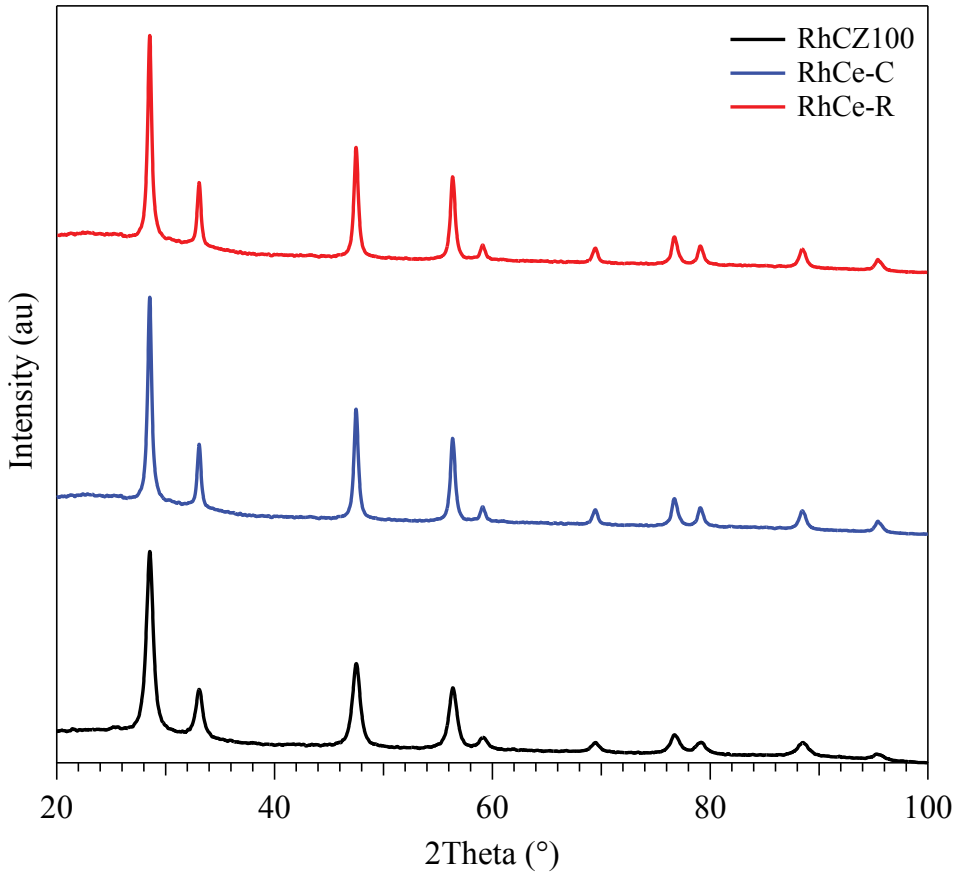

Figure 3.1 XRD spectra of 1%Rh/CeO_2 catalysts

Additional analyses of the X-ray diffraction profiles were carried out according to the method reported by Aneggi et al. [122] to see if XRD spectra of nanoceria-based catalysts can be used to characterize the morphological shape. Although the relative intensity of the peaks varies depending on the sample morphology (Table 3.2) these cannot be used to unambiguously identify the catalyst nanoshape, since there is no preferential exposure of ceria planes in XRD profiles. For this reason, also HRTEM analysis were carried on nanoshaped samples to define clearly their morphology.

Table 3.2 Relative intensity (%) from XRD according the exposed planes

Plane	CZ100	Ce-C	Ce-R	RhCZ100	RhCe-C	RhCe-R
[1 1 1]	100	100	100	100	100	100
[2 0 0]	27	32	26	27	30	28
[2 2 0]	51	52	40	51	52	45
[3 1 1]	43	36	28	34	40	35
[2 2 2]	7	6	4	7	7	6
[4 0 0]	7	6	4	7	7	6
[3 3 1]	15	11	7	13	12	10
[4 2 0]	9	6	5	8	8	6

Figure 3.2 shows an overview (left) and a high magnification (right) image of ceria nanocubes. It can be observed the well defined cubic geometry, with the exposure of CeO_2 (100) crystallographic planes as inferred from the spots at 2.71 Å of the Fourier transform image. Ceria nanorods are shown in Figure 3.3, and also in this case HRTEM images confirmed the expected morphology. The high magnification image allows to observe the roughness of the outer surface of ceria nanorods which are characterized by the presence of a large amount of defects and surface irregularities, most likely due to exposure of high index planes and surface faceting [152].

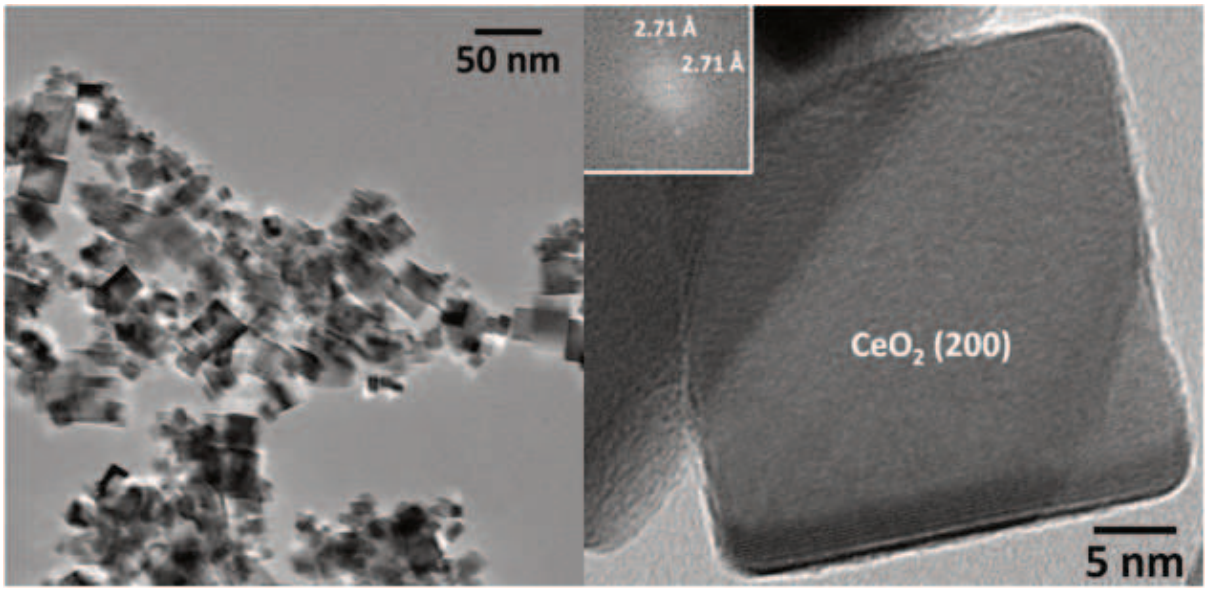

Figure 3.2 HRTEM image of ceria nanocubes. Left: Overview. Right: Magnification

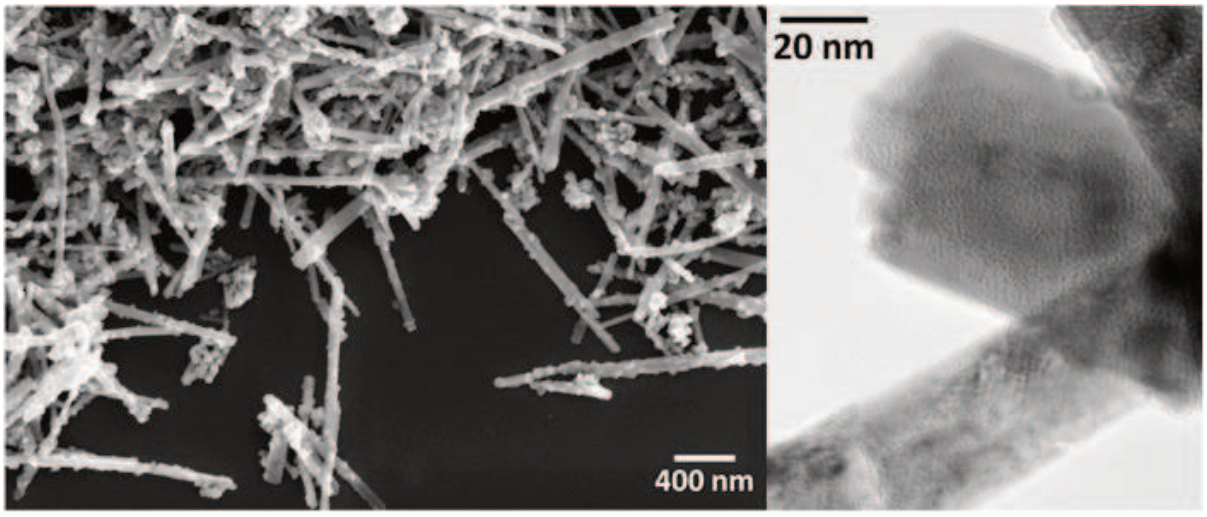

Figure 3.3 HRTEM image of ceria nanorods. Left: Overview. Right: Magnification

Moreover, polycrystalline ceria is shown in Figure 3.4. As it can be observed, no well-defined geometry can be inferred from figure 3.4 and ceria nanoparticles expose preferentially the (111) crystal plane.

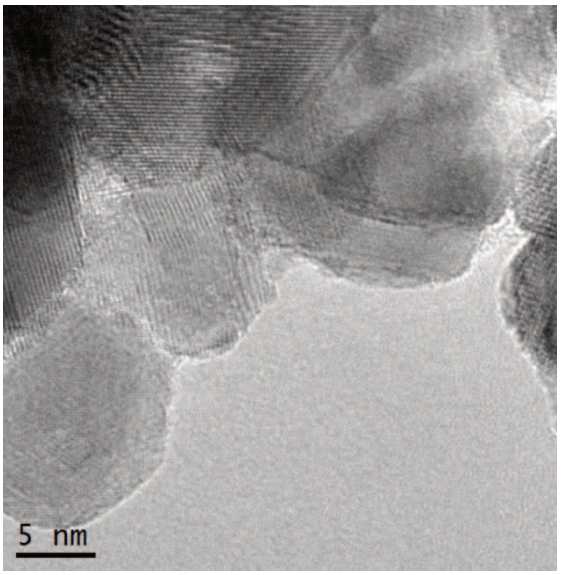

Figure 3.4 HRTEM image of polycristalline ceria

The morphological changes following low and high temperature reduction on Rh supported polycrystalline ceria were also followed by HRTEM. The aim of this analysis was to understand if and how the thermal treatments could modify the surface of the samples. According to the HRTEM pictures of RhCZ100 (see figure 3.5), only ceria particles comprised between 5 and 20 nm were detected. No significant differences between fresh and treated catalyst were observed, apart from a slight predominance of smaller particles on the fresh RhCZ100. On all samples the exposed planes were [1 1 1], [2 0 0] and [2 2 2], indicating the typical cubic fluorite structure of polycrystalline ceria and excluding any restructuring during LTR or HTR. In addition, Rh particles were not detected on any sample even if on a small portion of all samples the lattice fringes belonging to Rh_2O_3 could be observed. This indicates that Rh is easily oxidized in contact with air, and that it was not possible to draw any conclusion regarding Rh oxidation state on samples after LTR and HTR examined ex-situ.

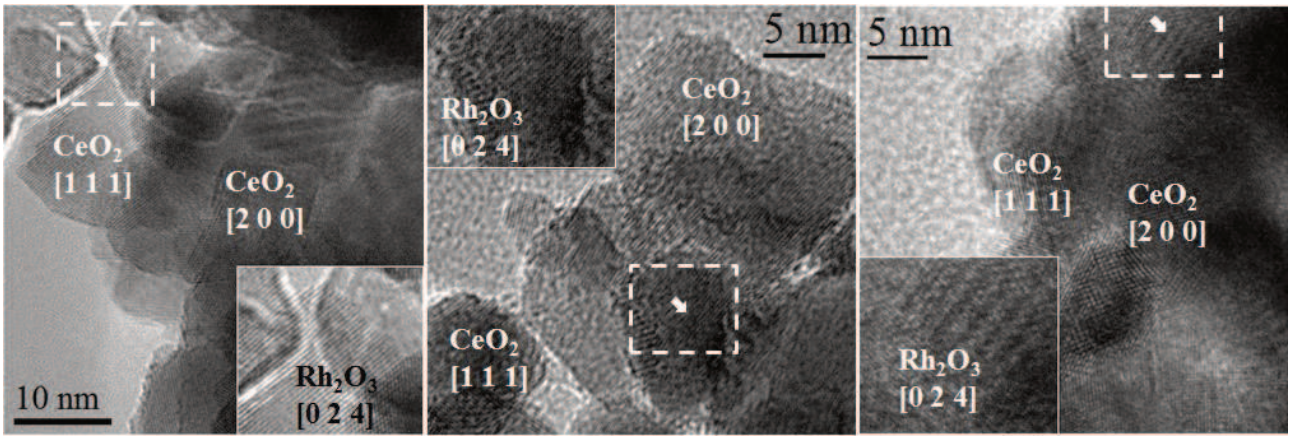

Figure 3.5 HRTEM analysis of Rh/CZ100 (left: fresh sample, middle: sample after LTR, right: sample after HTR)

3.2.1 Reduction studies

The reduction degree of the ceria-based catalysts was investigated first by recording of TPR signals associated with the bare supports (see figure 3.6). The TPR profile of polycrystalline ceria shows the typical profile with a low temperature peak ascribed to the reduction of surface Ce^{4+} species and a high temperature one related to the reduction of bulk ceria to Ce_2O_3 [70]. The reduction profile of nanoshapes is qualitatively similar to that of polycrystalline ceria, however, although there are no variations in the overall patterns of hydrogen consumption (i.e. the presence of two peaks related to surface and bulk reduction), some qualitative differences can be highlighted.

The reduction of surface Ce^{4+} is anticipated in nanoshaped ceria, and the onset of reduction is located at lower temperatures, as already reported in literature [122, 153], while there are no substantial modifications of the high-temperature peak. These facts suggest improvements in the surface reduction process due to the nano-oriented synthesis. In particular, the preferential orientation of the crystal exposing the {110} and {111} surfaces, facilitates redeuction, due to the higher reducibility of these surfaces compared to the {111}. The overall degree of reduction can be calculated from the TPR profiles according to reaction (Eq. 3.1) and it is reported in Table 3.3. The value is in agreement with the higher reducibiity of nanoshapes compared to polycrystalline ceria.

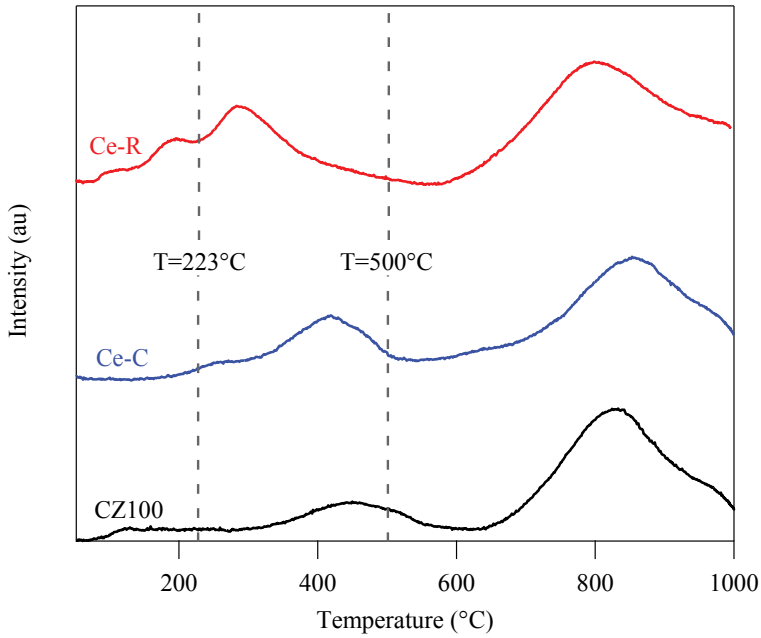

Figure 3.6 TPR results of ceria supports

$$CeO_2 + xH_2 \rightarrow CeO_{2-x} + xH_2O \qquad (Eq.3.1)$$

The TPR profiles of the Rh/CeO_2 catalysts are shown in Figure 3.7, where the effect of the presence of Rh on ceria reduction can be observed. It is well-known fact that in the presence of metal particles the reduction behavior of CeO_2 is deeply modified due to hydrogen spillover from the metal to the oxide that anticipates the reduction of ceria at lower temperatures [154-158]. Therefore, the impregnation of rhodium on these supports strongly modifies the low temperature reduction behavior of the catalysts. Indeed, the low temperature peaks are shifted to a much lower temperature, approximately between -30°C and 300°C. While the onset of reduction in RhCZ100 is at lower temperatures compared to RhCe-C and RhCe-R, the intensity of its peak is lower, suggesting a lower reduction degree. Surface reduction of RhCe-R shows also a shoulder after the main peak likely due to the presence of additional surface irregularities and effects in this sample.

The high temperature reduction peaks of ceria-based catalysts are similar indicating that Rh does not influence reduction characteristics of ceria bulk oxide.

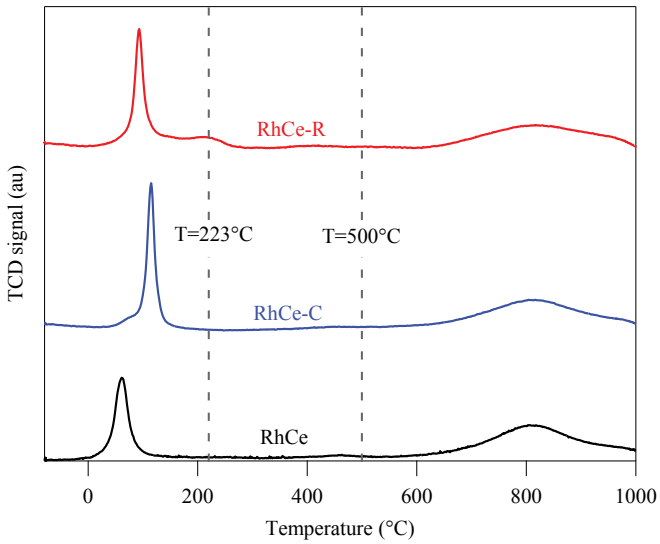

Figure 3.7 TPR profiles of Rh/CeO_2 catalysts

The quantitative analysis carried out assuming the complete reduction of rhodium oxide, according to equation (3.1) is reported in Table 3.3:

$$Rh_2O_3 + 3H_2 \rightarrow 2Rh + 3H_2O \qquad (Eq.\,3.2)$$

Table 3.3 Reduction characteristics of CeO_2 and Rh/CeO_2 samples.

Sample	x[a]	H_2 consumption ($mmol/g_{cat}$)[b]	x LT[c]	x HT[d]
CZ100	0.14	0.81	0.006	0.039
CeO_2-C	0.20	1.17	0.000	0.043
CeO_2-R	0.18	1.07	0.006	0.063
RhCZ100	0.15	1.04	0.028	0.036
RhCe-C	0.20	1.30	0.036	0.049
RhCe-R	0.19	1.25	0.044	0.058

[a] x from reaction (3.1) calculated at the end of a TPR run. In the cae of Rh-containing samples the calculations assume complete reduction of Rh_2O_3 to Rh according to reaction (3.2)
[b] Calculated at the end of TPR.
[c] Low-temperature reduction of CeO_2 according to (3.2) calculated at 223°C.
[d] High-temperature reduction of CeO_2 according to (3.2) calculated at 500°C

The rhodium presence slightly increases the reduction of polycrystalline and nanorod ceria, but not that of ceria nanocubes. The overall order of reduction degree is such that Nanocubes > nanorods > polycrystalline ceria, which is not depended on the rhodium impregnation. Previous reports have obtained similar results [102, 159]. By calculating the amount of reduction achieved under TPR

conditions at low and high temperature it is clear that for Rh supported samples the degree of reduction of ceria is higher for nanoshaped materials after both LT and HT and that after HT all cerias exhibit approximately 30% more reduction than after LT. The amount of reduction observed under TPR conditions does not necessarily reflect the amount of reduction that can be observed after isothermal reduction. To compare the two values a series of isothermal reduction experiments were followed in the TPR and TG apparatus as described in the experimental part. The results are summarized in Table 3.4 for RhCZ100 and RhCe-R and clearly show that the reduction degree after LTR and HTR is higher for nanorods compared to polycrystalline ceria.

Table 3.4 Quantitative results of TPR and TGA isotherm experiments

Sample	x TPR isotherm[a]	x TGA isotherm[b]
	LTR	
RhCZ100	0.041	0.021
RhCe-R	0.044	0.040
	HTR	
RhCZ100	0.051	0.043
RhCe-R	0.058	0.091

[a] x in CeO_{2-x} calculated from H_2 consumption in TPR of Rh/CeO_2 samples up to 223°C and treated for 2 hours at isothermal conditions.
[b] x in CeO_{2-x} calculated from H_2 consumption in TGA of Rh/CeO_2 samples up to 223°C and treated for 2 hours at isothermal conditions.

3.3 Catalytic activity

3.3.1 Pulse tests

Before starting the investigation of the new samples, the experiments carried out in the past were replicated to verify the occurrence of the expected transient behavior. This was necessary in order to check the correct operation of the setup, because as reported in the experimental part any leak, dead volume etc. could compromise the experiments. According to what explained in Chapter 2, before the methanation test each catalyst was pretreated exposing it to a reducing treatment in pure H_2 at

low (223°C, LTR) or high temperature (500°C, HTR). Figure 3.8 shows an example of the results obtained during pulse tests at 223°C, in agreement with the previous work [160]. By analyzing the catalytic behavior of RhCZ100, the results showed CO_2 conversion around 30-40% after LTR, almost constant from the first pulse onwards.

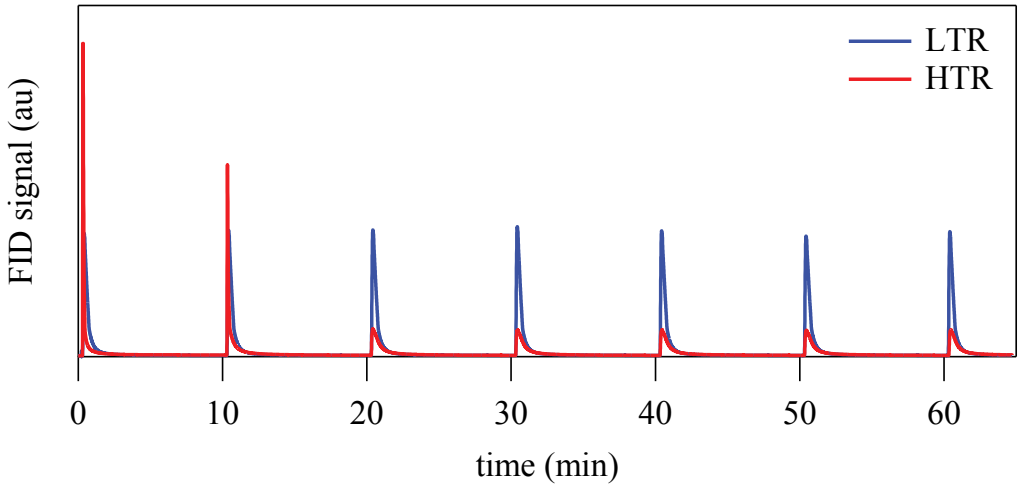

Figure 3.8 Typical results of pulse tests, as obtained on RhCZ100 at T=223°C

On the contrary, the catalytic performance after HTR varies depending on the pulse to be considered. In this respect, the conversion during the first pulse is always slightly lower than that after LTR, but the highest one of the test after HTR. The conversion then decreases in the following 3-4 pulses until its stabilization (about 10-15% CO_2 conversion). A stable behavior was observed from the fourth pulse onwards, and constant CH_4 production was detected for about 20 pulses. Even if the overall HTR conversion during the first pulse is lower than LTR conversion, the methane production is much faster as it can be observed from Figure 3.9: the first pulse after HTR is sharper and higher, indicating a very high transient activity that declines very fast, whereas the transient activity after LTR is negligible compared to HTR.

This different behavior after LTR and after HTR was the driving force of the investigation: why do we observe such a high transient activity after the sample has been reduced at high temperature (500°C)? The hypothesis was that the effect could be related to the oxygen vacancies formed on ceria, as reported also for Rh/TiO_2 [43] and for Ru/CeO_2 [161], and the study of samples with

different redox properties as cubes and rods could help to shed some light on this point. For this purpose, transient experiments were performed in which CO_2 methanation was studied over a 60 min time period at constant temperature (see Experimental Section, Chapter 2).

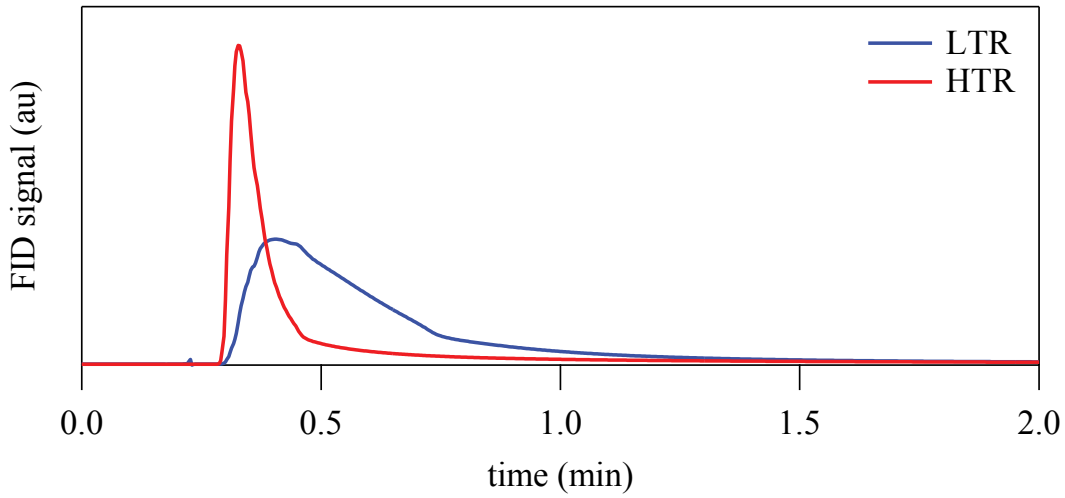

Figure 3.9 First-peak result, obtained on RhCZ100 at T=223°C

3.3.2 Transient tests

Figures 3.10, 3.11 and 3.12 show the results of the transient tests carried out at 150°C on RhCZ100, RhCe-C and RhCe-R, respectively. The first thing to be observed is that at this temperature the transient and overall activity after LTR is negligible in comparison with that after HTR. Also, the presence of the transient high activity peak is related to the high temperature reduction with the interesting exception of RhCe-R for which a small transient peak is detected also after LTR. This feature is likely related to the fact that the degree of reduction of RhCe-R at 223°C (LTR) is higher than that of the other two samples. Focusing on the shape of this transient peak after HTR, it is important to distinguish between polycrystalline ceria on one side, and cubes and rods on the other. For RhCZ100 in fact the peak is narrower and the steady state condition is reached after about 20 mins of reaction, whereas for RhCe-C and RhCe-R a steady state is not reached within the 60

minutes of the experiment. The quantitative analysis of the methane produced during the transient high activity peak is reported in Figure 3.13 for all samples.

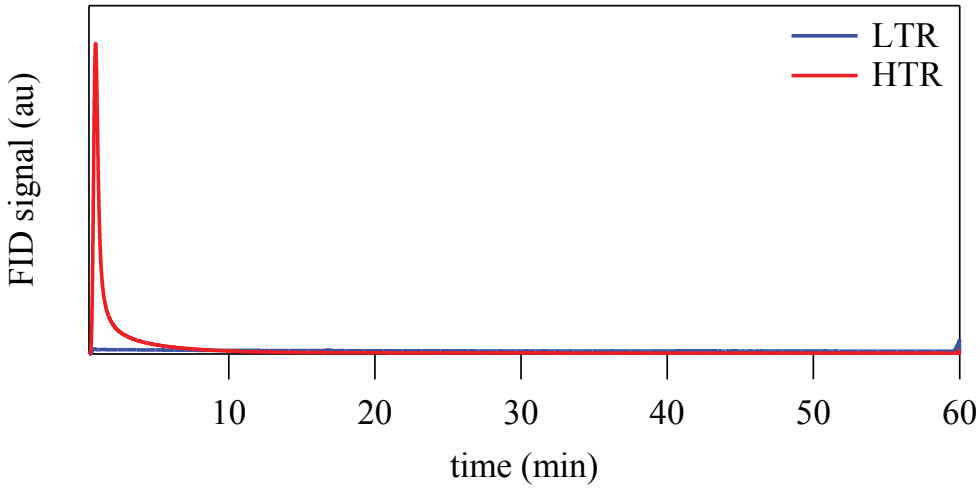

Figure 3.10 Transient test results at 150°C over RhCZ100 after LTR and HTR

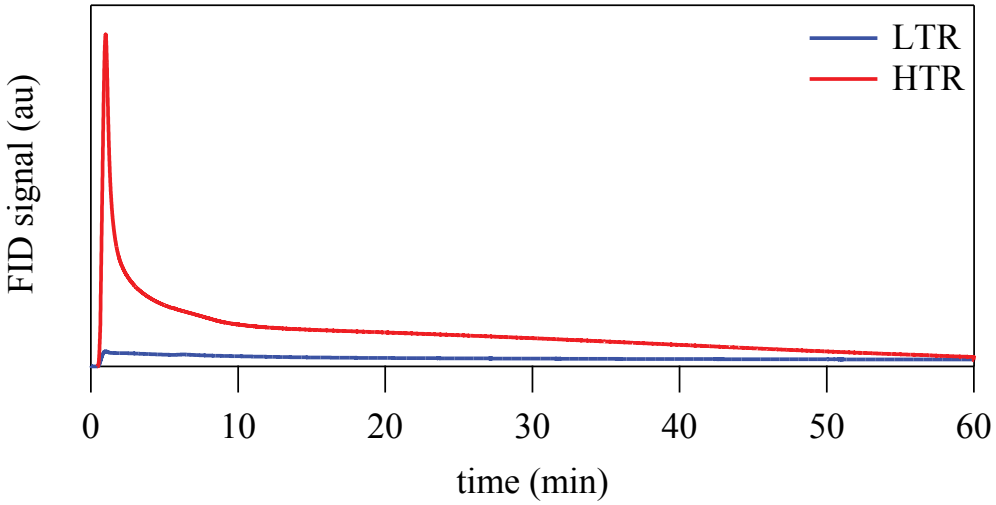

Figure 3.11 Transient test results at 150°C over RhCe-C after LTR and HTR

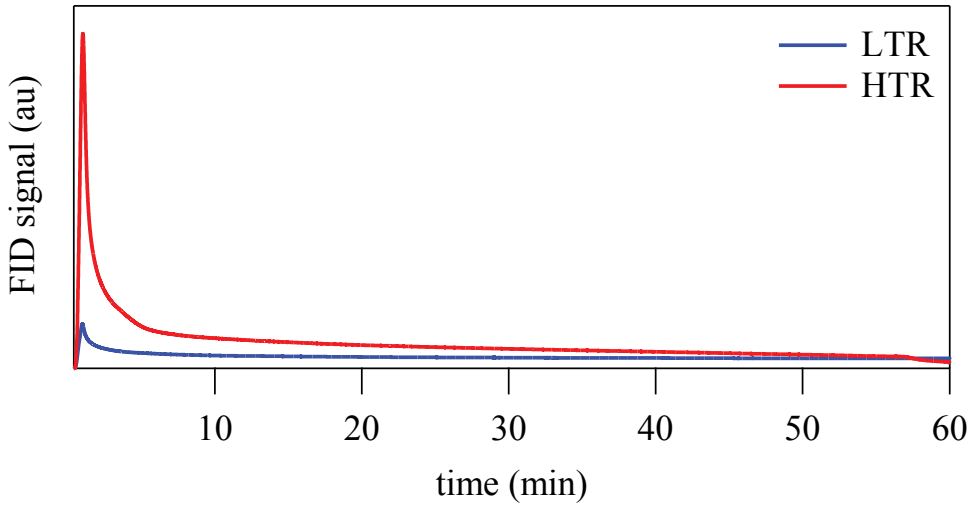

Figure 3.12 Transient test results at 150°C over RhCe-R after LTR and HTR

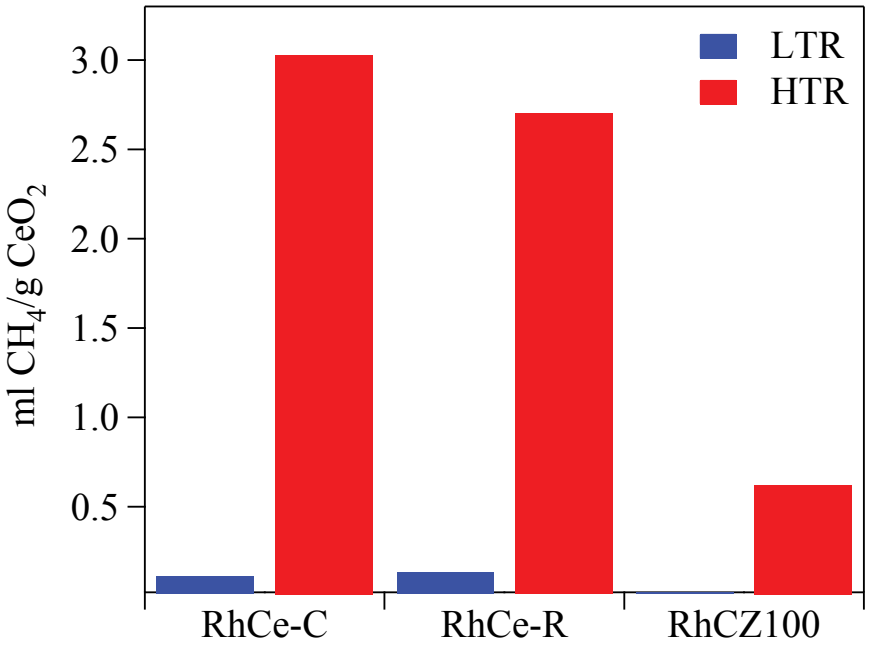

Figure 3.13 Methane produced in the transient high activity peak at T=150°C

The difference between the amount of methane produced over the nanoshaped ceria and over RhCZ100 is evident, especially for the test carried out after HTR. These results indicate that not only the higher degree of reduction of RhCe-C and RhCe-R plays a role on the catalytic performance, but also that the different redox patterns observed during TPR are reflected in the transient high activity. This transient activity in fact is prolonged over a longer period on nanoshaped ceria, and this is likely due to the fact that there are more oxygen vacancies which take a longer time to be reoxidized by CO_2 or water formed during the reaction, according to the mechanism proposed by de Leitenburg et al. [45].

When the reaction is carried out at 223°C, the general picture is similar but the amount of methane produced is of course much higher, and the difference between methane production after LTR and after HTR is smaller compared to the one recorded at 150°C (see Figure 3.14).

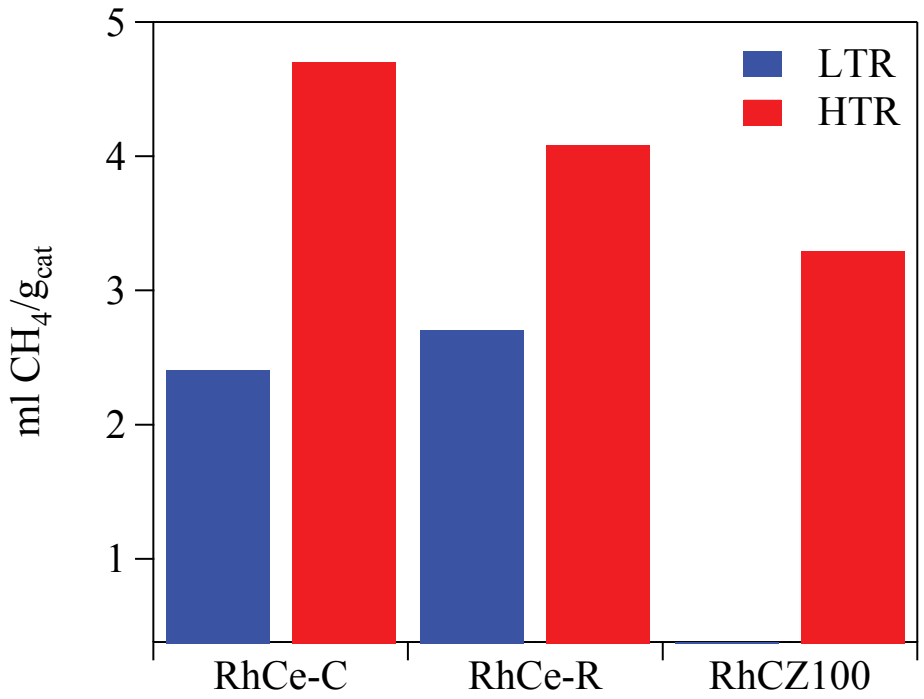

Figure 3.14 Methane produced at T=223°C in the transient high activity peak

Figures 3.15, 3.16 and 3.17 show the evolution of methane production over time at 223°C after low and high temperature reduction for RhCZ100, RhCe-C and RhCe-R, respectively. Again, we observe the presence of a pronounced transient high activity peak after LTR only on RhCe-R. On RhCe-C, and to a lesser extent on RhCZ100, the peak is much less evident and requires more time to reach the baseline (see Figure 3.14). The transient peak after HTR is broader on RhCe-C and RhCe-R compared to RhCZ100, similarly to what detected when the reaction is carried out at 150°C, but in this case also for Rh supported on ceria cubes and rods this transient activity is concluded within about 10 minutes of reaction. This indicates that at 223°C the active sites formed after HTR are more active but deactivate faster than at 150°C, and both effects are likely due to the higher temperature of reaction.

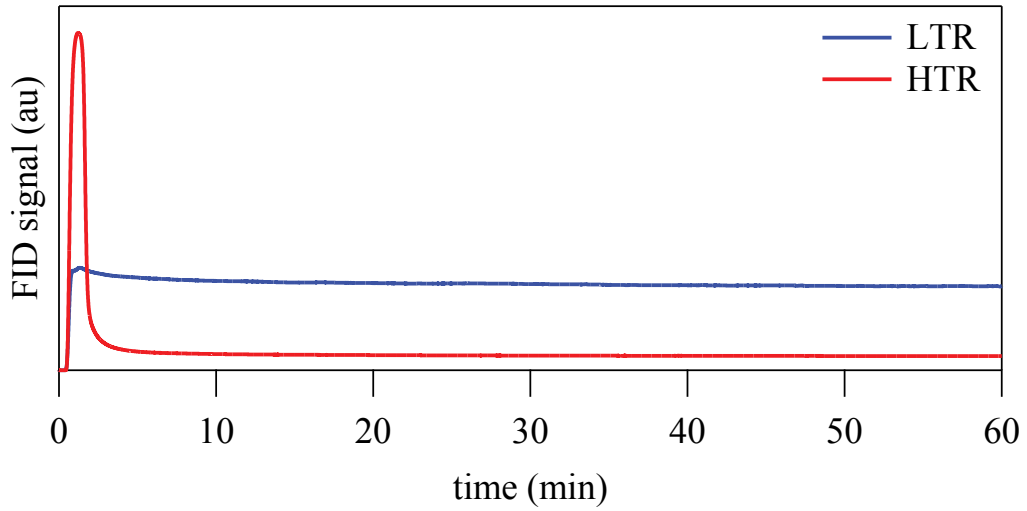

Figure 3.15 Transient test results at 223°C over RhCZ100 after LTR and HTR

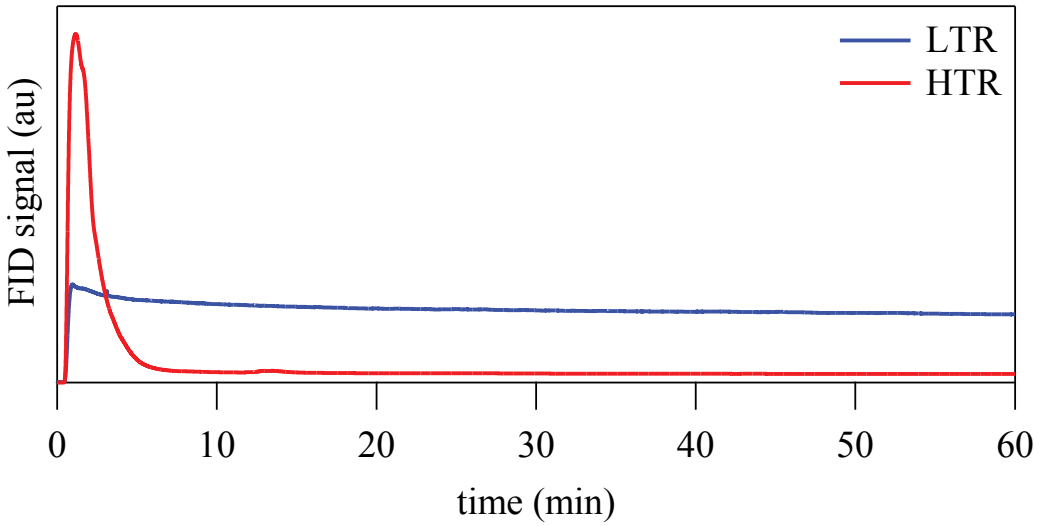

Figure 3.16 Transient test results at 223°C over RhCe-C after LTR and HTR

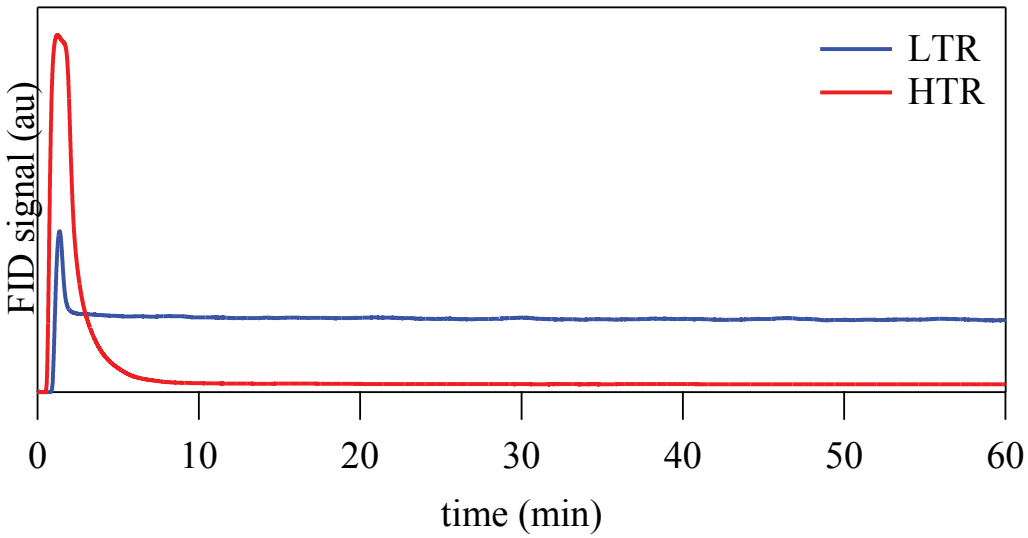

Figure 3.17 Transient test results at 223°C over RhCe-R after LTR and HTR

It is also worth noting that the methane production during steady state at 223°C is much higher after LTR than after HTR, irrespective of the support: once the active sites are used during the high transient peak, the activity of the catalyst is suppressed. This happens on all ceria-based samples: the active sites formed during HTR are consumed faster and more completely with respect to those formed after LTR.

Comparing the transient activity after HTR at 150°C and 223°C in the first minutes of reaction (Figures 3.18 and 3.19, respectively), these aspects are clearer and other considerations can be made. At 150°C the transient high activity peak is sharper, while at 223°C the peak width is much larger suggesting that increasing the temperature one could try to stabilize the high activity. Moreover, the absolute intensity of the peak on RhCZ100 is higher than on RhCe-C and RhCe-R, but its width is much smaller at both temperatures. This observation is a further confirmation that the more active the CO_2 methanation sites, the faster they deactivate.

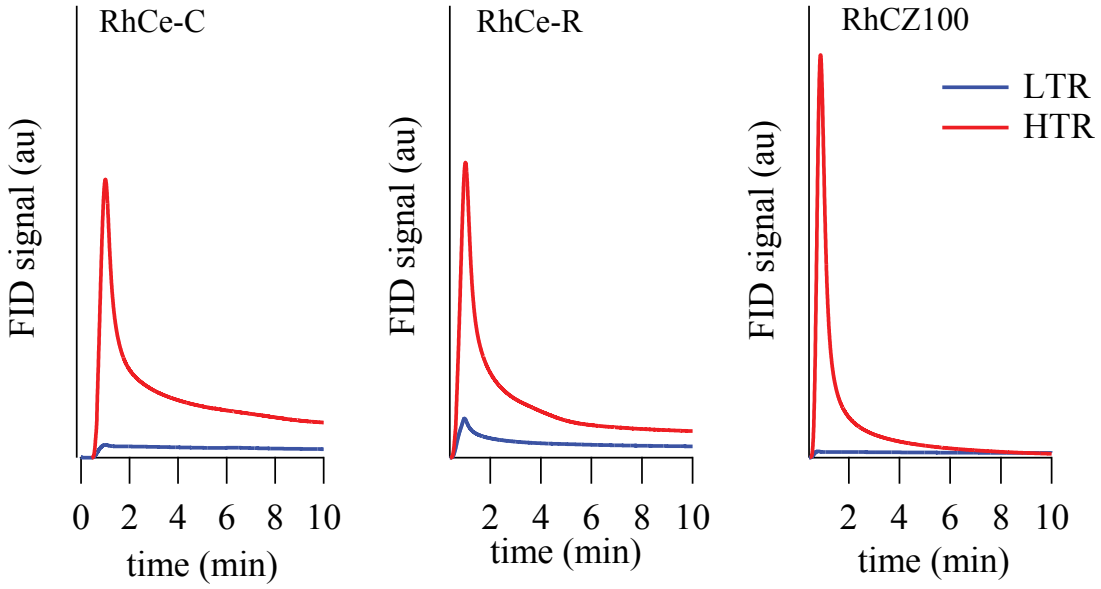

Figure 3.18 Transient test results at T=150°C (first 10 minutes of experiment)

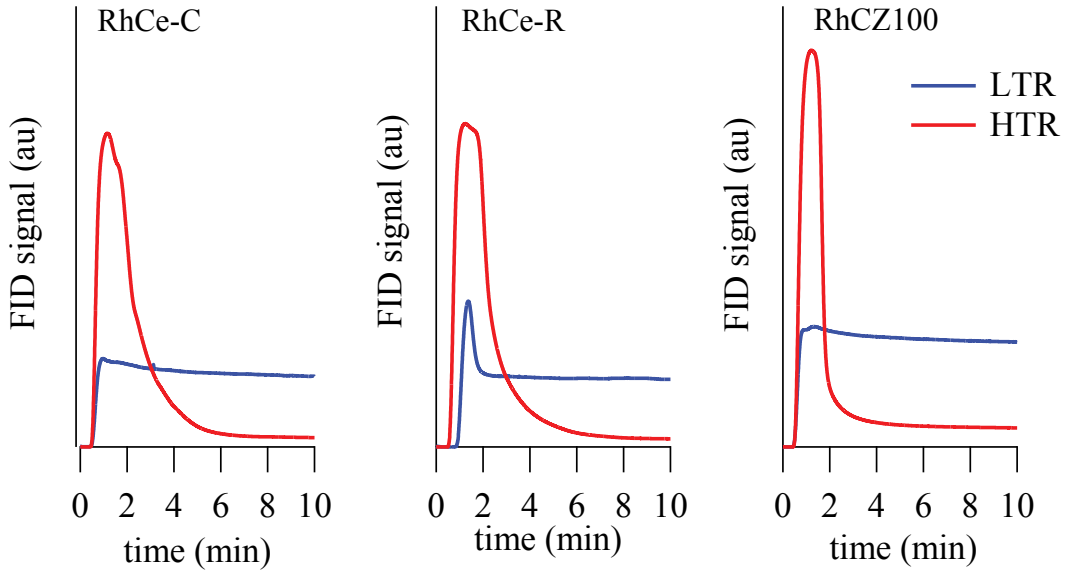

Figure 3.19 Transient test results at T=223°C (first 10 minutes of experiment)

The combined analysis of the results obtained during transient tests on RhCZ100, RhCe-C and RhCe-R at 150°C and 223°C indicate that the catalytic activity follows different pathways to reach the steady state, depending upon three factors: (i) the temperature of reaction, (ii) the temperature of the pretreatment (LTR or HTR), and (iii) the nature of the support. The third aspect is the one that rules the game in terms of active sites: these are formed preferentially at high temperature (i.e. after HTR) and are related to the redox properties of the material, being present in higher amount on ceria cubes and rods, irrespective of the reaction temperature, as shown in Figures 3.13 and 3.14.

The comparison between the mmoles of methane produced and the mmoles of reduced ceria on the different ceria-based catalysts (Figures 3.20 and 3.21) gives a clear indication of the weight of the oxygen vacancies on the catalytic activity for each sample. The mmoles of reduced ceria have been calculated at 223°C (LTR) and at 500°C (HTR), according to Table 3.3.

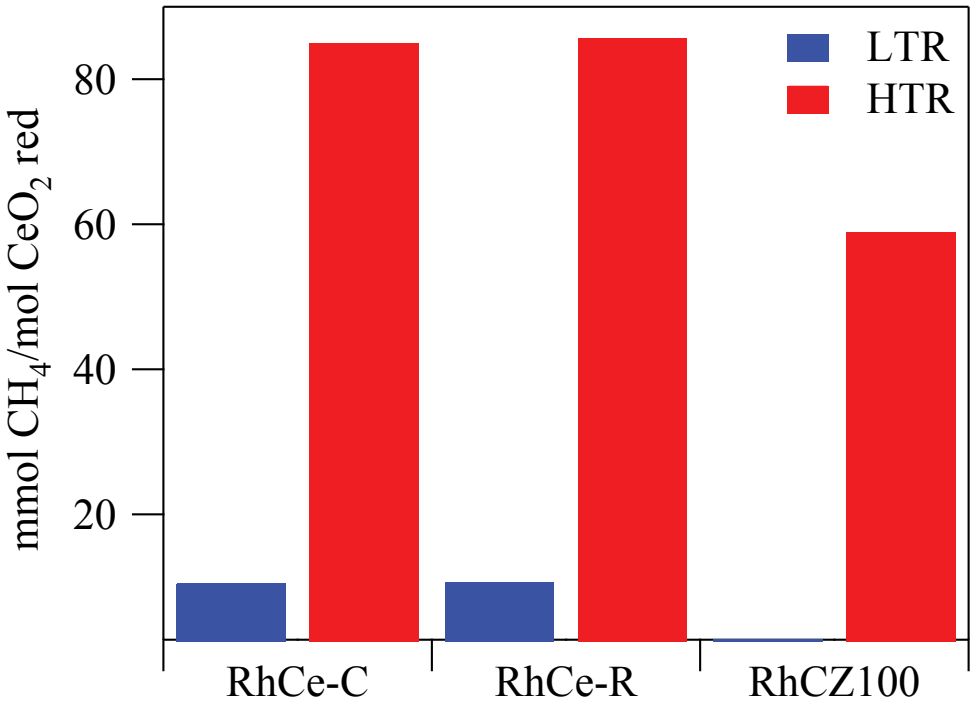

Figure 3.20 Methane produced in transient conditions at 150°C with respect to reduced ceria

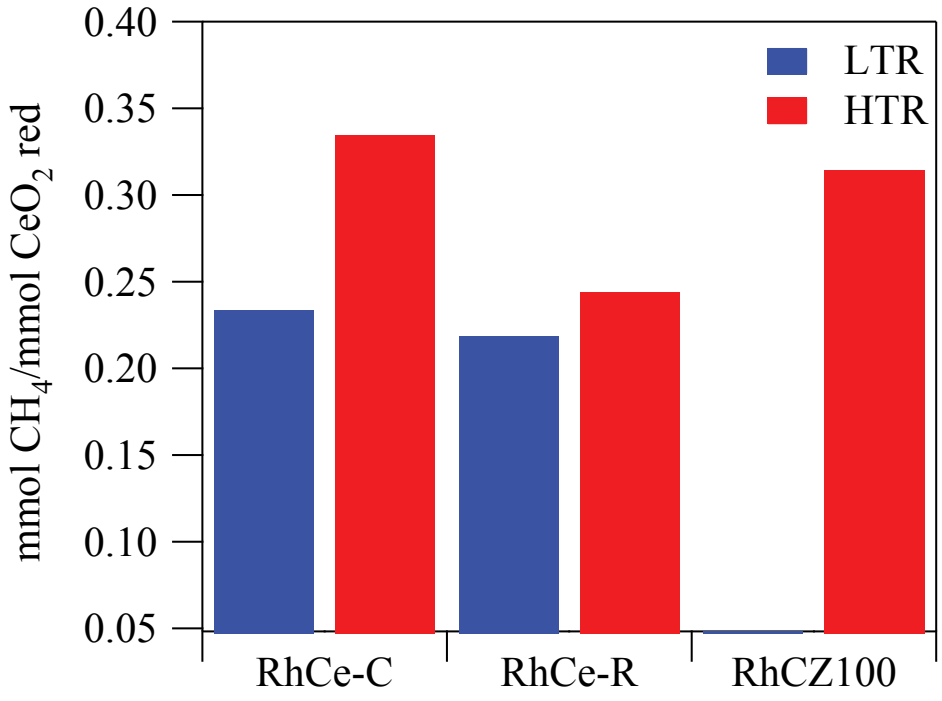

Figure 3.21 Methane produced in transient conditions at 223°C with respect to reduced ceria

At low temperature (150°C) the most reducible supports exhibit also the more active vacancies, with a higher amount of methane produced per mmole of reduced ceria, this being true both after LTR and after HTR. At 223°C the situation is the same after LTR, i.e. the vacancies formed on

ceria nanocubes and nanorods during low temperature reduction are much more active than those formed over polycrystalline ceria. After HTR instead, it can be observed that the trend of methane production per mmole of reduced CeO_2 follows the order RhCe-C > RhCZ100 > RhCe-R. This might be due to a change in the redox properties of nanorods, which have been shown to modify their behavior towards oxygen adsorption after a reduction treatment at 500°C, differently from what happens on nanocubes and nano-octahedra [162]. Probably at 150°C the temperature (and the activity) is too low to evidence this effect. Despite the apparent discrepancy, this is in fact a further confirmation of the relationship between sample redox properties and catalytic activity for CO_2 methanation.

Chapter 4. Ceria-Zirconia supported catalysts

4.1 Overview

The transient effect observed on ceria-based catalysts during CO_2 methanation after high temperature reduction (HTR), and more pronounced on nanoshaped ceria with enhanced reducibility, raised many questions. First of all, since the effect is likely related to the formation of oxygen vacancies on ceria, one can ask whether there is a way to enhance it by increasing ceria reducibility. Also, can the vacancies be stabilized, and thus the effect prolonged, by the addition of suitable dopants? Obviously the goal under these issues was not only to try to increase the CO_2 methanation activity of Rh-based catalysts, but also to shed some light on the mechanism taking place during the reaction. Trying to answer to these questions, this part of the work has been focused on ceria-zirconia supported samples.

The mixed ceria-zirconia catalysts have been employed in TWCs, due to their better thermal stability, as well as their enhanced oxygen storage capacity [163-165]. According to the results of several studies, the lower atomic radius of zirconium alters the positions of the atoms into ceria lattice, resulting in an improved oxygen mobility and enhanced reduction properties in ceria-zirconia mixed oxides [166]. For these reasons ceria-zirconia supports with different Ce-Zr ratio have been prepared, according to the procedure reported in Chapter 2, and tested for CO_2 hydrogenation.

4.2 Characterization

Looking at the data in Table 4.1, the pure oxide catalysts (RhCZ100 and RhCZ0) have similar surface areas which are the lowest of the series. The mixed-oxide catalysts show higher surface areas, especially at high ceria content.

Table 4.1 BET and porosimetry analysis of Ce-Zr and 1%Rh/Ce-Zr samples

Catalyst	BET S.A. (m^2/g)	Pore volume (cm^3/g)	Pore size (Å)	Crystal size (nm)
RhCZ0	29.0	0.19	152	59
CZ0	47.1	0.29	182	21
RhCZ10	33.0	0.13	95	25
CZ10	63.2	0.16	80	17
RhCZ50	55.9	0.28	160	13
CZ50	84.8	0.22	97	32
RhCZ75	54.8	0.23	135	21
CZ75	63.5	0.30	160	37
RhCZ100	25.5	0.10	114	21
CZ100	51.7	0.18	116	19

The XRD spectra show the effect of zirconium presence into ceria lattice, and can be used to assess the formation of Ce-Zr solid solution since no segregation of zirconia could be detected. Regarding the pure oxides, the x-ray diffraction pattern of RhCZ100 presents the typical features of cubic ceria, while for RhCZ0 a mixed structure of monoclinic and tetragonal zirconia is identified. The structure of ceria-zirconia based samples gradually change at increasing zirconium content, from cubic (RhCZ75) to tetragonal structure (RhCZ50 and RhCZ10).

From XRD patterns it has been possible to calculate the crystal size by using the Scherrer equation (1) (See table 4.1):

$$\tau = \frac{K\lambda}{\beta \cos\theta} \qquad (Eq. 4.1)$$

where:

τ: mean crystal size

K: Shape Factor (0.9).

β: Line boadening at half the maximum intensity

θ: Bragg angle

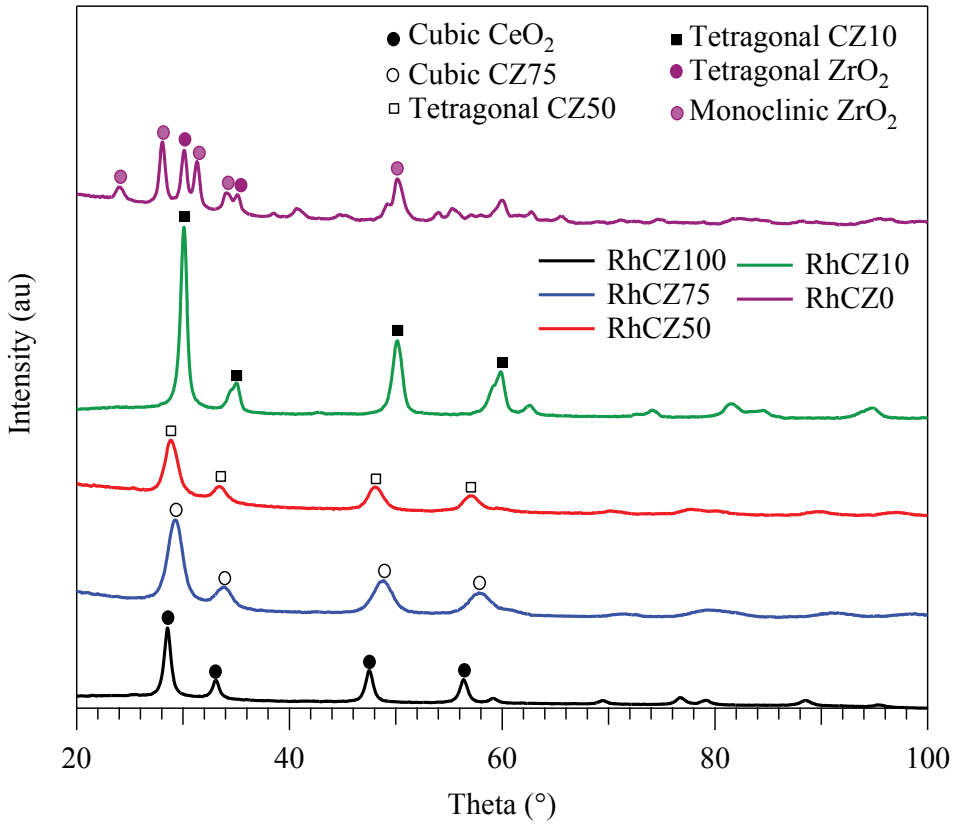

Figure 4.1 XRD analysis of 1%Rh/CeO_2-ZrO_2 catalysts

Figure 4.2 shows the TPR profiles of ceria-zirconia supports. As expected, after the incorporation of Zr into ceria lattice a modification of the hydrogen consumption profile is observed. The high temperature peak almost disappears, while the presence of a medium temperature peak (between 400 and 750°C) is detected on CZ50 and CZ75. This is in agreement with the literature on the reduction of ceria-zirconia mixed oxides [167].

The results of TPR experiments on Rh containing catalysts are shown in Figure 4.3. The first thing to be observed is that in presence of rhodium almost all the hydrogen consumption takes place at

low temperature. This is due to the hydrogen spillover effect: the reduction of Rh_2O_3 to Rh^0 promotes the spillover of H_2 onto the ceria support causing its simultaneous reduction [156, 168], as it can be inferred also looking at the quantitative data reported in Table 4.2. The general trend of hydrogen consumption reflects the expected enhanced reducibility of Ce-Zr mixed oxides with respect to pure ceria.

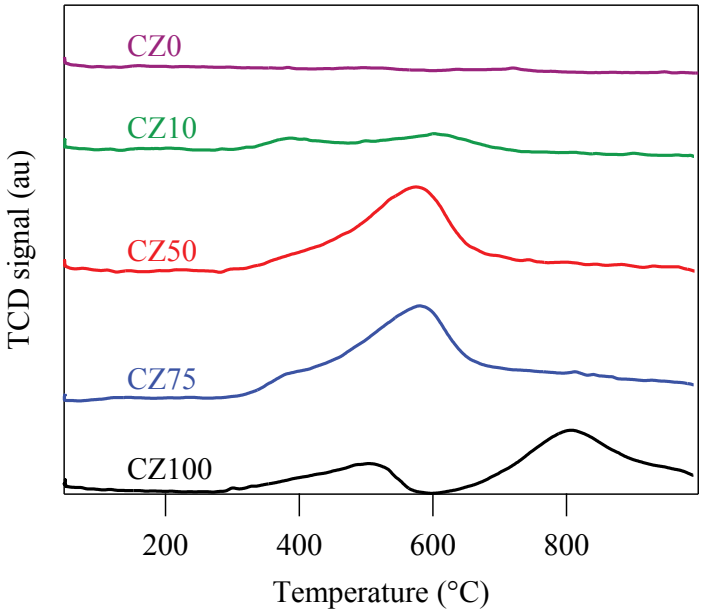

Figure 4.2 TPR results of CeO_2-ZrO_2 supports

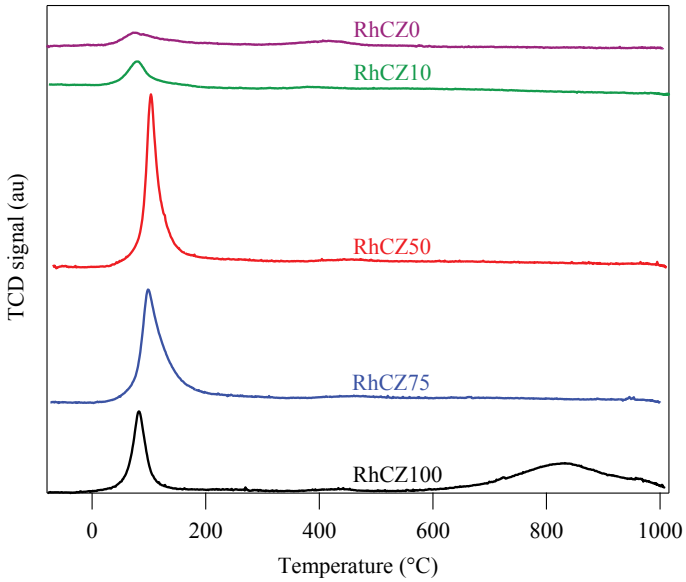

Figure 4.3 TPR profiles of 1%Rh/CeO_2-ZrO_2 catalysts

Table 4.2 TPR results of 1%Rh/CeO_2-ZrO_2 catalysts

Sample	H_2 consumption (mmol/g_{cat})	% of CeO_2 reduction[a]
CZ0	/	/
CZ10	0.36	91
CZ50	1.16	68
CZ75	1.25	53
CZ100	0.91	30
RhCZ0	0.10	/
RhCZ10	0.35	53
RhCZ50	1.56	84
RhCZ75	1.57	61
RhCZ100	1.02	31

[a] calculated assuming 100% of Rh_2O_3 reduction

4.3 Catalytic activity

4.3.1 Pulse experiments

Pulse experiments were performed in order to verify the occurrence of the transient effect observed on ceria-supported samples. As an example, Figure 4.4 shows a typical pulse test carried out on RhCZ75 at T=223°C. It can be observed that all pulses have a similar area after low temperature reduction, whereas after HTR the first three pulses are different and decrease in amplitude, stabilizing to a similar value with respect to pulses recorded after LTR (see figure 4.5). The overall conversion after LTR was about 37%, being stable during all the test, while the general conversion after HTR was about 27% (from the third peak onwards). Overall, the behavior is very similar to what detected for rhodium supported on pure ceria, with the first pulse after HTR showing clearly the transient high methanation activity. Nevertheless, some differences can be highlighted after a careful analysis of the shape of the pulses (Figure 4.5).

Unlike ceria-based samples, where high and narrow peaks were observed, ceria-zirconia catalysts show broader peaks with a small shoulder at the peak's top (except for the HTR's first two), no matter what pretreatment (i.e. HTR or LTR). It is also remarkable that on these samples the peak

width is almost identical after LTR or HTR, with a similar peak tail: this was not the case of Rh/CeO_2, on which peaks after HTR where narrower and took place in a shorter time span compared to those after LTR. Moreover, the difference between pulses after LTR and HTR is smaller if compared to that on pure ceria (see Figures 3.8 and 3.9, Chapter 3). The direct comparison of pulses after LTR and HTR on RhCZ100 and RhCZ75, reported in Figure 4.6, provides further insights on the behavior of ceria-zirconia samples.

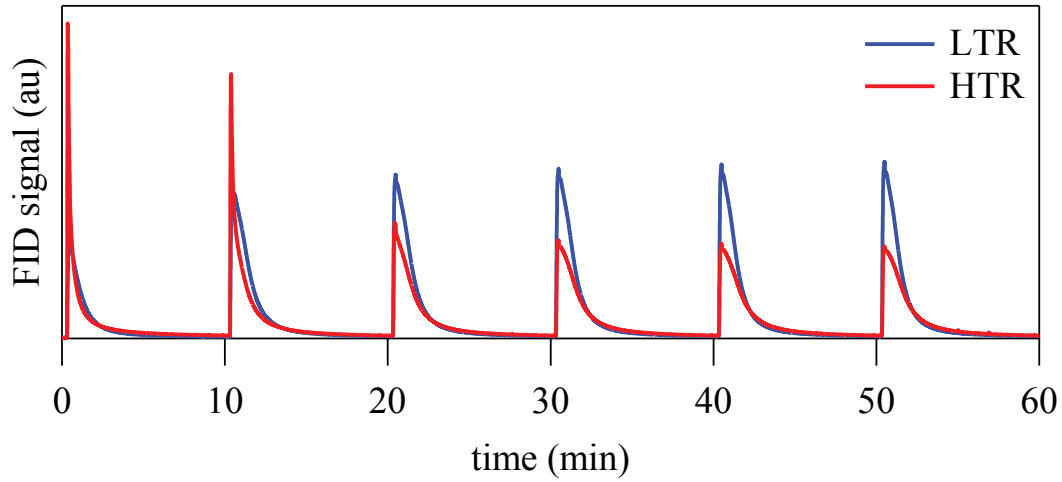

Figure 4.4 Typical results of pulse tests, obtained on RhCZ75 at T=223°C

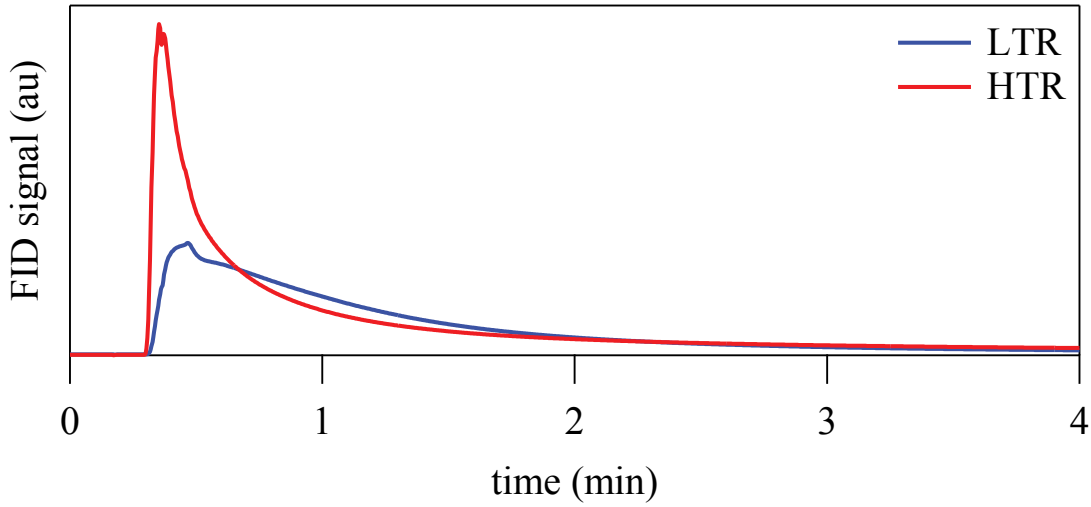

Figure 4.5 First-peak result, obtained on RhCZ75 at T=223°C

It can be observed that on RhCZ100 the peaks are sharper, and higher, both after LTR and during the first two pulses after HTR, whereas on RhCZ75 the peaks show a more pronounced tail and take

a longer time to reach the baseline. It appears that on RhCZ100 the transient component of the catalytic behavior is strongly emphasized with respect to RhCZ75, especially after HTR.

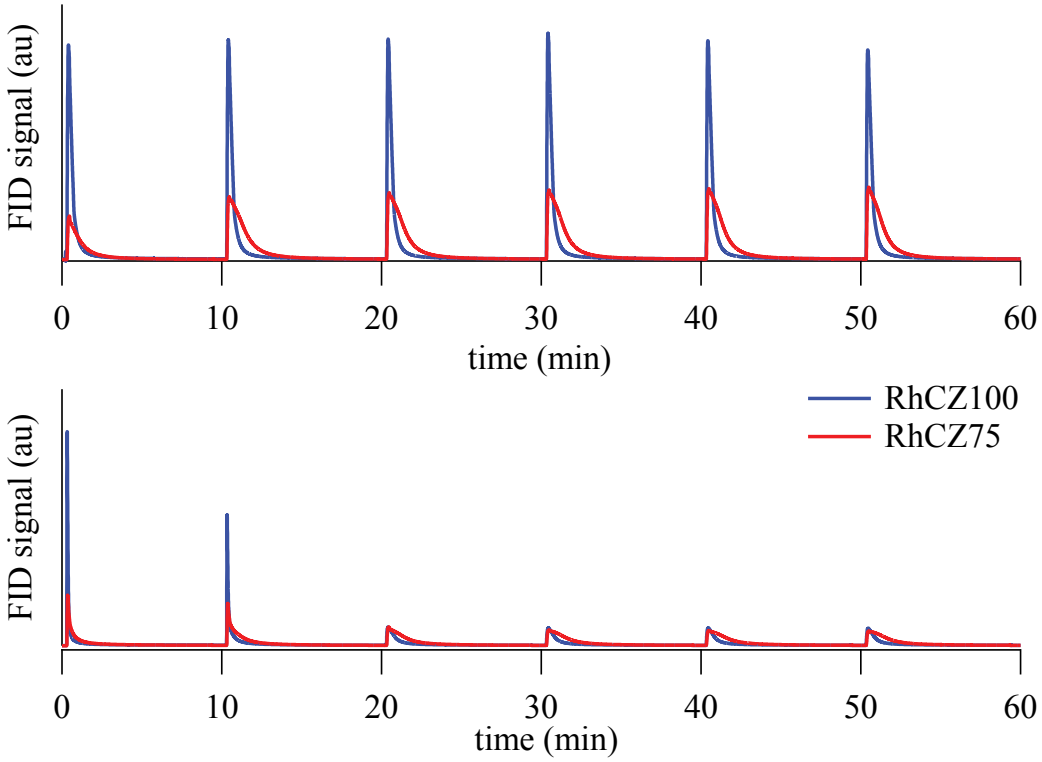

Figure 4.6 Pulse tests after LTR (top) and after HTR (bottom) on RhCZ75 and RhCZ100

These results indicate likely that on these samples the introduction of zirconia improves the steady state activity at the expenses of the transient high activity peak, as it will be clearer by looking at the transient experiments described in the following.

For a reference sample (RhCZ75) also a reduction at 400°C has been performed, in order to assess which is the minimum temperature for the high activity peak to occur. Figure 4.7 shows the result of pulse test carried out after the reduction at 400°C, compared to those obtained after HTR and LTR treatments. In this case only a small hint of the transient high activity can be observed during the first pulse, whereas from the second one onwards all peaks are similar and slightly higher than after HTR (at 500°C). It can be inferred that a minimum temperature comprised between 400°C and 500°C is required to activate the sites responsible of the high transient activity.

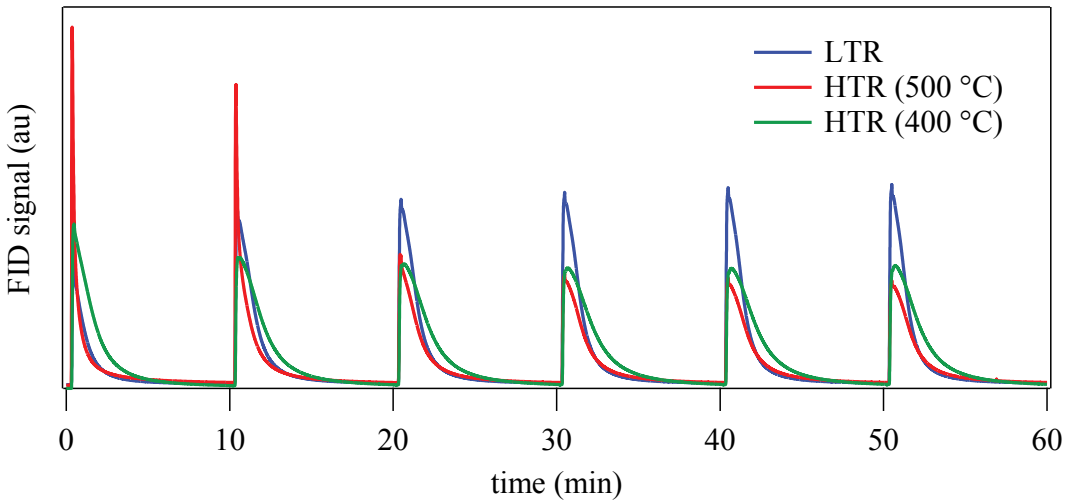

Figure 4.7 Comparison pulse tests at different HTR conditions (RhCZ75)

4.3.2 Transient test

Transient tests carried out on ceria-zirconia samples at 150°C and 223°C are shown in Figure 4.8 and 4.9, respectively. The first thing to be observed is that the steady state methanation activity is much higher on zirconia-rich samples, decreasing linearly at increasing Ce content (RhCZ0 > RhCZ10 > RhCZ50 > RhCZ75 > RhCZ100). This is true for the experiments carried out after both LTR and HTR treatments, and it is more evident at T_r=223°C. Another important feature is the presence of an apparent transient peak also on RhCZ0 at 150°C. This seems in contrast with the hypothesis of a direct link between the transient activity peak and the oxygen vacancies on ceria, but the results obtained on ceria-zirconia instead point to that direction. For ceria-zirconia based catalysts in fact, the presence of the transient high activity peak after LTR at 150°C can be interpreted as for ceria rods: the higher reducibility of these samples compared to RhCZ100 induces the formation of the transient peak already under mild conditions. For zirconia, it has to be underlined that (i) the steady state activity is always higher than on the other samples and the contribution of the transient peak is very low, (ii) on RhCZ100, RhCZ75 and RhCZ50, as well as on RhCe-C and RhCe-R, the transient high activity peak increases with temperature, while for RhCZ0

and RhCZ10 the trend is opposite, and (iii) it is recognized that the mechanisms of CO_2 hydrogenation on reducible and non-reducible supports follow different pathways [138, 169, 170].

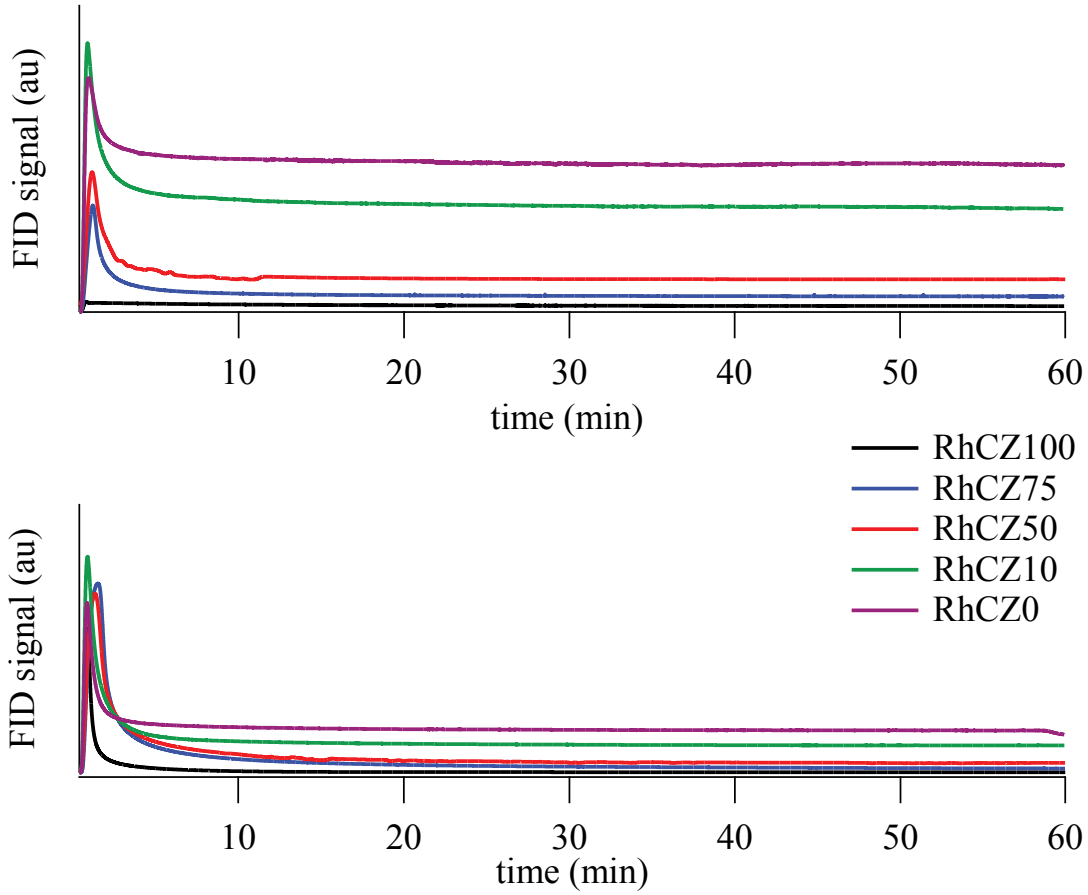

Figure 4.8 Transient tests carried out at 150°C after LTR (top) and after HTR (bottom) on ceria-zirconia samples

Focusing on the two different tests at T_r=223°C (after LTR and after HTR), it is worth noting that, similarly to what detected on nanoshaped ceria, again the samples with higher reducibility (i.e. ceria-zirconia ones) take a longer time to reach the baseline after HTR and show a pronounced transient high activity peak also after LTR, as it happened for rhodium supported on ceria nanorods (Chapter 3).

Comparing the methanation activities at 223°C on the same sample, it can be observed that on RhCZ0 the steady state methane production after HTR is higher than after LTR (Figure 4.10), whereas on RhCZ10 (Figure 4.11) the steady state activities are almost the same. On the other side, for RhCZ50 and RhCZ75 the steady state activities reflect the reduction treatment before the

experiment as it happened for Rh supported over pure ceria, with higher methane production after LTR than after HTR (see Figures 4.12 and 4.13, respectively).

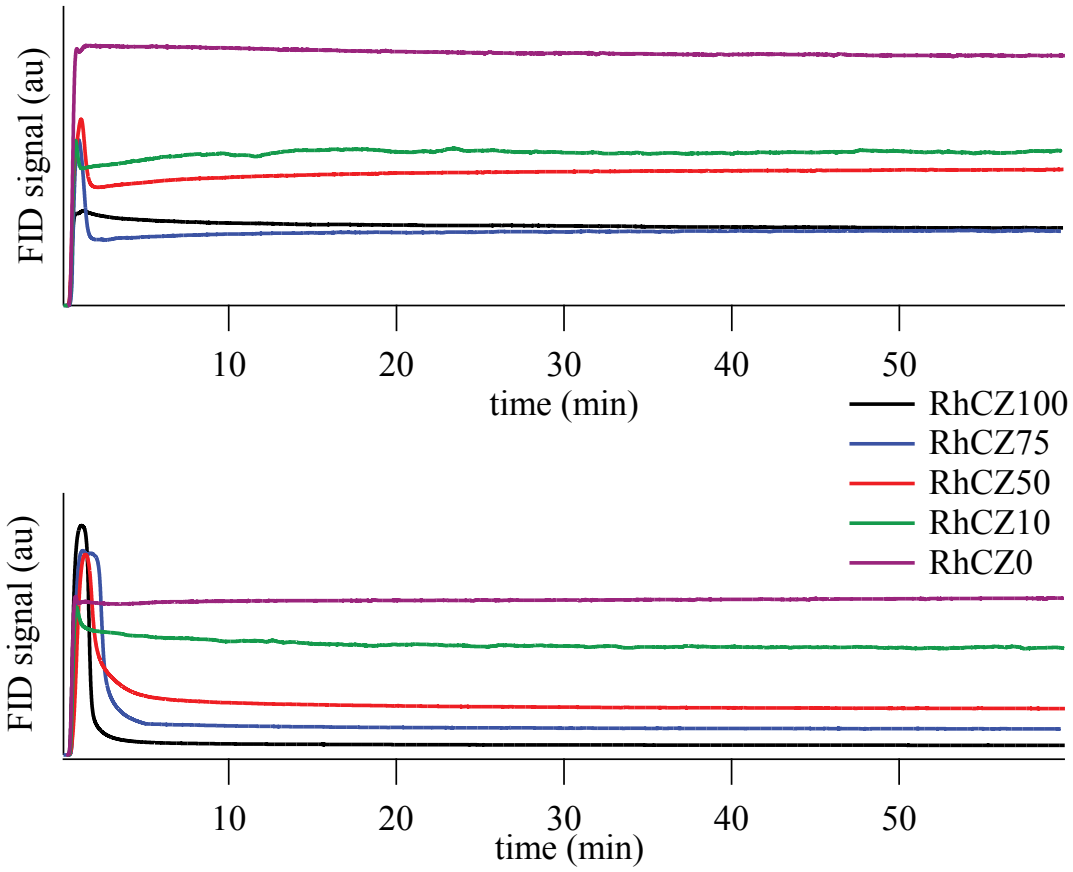

Figure 4.9 Transient tests carried out at 223°C after LTR (top) and after HTR (bottom) on ceria-zirconia samples

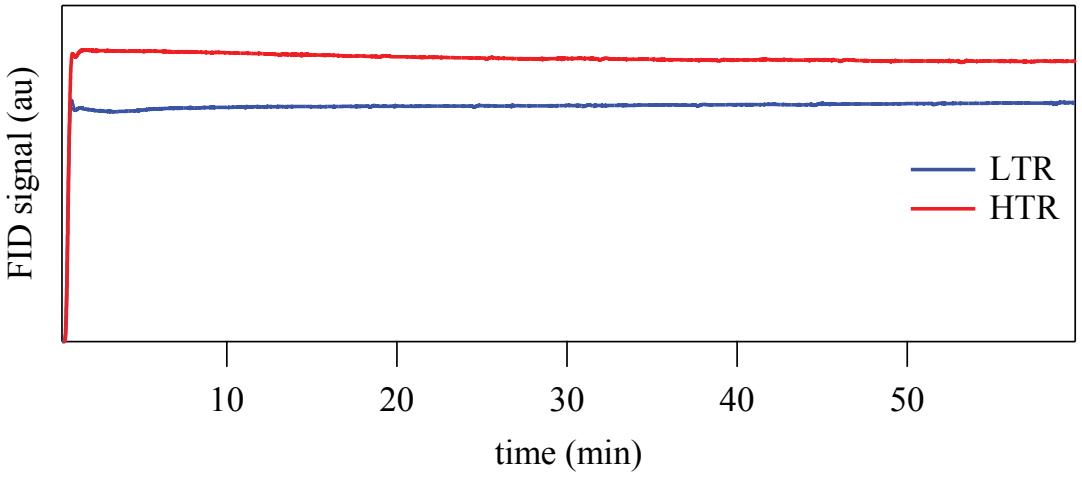

Figure 4.10 Methane production at 223°C during transient test over RhCZ0 after LTR and HTR

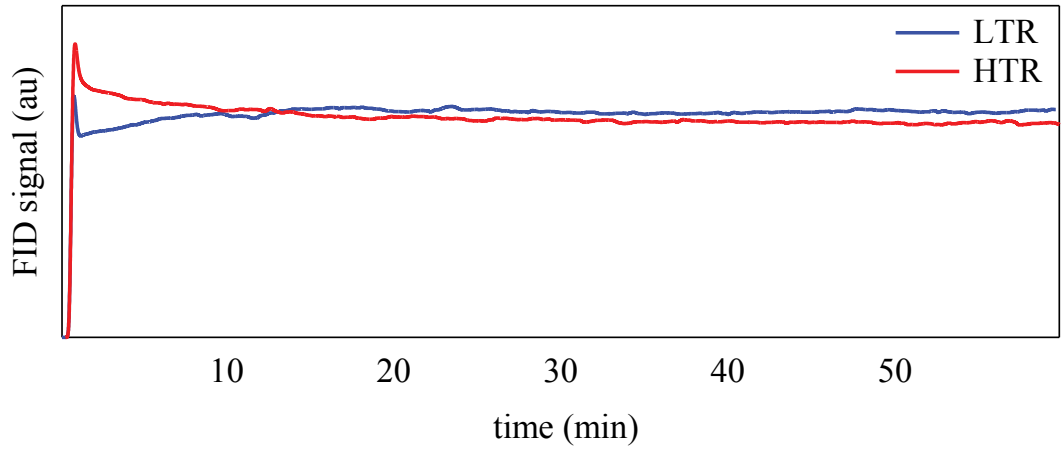

Figure 4.11 Methane production at 223°C during transient test over RhCZ10 after LTR and HTR

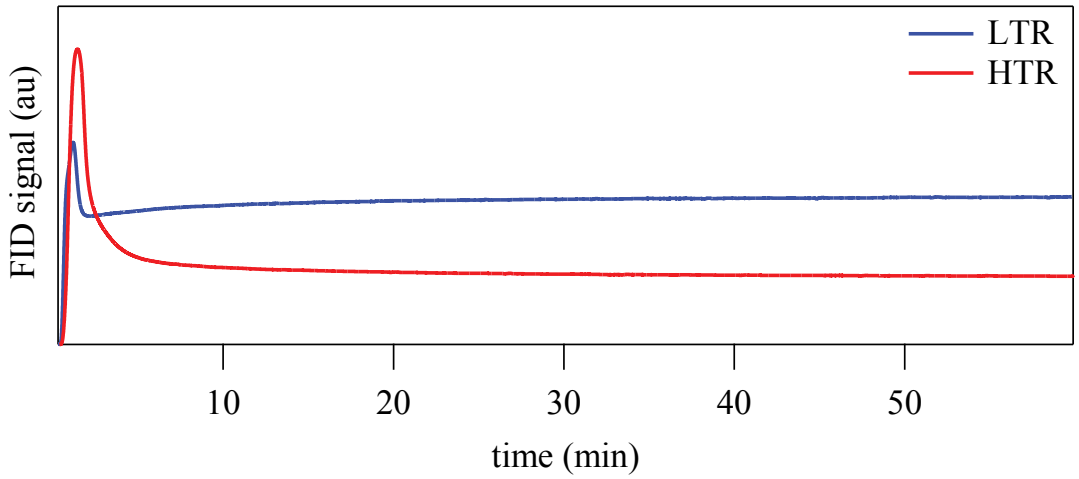

Figure 4.12 Methane production at 223°C during transient test over RhCZ50 after LTR and HTR

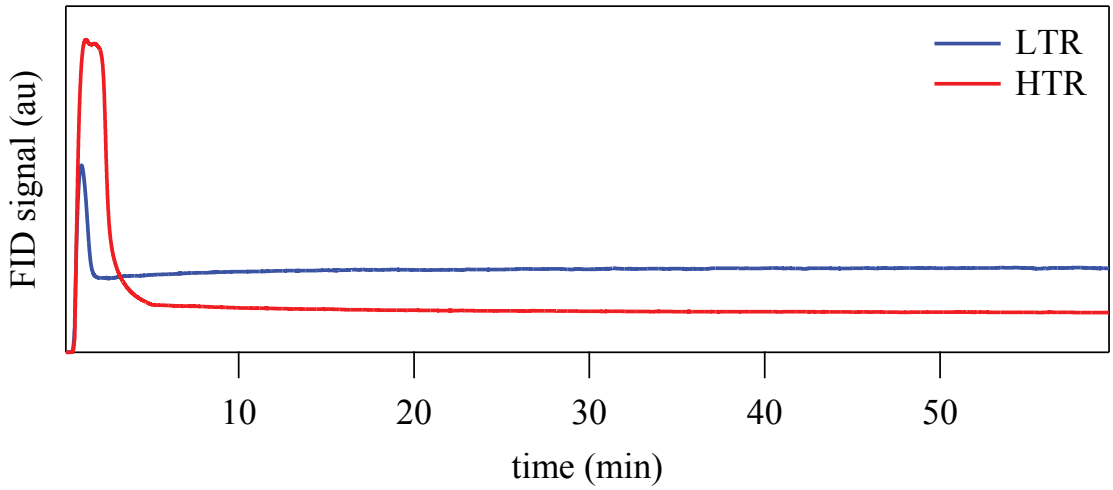

Figure 4.13 Methane production at 223°C during transient test over RhCZ75 after LTR and HTR

These findings indicate that for samples on which methane production takes place with the transient high activity peak (i.e. high ceria content or pure ceria) the steady state conversion after HTR is attenuated with respect to that obtained after LTR. The reason for this behavior is likely in the nature of the active sites: the ones formed during high temperature reduction react faster and, being more reactive, are also consumed (or reoxidized) faster than those formed after LTR. As observed for rhodium supported over pure ceria, this happens only when the methanation is carried out at 223°C, meaning that at 150°C the temperature is too low to appreciate the effect of the pretreatment (see Figures 4.14-4.16).

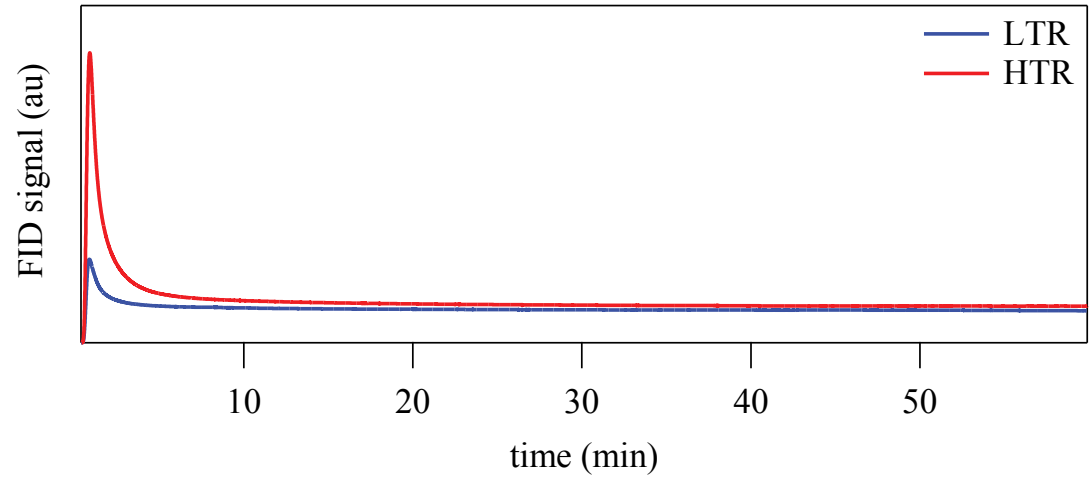

Figure 4.14 Methane production at 150°C during transient test over RhCZ10 after LTR and HTR

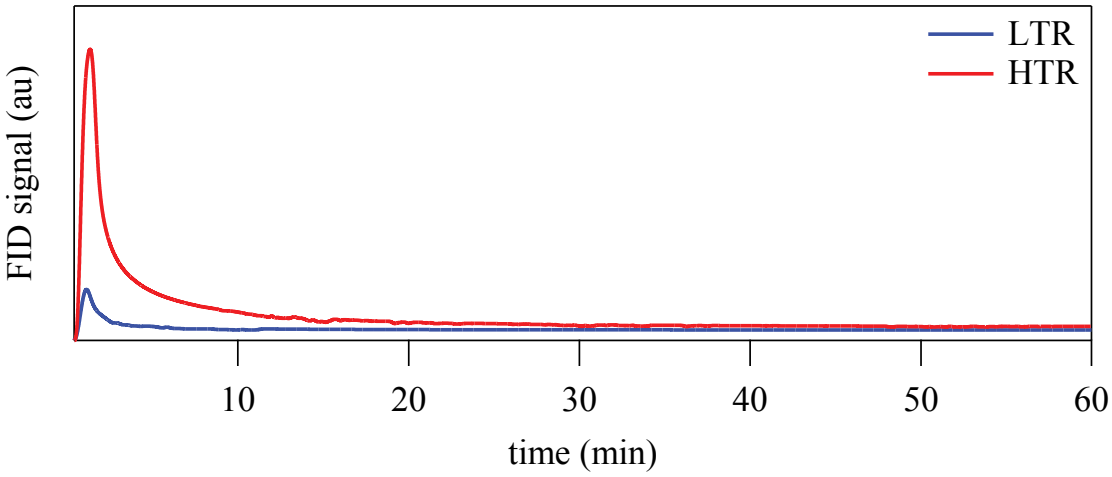

Figure 4.15 Methane production at 150°C during transient test over RhCZ50 after LTR and HTR

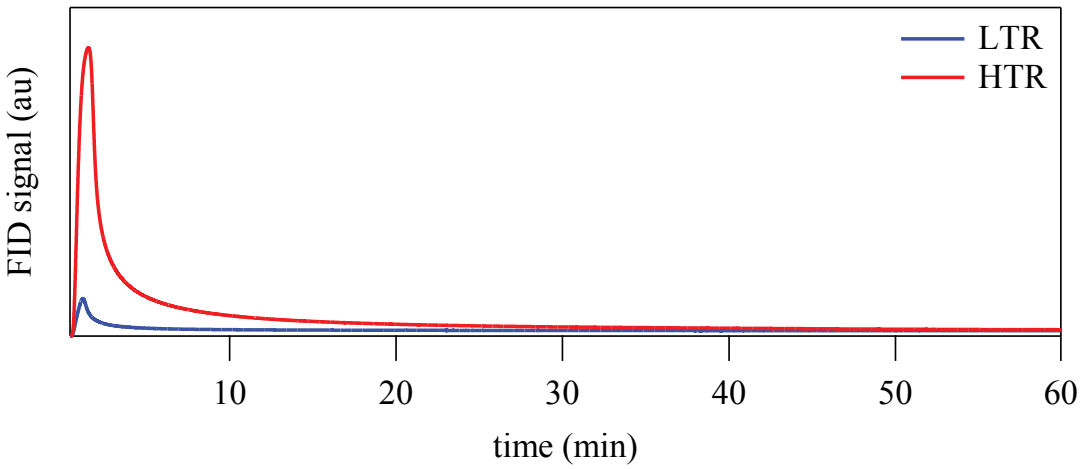

Figure 4.16 Methane production at 150°C during transient test over RhCZ75 after LTR and HTR

Quantitative analysis referred to the methane produced at 150°C and 223°C during the transient high activity peak, before reaching the steady state, is reported in Figure 4.17 and 4.18, respectively. The activity after LTR is always negligible compared to that after HTR and the activity at 150°C is much lower than at 223°C, similarly to what observed for pure ceria (the data for RhCZ100 is included in the graph for comparison).

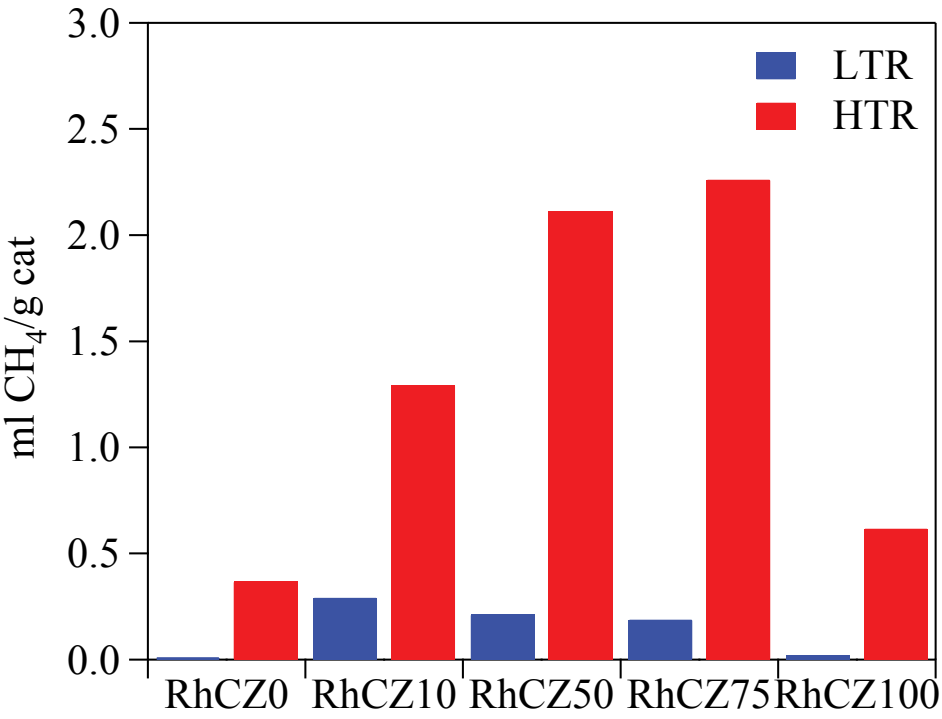

Figure 4.17 Methane produced in transient conditions (high activity peak) at 150°C

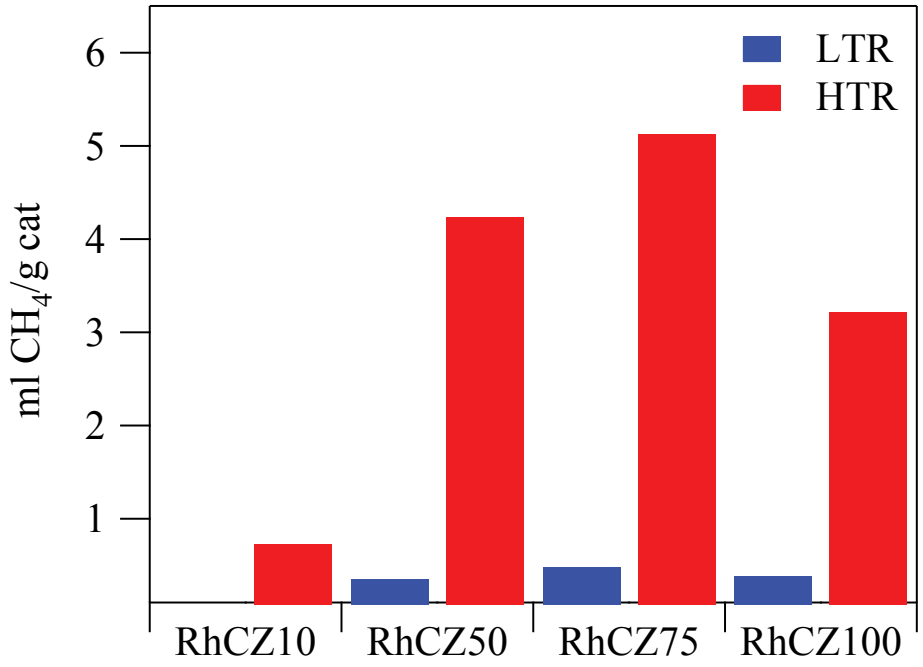

Figure 4.18 Methane produced in transient conditions (high activity peak) at 223°C

As it can be observed, RhCZ10 produces more methane in transient conditions at 150°C than at 223°C. This is likely due to the very low cerium content: on this sample the activity is only partly explained by a redox mechanism involving oxygen vacancies on ceria, the major contribution being given by rhodium on zirconia which presents a pseudo-transient effect only at low temperature (150°C, RhCZ0). As stated before, this transient effect though should not be confused with the one taking place on ceria-containing samples. The aspect will be better discussed in Chapter 5. Here it is important to highlight that the samples with higher reducibility and high cerium content, namely RhCZ50 and RhCZ75, produce the highest amount of methane during the transient high activity peak compared to the other catalysts, in line with the results obtained for nanoshaped ceria and thus confirming the correlation between sample reducibility and catalytic activity.

To further investigate this point, experiments have been carried out in the TPR apparatus in which we reproduced the low or high temperature reduction pretreatments. In these experiments the catalysts were exposed to the reducing mixture (5% H_2 in N_2) at 223°C (LTR) or at 500°C (HTR) for 2 hours, monitoring hydrogen consumption. Quantitative results are reported in Table 4.4.

Table 4.3 Results of modified TPR experiments

Sample	LTR		HTR	
	ml H_2 consumed	mmol CeO_2 red[a]	ml H_2 consumed	mmol CeO_2 red[a]
RhCZ10	0.35	0.0142	0.61	0.0359
RhCZ50	0.67	0.0435	1.64	0.1221
RhCZ75	0.90	0.0597	4.56	0.1145
RhCZ100	0.45	0.0213	0.69	0.0417

[a] It is calculated assuming the total reduction of Rh_2O_3 to Rh^0

As expected, there is a trend in hydrogen consumption that depends upon the addition of zirconia, in line with what reported in the literature [167]. This is clearer looking at Figure 4.19 where the relative amount of ceria reduction is reported.

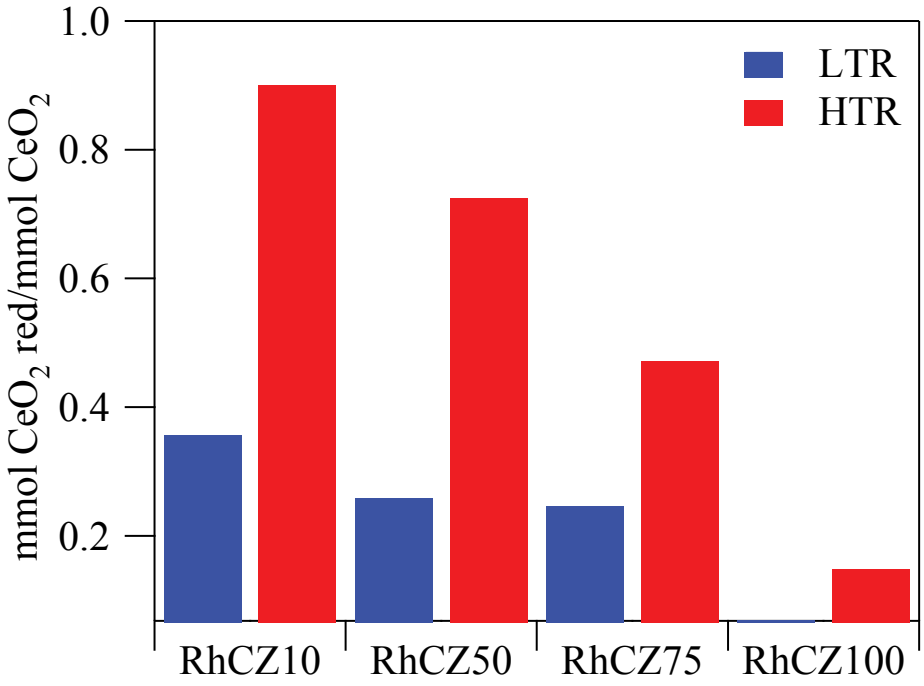

Figure 4.19 Reduced ceria with respect to the total cerium content of samples

In the past, Teschner et al. reported a higher hydrogen consumption and spillover effect for 2%Rh/CeO_2 reduced at low temperature (300°C) with respect to the same sample treated at 500°C [156]. For this reason, and to exclude a drift of the TCD signal during the isotherm, the LTR and HTR treatments have been repeated also in a TGA apparatus monitoring the weight loss of the samples. It has to be recalled that in these experiments the weight loss is due to the reduction of the

sample, that looses a H_2O molecule for every mole of H_2 consumed. From the results reported in Figures 4.20 and 4.21, it appears that the main H_2 consumption takes place during the temperature ramp (corresponding to the peak of TPR profile). The weight loss is proportional to the reducibility of the catalyst in agreement with TPR results, with the higher decrease in weight observed for RhCZ50 and RhCZ75.

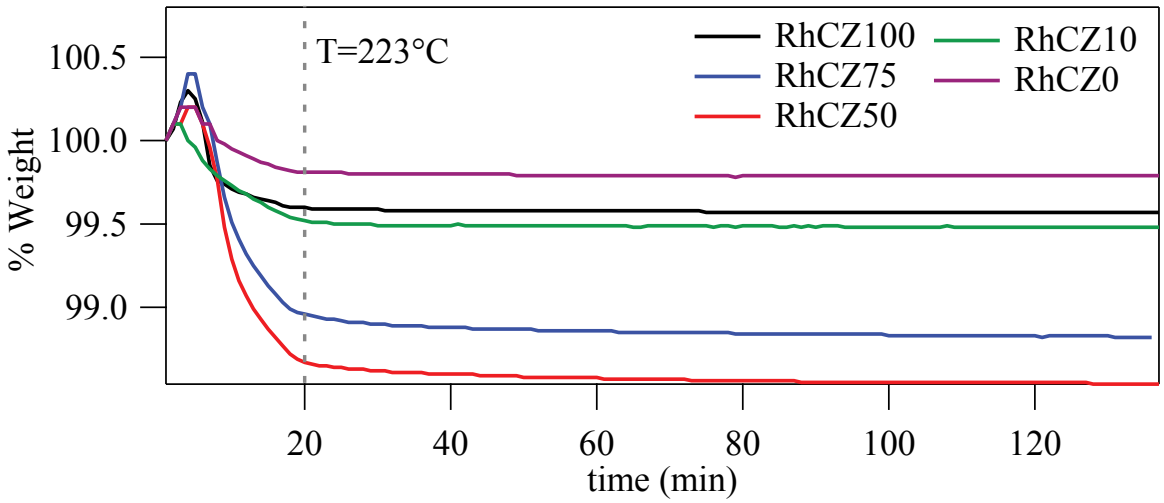

Figure 4.20 Weight loss of Rh/CeO_2-ZrO_2 samples during LTR (223°C) in TGA apparatus

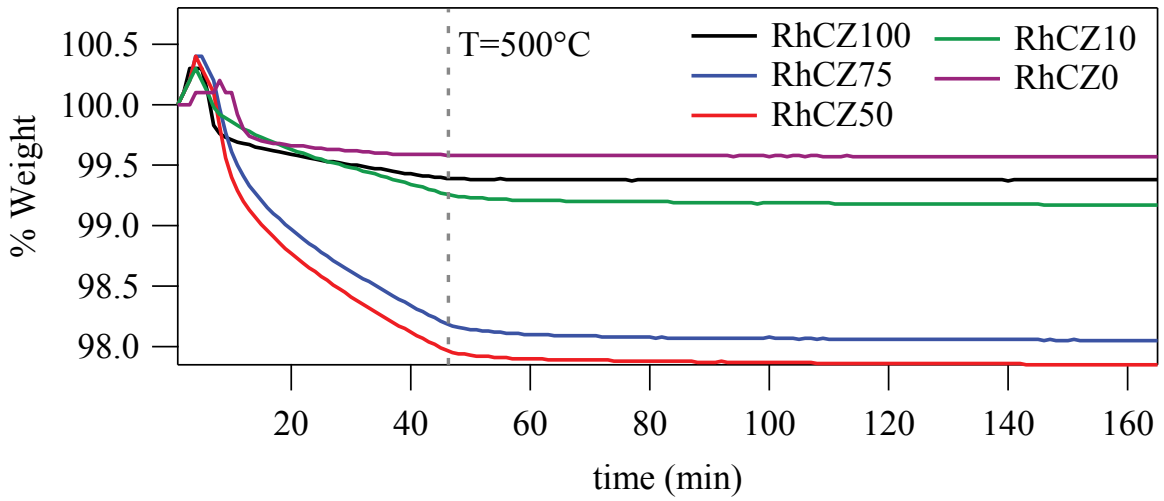

Figure 4.21 Weight loss of Rh/CeO_2-ZrO_2 samples during HTR (500°C) in TGA apparatus

It should be observed also that the weight loss after LTR and after HTR for RhCZ100 is very similar, while for the zirconia containing samples the difference is much more pronounced confirming the data of Table 4.3 and indicating that the high temperature reduction treatment induces a more significant change on these catalysts with respect to pure ceria. The difference with

the results obtained by Teschner et al. might be explained keeping in mind that their samples were calcined at a lower temperature (300°C) and they were prepared using an aqueous solution of rhodium chloride, which is known to have strong effects on catalyst redox properties [171].

A comparison of the methane produced during the transient high activity peak with the amount of reduced ceria obtained from TPR experiments gives interesting insights. At 150°C no significant trend could be observed, but we have already noted that this temperature is too low to emphasize the transient behavior. At 223°C instead, it is noteworthy that the ratio between the mmoles of methane produced and the mmoles of ceria reduced increases linearly with increasing ceria content in the samples (see Figure 4.22).

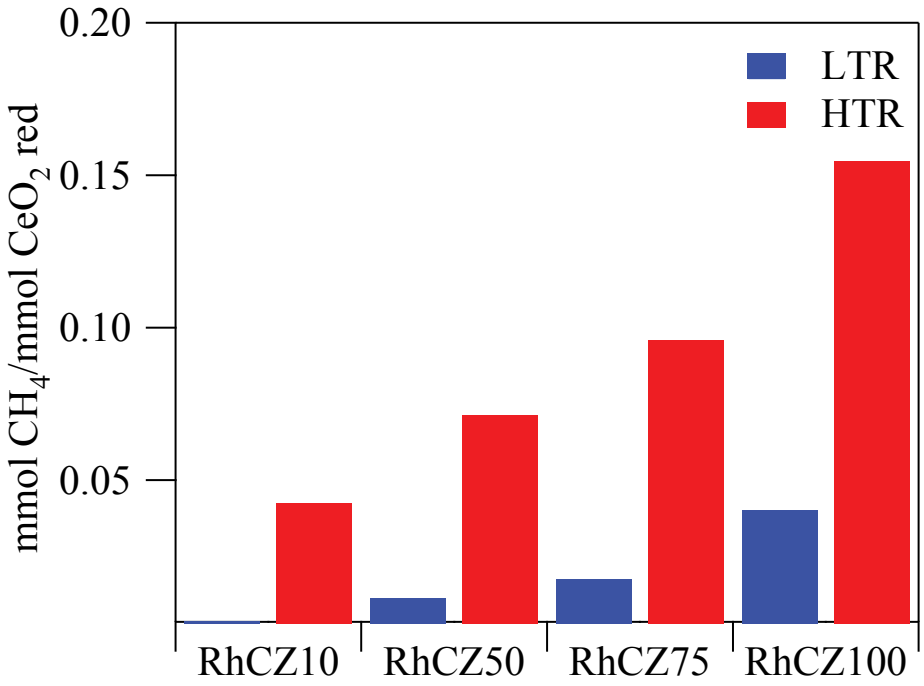

Figure 4.22 CH_4 produced during transient time at T=223°C with respecto to reduced ceria

This indicates that, if we accept the correspondence between oxygen vacancies and transient hydrogenation activity, the vacancies created on CeO_2 are more active than those formed over ceria-zirconia, even if on an absolute basis the higher number of active sites on RhCZ50 and RhCZ75 produces a higher amount of methane (see Figure 4.18 for comparison). This situation might be

related to the different nature of the vacancies of pure cerium oxide and of mixed ceria-zirconia [172, 173].

Trying to better understand this last point, and in order to define whether there was a role of OH groups on the catalytic activity as indicated by some authors [16], specific experiments have been designed in which the high temperature treatment has been carried out also in inert gas (helium). In detail, the sequence of treatments proceeded as follows:

- Low temperature reduction in H_2 (LTR, 223°C) for 2 h → catalytic test (223°C).
- Oxidation at 500°C for 1 hour.
- High temperature reduction in He (HTR, 500°C) for 2 h → catalytic test (223°C).
- Oxidation at 500°C for 1 h.
- LTR at 223°C in H_2 for 2 h followed by a HTR at 500°C in He for 2 h → catalytic test (223°C).

The results of these modified transient experiments are shown in Figure 4.23 for RhCZ100 and RhCZ75, that have been chosen as representative samples; the curve of methane production at 223°C after standard HTR (500°C in H_2 for 2 hours) is reported for comparison (purple line). On both samples it is clear that only the high temperature reduction in H_2 leads to the formation of a pronounced transient high activity peak, thus linking strictly this phenomenon to the reduction of ceria at relatively high temperature (T = 500°C; it is useful to remember that after HTR at 400°C in pulse experiments this peak was not detected, see Figure 4.7). The fact that this transient high activity peak does not appear on both samples after HTR in He (red line) excludes the involvement of OH groups in its formation, as suggested by alternative mechanisms proposed for CO_2 hydrogenation [23].

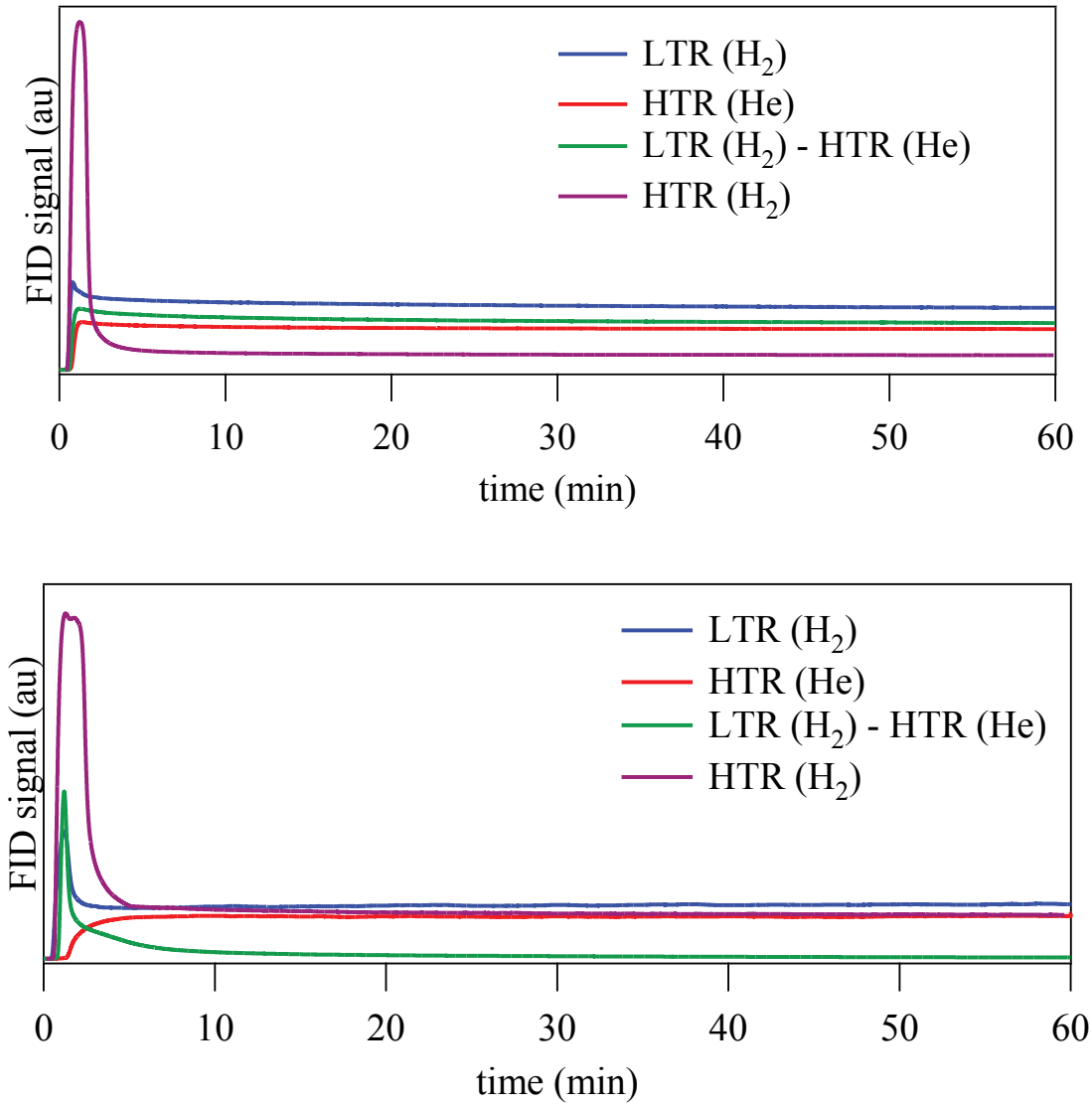

Figure 4.23 Modified methanation experiments on RhCZ100 (top) and RhCZ75 (bottom)

Focusing on the steady state activity (SSA), it can be observed that on RhCZ100 it is only slightly affected by the pretreatment (when the transient high activity peak is not present), whereas on RhCZ75 the situation is completely different. For this sample, the modified experiments confirm that the low temperature reduction is enough to induce the formation of the transient high activity peak, likely due to the higher reducibility of ceria-zirconia support. When the LTR and HTR(He) treatments are separated by an oxidation (blue and red lines), this peak is not present while the SSA is similar. Instead, when LTR and HTR(He) are carried out subsequently with no oxidation in between (green line), the transient high activity peak is formed but the steady state activity decreases dramatically. This might indicate that on ceria-zirconia the SSA is boosted by the

oxidation of the catalyst, but this explanation has to be ruled out since also after a standard HTR treatment (purple line) the steady state methane production is higher. What seems more likely to occur is that the active sites responsible of the steady state activity formed upon reduction at 223°C are somehow annihilated by the subsequent treatment in He at 500°C. The oxidation at 500°C carried out between LTR and HTR(He) regenerates the starting material: at this point the treatment in He at 500°C is not enough to restore the transient high activity peak, but, acting as a mild reduction on the oxidized sample, might activate the sites responsible of steady state activity (red line).

4.3.3 Transient tests at different temperatures over CZ50 and CZ75 supported catalysts

Once we have established that the highest transient activity is recorded over RhCZ50 and RhCZ75, we decided to test these samples for CO_2 methanation in a wider range of temperatures. After low temperature reduction, the samples were not active at the lowest temperatures (50 and 100°C), while after HTR CO_2 methanation was recorded as low as 50°C. Qualitative results (in terms of FID signal) obtained after HTR are shown in Figure 4.24.

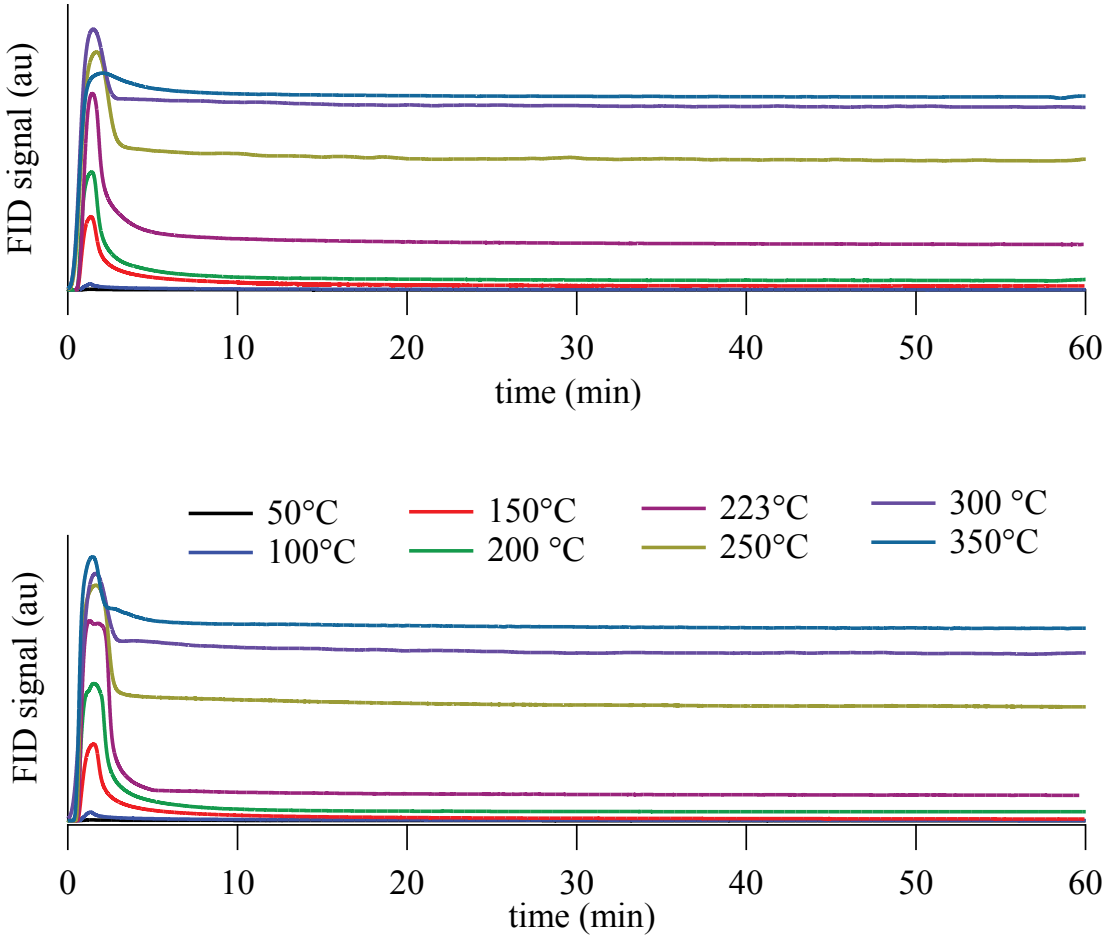

Figure 4.24 CO_2 methanation activity for RhCZ50 (top) and RhCZ75 (bottom) in the 50-350°C temperature range after HTR treatment

It can be observed that at increasing temperature the high activity peak becomes smaller, while the steady state activity increases. This is more evident for RhCZ50, which at 350°C has lost almost all its transient activity. Figure 4.25 is a magnification of the results obtained at T=50°C and T=100°C, from which it can be observed that at these low temperatures both samples present the transient high activity peak, indicating that the sites responsible of the transient activity (TA) are activated even at very low temperature.

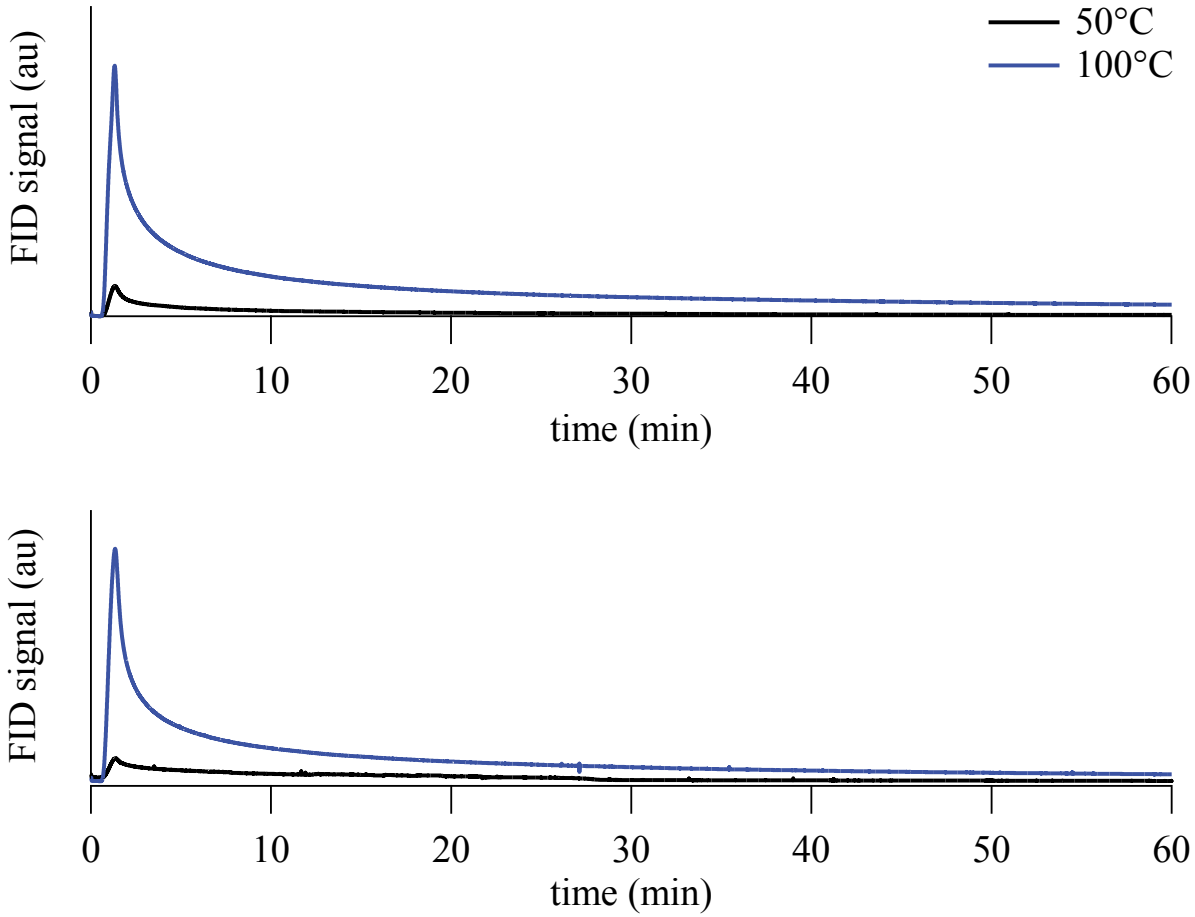

Figure 4.25 CO_2 methanation activity for RhCZ50 (top) and RhCZ75 (bottom) at T=50°C and T=100°C after HTR treatment

Quantitative analysis of the methane produced during the transient high activity peak is shown in Figure 4.26. For both samples there is a maximum at 223°C; beyond this temperature the TA starts to decline, probably because the oxygen vacancies responsible of this phenomenon are filled faster due to the higher temperature. Above 223°C the contribution of the SSA becomes more important (see Figure 4.27), indicating that likely other pathways are involved in the methanation reaction beside the oxygen exchange capability of the support.

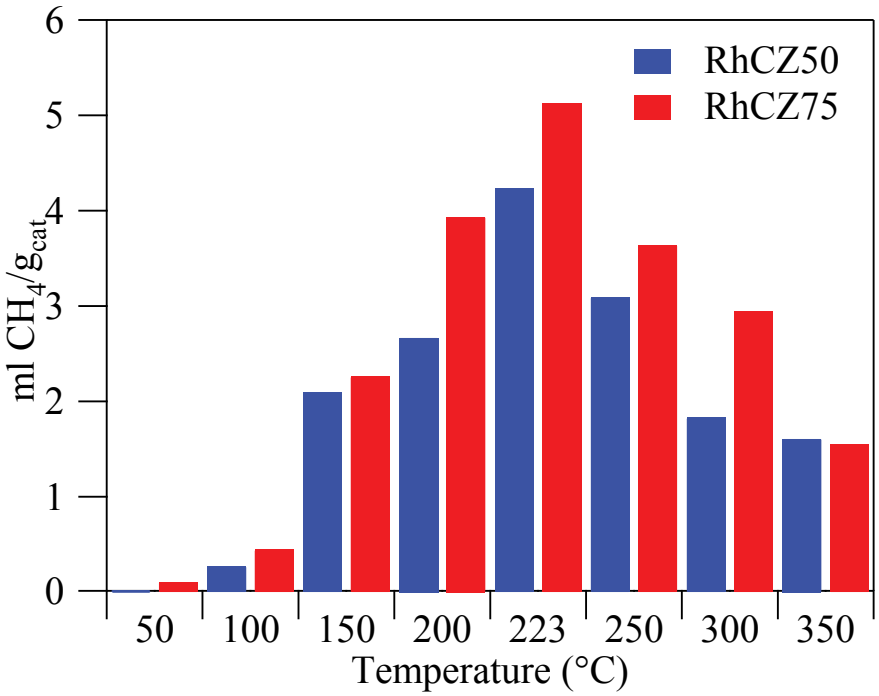

Figure 4.26 Methane production in the transient high activity peak after HTR

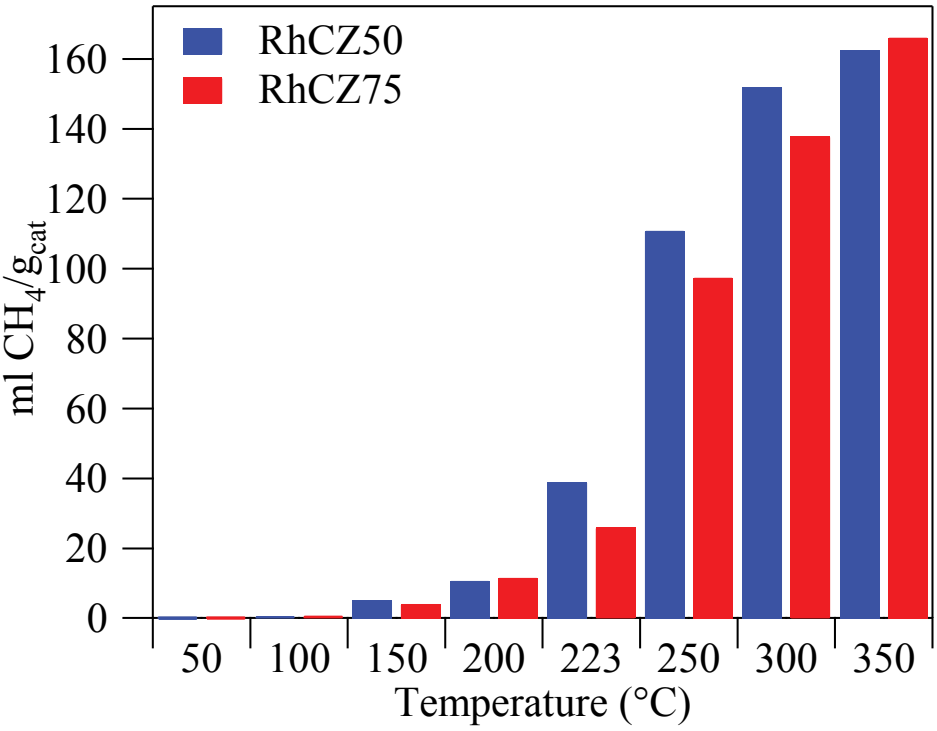

Figure 4.27 Methane production at steady state after HTR

Chapter 5. Discussion of results

The investigation of the CO_2 methanation reaction carried out over Rh-based catalysts has given some insights on the transient effects related to the reducibility of the support. The results obtained in our group in the past [45, 133, 142, 160] have been extended in order to include systems with increased reducibility and oxygen mobility. In particular, nanoshaped ceria with preferential exposure of more reactive planes and ceria-zirconia solid solutions have been tested as rhodium supports for CO_2 hydrogenation. The higher reducibility of these catalysts compared to polycrystalline ceria has been ascertained by TPR and TGA-H_2 measurements before methanation experiments. The tests carried out on these materials have allowed to prove that the most reducible supports are indeed more active for CO_2 hydrogenation under transient conditions, and that the mechanism proposed for CO_2 methanation over rhodium supported on CeO_2 [45] and on TiO_2 [43] well explains the results obtained also for ceria cubes and rods, and for ceria-zirconia. In particular, it has been observed that on these supports not only the methane produced during the transient high activity peak is higher, but also the transition from transient to steady state activity requires a longer time to be completed compared to polycrystalline ceria, due to the slower filling of oxygen vacancies. This aspect indicates that the increase of vacancies is the right way to enhance the catalytic activity for CO_2 methanation. Moreover, on the samples with the highest reducibility, these sites can be activated also by a low temperature reduction (LTR, 223°C), while for pure ceria a reduction at 500°C is needed.

The study of rhodium supported on ceria-zirconia solid solutions prompted us to investigate also the behavior of Rh on pure ZrO_2. Rh/ZrO_2 is known to be a good catalyst for CO_2 hydrogenation [31, 174], and in our experiments we have observed that in fact its steady state activity outperforms that of the other samples both at 150°C and 223°C. If we consider the ratio of the amount of methane

produced in transient and steady state conditions after HTR, we can observe that this amount is negligible for RhCZ0 and RhCZ10 and it increases at increasing cerium content. The quantitative results for the reaction carried out at 150°C and 223°C are shown in Figure 5.1 and 5.2, respectively.

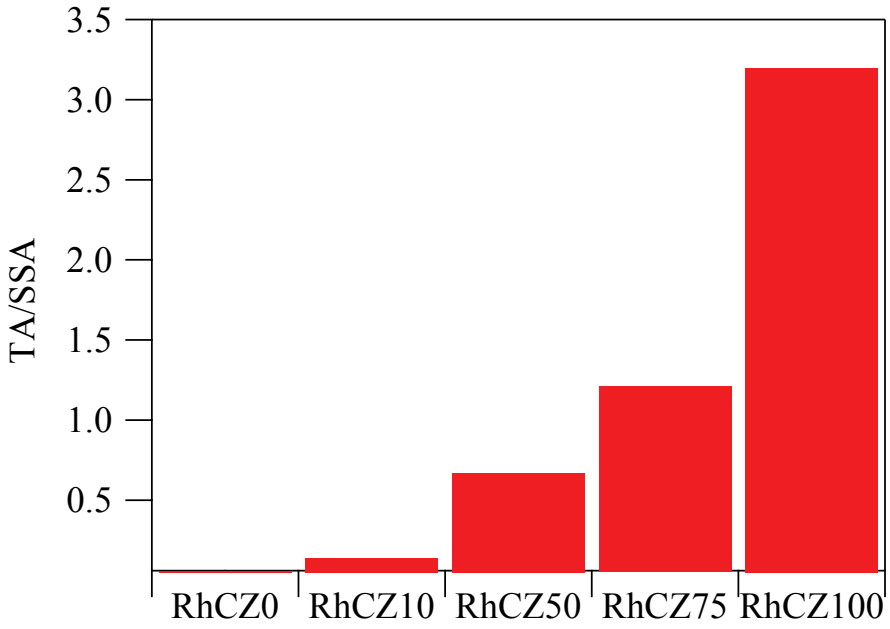

Figure 5.1 Ratio between transient (TA) and steady state activity (SSA) for CO_2 methanation carried out at 150°C after HTR

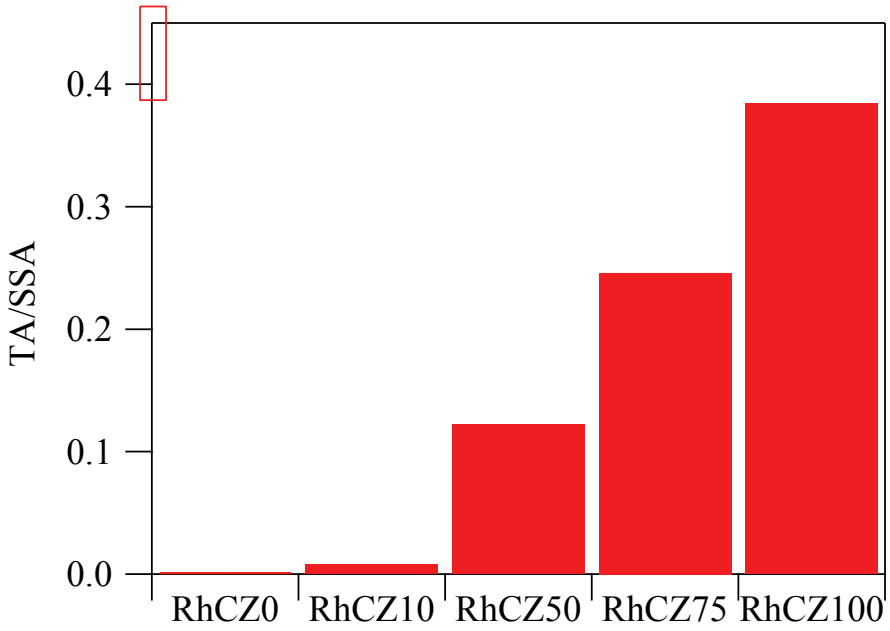

Figure 5.2 Ratio between transient (TA) and steady state activity (SSA) for CO_2 methanation carried out at 223°C after HTR

After the low temperature reduction (223°C) the situation is slightly different, with the highest TA/SSA ratio observed for RhCZ75 at both 150°C and 223°C (Figures 5.3 and 5.4, respectively). This is well in agreement with the observation that the low temperature reduction is more effective on ceria-rich CeZr catalysts.

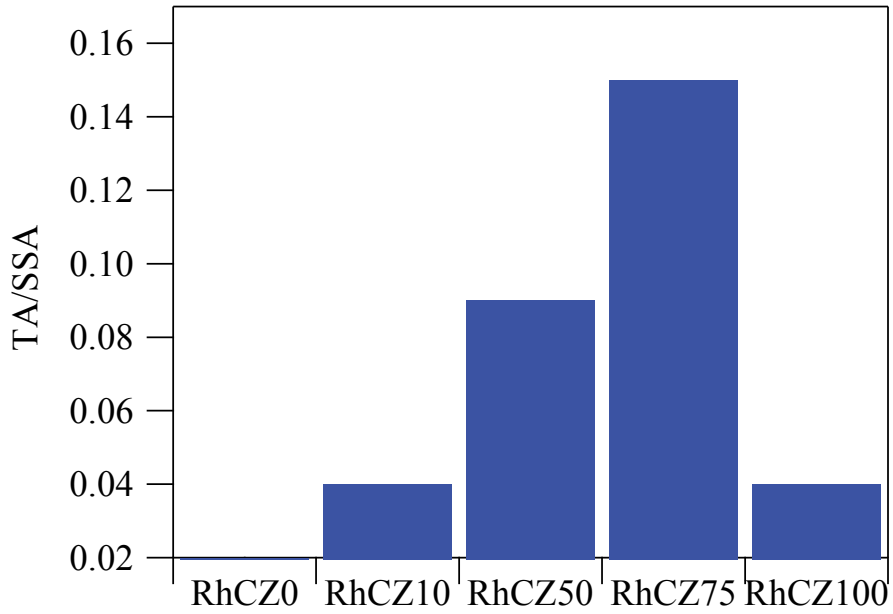

Figure 5.3 Ratio between transient (TA) and steady state activity (SSA) for CO_2 methanation carried out at 150°C after LTR

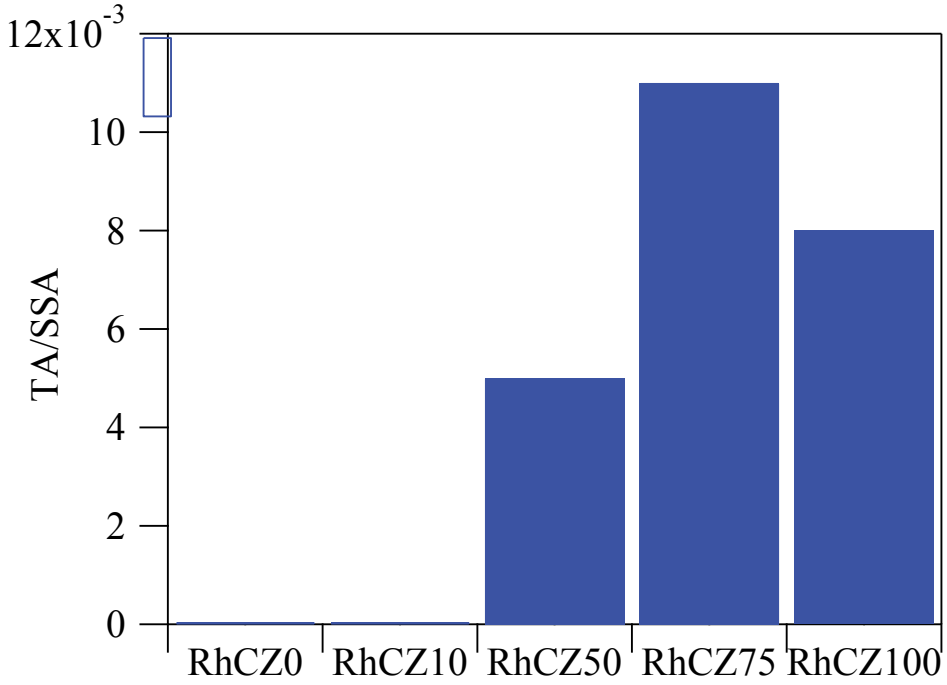

Figure 5.4 Ratio between transient (TA) and steady state activity (SSA) for CO_2 methanation carried out at 223°C after LTR

As already discussed in Chapter 4, the presence of a transient effect on RhCZ0, and partly on RhCZ10, when the reaction is carried out at 150°C should not be confused with the transient high activity dependent upon oxygen vacancies observed on ceria-containing catalysts. Here it is useful to recall that this effect decreases at increasing temperature, an opposite trend with respect to RhCZ50, RhCZ75 and RhCZ100, and opposite also to the formation of oxygen vacancies that is higher at higher temperature (see Chapter 4, and [175]). Moreover, Bedrane et al. observed that the rate of oxygen homoexchange reaction, that can be considered a measure of the activation for metal based catalysts, increased with temperature on Rh/CeO_2 and Rh/CeZr [176]. Recently some authors reported a peculiar interaction taking place between rhodium and ceria in different conditions [177-179]; this unique Rh-Ce interaction, in particular the tendency of Rh to diffuse into the lattice and the redox interplay between the two components, is likely to have a key role in the transient high methanation activity. Based on these evidences, it is then reasonable to assume that on RhCZ0 (and partly on RhCZ10) the activity for CO_2 methanation is more related to the acid/basic and adsorption properties of zirconia [16] and/or to an electronic effect [180], differentiating the process from what happens on ceria-based catalysts. A recent work by Wang et al. indicates that there are two different mechanisms on Ru-based catalysts in presence (Ru/CeO_2) or in absence (Ru/Al_2O_3) of oxygen vacancies: the formate or the CO route, respectively [161]. In the first route the methanation of CO_2 involves the conversion of CO_2 to $CO_2^{\delta-}$ thanks to a reduced ceria site, its evolution into formate species ($HCOO^-$) with the contribution of surface OH and the following formate dissociation catalyzed by an oxygen vacancy. The second route implies the formation of carbonyls on the metal sites, in the form of chemisorbed CO. It is likely that also for Rh-supported catalysts CO_2 methanation follows the formate route, with a preferential role of oxygen vacancies on ceria-based materials and a more significant contribution of the metal and/or other support properties on zirconia.

Noteworthy, the evidences reported by Wang et al. clearly support our explanation for the transient high activity observed on ceria-rich samples. On highly reduced catalysts, at the beginning of the

experiment the surface oxygen vacancies on ceria are continuously reformed thanks to oxygen mobility from the bulk, giving rise to the high transient activity. Afterwards, they get filled by the CO_2 dissociation taking place on reduced ceria sites [161, 181], thus decreasing dramatically the catalytic activity. This decrease is less pronounced when the reaction is carried out at 150°C and it takes place more slowly on samples with increased reducibility, on which the vacancies are formed more easily. The connection between the transient high activity peak and the bulk oxygen vacancies is corroborated by another observation: on CeZr supported samples, this peak is significant also after the LTR treatment, in agreement with the lower bulk reduction energies of ceria-zirconia systems, comparable to those of the surface reduction of pure ceria [182]. In other words, on RhCZ100 the reduction at 223°C produces only, or mainly, surface vacancies, while on RhCZ50 and RhCZ75 bulk vacancies are formed already at this temperature, giving rise to the transient phenomenon observed on these catalysts after low temperature reduction.

5.1 Concluding remarks

This thesis work has shed some light on the mechanisms of CO_2 hydrogenation on Rh-based catalysts, defining the role of highly reducible supports such as nanoshaped ceria and ceria-zirconia on the transient high activity observed on these systems. Nevertheless, for a deeper understanding of the complex phenomena taking place on Rh/CeO_2 and $Rh/CeZrO_2$, it would be useful to apply more advanced techniques such as for example *operando* spectroscopy methodology as it has been done for Ru/CeO_2 [161]. Also an investigation of the active sites in terms of acidic/basic properties would give additional information to discriminate between the role of the support and that of the metal on the different Rh-based systems. Moreover, additional studies involving diffrerent synthesis methods and aging protocols could give more information regarding the transient state.

From the point of view of practical applications, it is remarkable that after HTR treatment the maximum of the transient activity peak of the ceria-containing catalysts is higher than the steady state activity on RhCZ0. It would be desirable to find a way to maintain the methanation activity as high as the maximum of the transient activity, and we know that this can be obtained by preserving the oxygen vacancies on the surface. To reach this goal, one might envisage a system operating with more diluted CO_2 feed (or high excess of hydrogen) in order to avoid the filling of vacancies driven by CO_2 dissociation. In addition, several water-removing systems (e.g. membrane reactor, reactive distillation) could also be assessed.

References

1. D'Alessandro, D.M., B. Smit, and J.R. Long, *Carbon Dioxide Capture: Prospects for New Materials.* Angewandte Chemie International Edition, 2010. **49**(35): p. 6058-6082.
2. Li, B., et al., *Advances in CO_2 capture technology: A patent review.* Applied Energy, 2013. **102**: p. 1439-1447.
3. Cozier, M., *The UN COP21 Climate Change Conference and the role of CCS.* Greenhouse Gases: Science and Technology, 2015. **5**(6): p. 697-700.
4. Global Monitoring Division. *Trends in Atmospheric Carbon Dioxide*. 2017 [cited 2017 August 01]; Available from: https://www.esrl.noaa.gov/gmd/ccgg/trends/global.html.
5. Yu, K.M.K., et al., *Recent Advances in CO_2 Capture and Utilization.* ChemSusChem, 2008. **1**(11): p. 893-899.
6. Council Decision of the European Union, *Council Decision of 03 December 2013 estabisling the especific programme implementing Horizon 2020 - the Framework Programme for Research and Innovation (2014-2020) and reapeling Decisions 2006/971/EC, 2006/972/EC, 2006/973/EC, 2006/974/EC and 2006/975/EC*, Council Decision of the European Union, Editor. 2013: Brussels.
7. MacDowell, N., et al., *An overview of CO_2 capture technologies.* Energy & Environmental Science, 2010. **3**(11): p. 1645-1669.
8. Boot-Handford, M.E., et al., *Carbon capture and storage update.* Energy & Environmental Science, 2014. **7**(1): p. 130-189.
9. Topham, S., et al., *Carbon Dioxide*, in *Ullmann's Encyclopedia of Industrial Chemistry*. 2000, Wiley-VCH Verlag GmbH & Co. KGaA.

10. Centi, G., E.A. Quadrelli, and S. Perathoner, *Catalysis for CO_2 conversion: a key technology for rapid introduction of renewable energy in the value chain of chemical industries.* Energy & Environmental Science, 2013. **6**(6): p. 1711-1731.

11. Aresta, M., A. Dibenedetto, and A. Angelini, *Catalysis for the Valorization of Exhaust Carbon: from CO_2 to Chemicals, Materials, and Fuels. Technological Use of CO_2.* Chemical Reviews, 2014. **114**(3): p. 1709-1742.

12. Bertau, M., et al., *Methanol: The Basic Chemical and Energy Feedstock of the Future: Asinger's Vision Today*. 2014: Springer Berlin Heidelberg.

13. Schlögl, R., *The Revolution Continues: Energiewende 2.0.* Angewandte Chemie International Edition, 2015. **54**(15): p. 4436-4439.

14. Vander Wiel, D.P., et al. *Carbon Dioxide Conversions in Microreactors.* in *4th International Conference on Microreaction Technology: topical conference proceedings. AIChE Spring National Meeting,* . 2000. Atlanta, GA: American Institute of Chemical Engineers.

15. Thampi, K.R., J. Kiwi, and M. Gratzel, *Methanation and photo-methanation of carbon dioxide at room temperature and atmospheric pressure.* Nature, 1987. **327**(6122): p. 506-508.

16. Wang, W., et al., *Recent advances in catalytic hydrogenation of carbon dioxide.* Chemical Society Reviews, 2011. **40**(7): p. 3703-3727.

17. Du, G., et al., *Methanation of carbon dioxide on Ni-incorporated MCM-41 catalysts: The influence of catalyst pretreatment and study of steady-state reaction.* Journal of Catalysis, 2007. **249**(2): p. 370-379.

18. Tada, S. and R. Kikuchi, *Mechanistic study and catalyst development for selective carbon monoxide methanation.* Catalysis Science & Technology, 2015. **5**(6): p. 3061-3070.

19. Schild, C., A. Wokaun, and A. Baiker, *On the mechanism of CO and CO_2 hydrogenation reactions on zirconia-supported catalysts: a diffuse reflectance FTIR study.* Journal of Molecular Catalysis, 1990. **63**(2): p. 243-254.

20. Falconer, J.L. and A.E. Zağli, *Adsorption and methanation of carbon dioxide on a nickel/silica catalyst.* Journal of Catalysis, 1980. **62**(2): p. 280-285.

21. Weatherbee, G.D. and C.H. Bartholomew, *Hydrogenation of CO_2 on group VIII metals.* Journal of Catalysis, 1982. **77**(2): p. 460-472.

22. Peebles, D.E., D.W. Goodman, and J.M. White, *Methanation of carbon dioxide on nickel(100) and the effects of surface modifiers.* The Journal of Physical Chemistry, 1983. **87**(22): p. 4378-4387.

23. Marwood, M., R. Doepper, and A. Renken, *In-situ surface and gas phase analysis for kinetic studies under transient conditions The catalytic hydrogenation of CO_2.* Applied Catalysis A: General, 1997. **151**(1): p. 223-246.

24. Panagiotopoulou, P., D.I. Kondarides, and X.E. Verykios, *Mechanistic aspects of the selective methanation of CO over Ru/TiO_2 catalyst.* Catalysis Today, 2012. **181**(1): p. 138-147.

25. Panagiotopoulou, P., D.I. Kondarides, and X.E. Verykios, *Mechanistic Study of the Selective Methanation of CO over Ru/TiO_2 Catalyst: Identification of Active Surface Species and Reaction Pathways.* The Journal of Physical Chemistry C, 2011. **115**(4): p. 1220-1230.

26. Erdöhelyi, A., M. Pásztor, and F. Solymosi, *Catalytic hydrogenation of CO2 over supported palladium.* Journal of Catalysis, 1986. **98**(1): p. 166-177.

27. Wang, X., et al., *Mechanism of CO_2 Hydrogenation on Pd/Al_2O_3 Catalysts: Kinetics and Transient DRIFTS-MS Studies.* ACS Catalysis, 2015. **5**(11): p. 6337-6349.

28. Heyl, D., U. Rodemerck, and U. Bentrup, *Mechanistic Study of Low-Temperature CO_2 Hydrogenation over Modified Rh/Al_2O_3 Catalysts.* ACS Catalysis, 2016. **6**(9): p. 6275-6284.

29. Miyao, T., et al., *Mechanistic study of the effect of chlorine on selective CO methanation over Ni alumina-based catalysts.* Applied Catalysis A: General, 2014. **486**: p. 187-192.

30. Beuls, A., et al., *Methanation of CO_2: Further insight into the mechanism over Rh/γ-Al_2O_3 catalyst.* Applied Catalysis B: Environmental, 2012. **113–114**(0): p. 2-10.

31. Iizuka, T., Y. Tanaka, and K. Tanabe, *Hydrogenation of CO and CO_2 over rhodium catalysts supported on various metal oxides.* Journal of Catalysis, 1982. **76**(1): p. 1-8.

32. Solymosi, F., I. Tombácz, and M. Kocsis, *Hydrogenation of CO on supported Rh catalysts.* Journal of Catalysis, 1982. **75**(1): p. 78-93.

33. Takenaka, S., T. Shimizu, and K. Otsuka, *Complete removal of carbon monoxide in hydrogen-rich gas stream through methanation over supported metal catalysts.* International Journal of Hydrogen Energy, 2004. **29**(10): p. 1065-1073.

34. Tada, S., et al., *Effect of reduction pretreatment and support materials on selective CO methanation over supported Ru catalysts.* Applied Catalysis A: General, 2011. **404**(1–2): p. 149-154.

35. Tada, S., et al., *Study of RuNi/TiO_2 catalysts for selective CO methanation.* Applied Catalysis B: Environmental, 2013. **140–141**: p. 258-264.

36. Tada, S., et al., *Promotion of CO_2 methanation activity and CH_4 selectivity at low temperatures over Ru/CeO_2/Al_2O_3 catalysts.* International Journal of Hydrogen Energy, 2014. **39**(19): p. 10090-10100.

37. Tada, S., et al., *Ni/CeO_2 catalysts with high CO_2 methanation activity and high CH_4 selectivity at low temperatures.* International Journal of Hydrogen Energy, 2012. **37**(7): p. 5527-5531.

38. Erhan Aksoylu, A. and Z. İlsenÖnsan, *Hydrogenation of carbon oxides using coprecipitated and impregnated Ni/Al_2O_3 catalysts.* Applied Catalysis A: General, 1997. **164**(1): p. 1-11.

39. Li, C., et al., *Photohole-oxidation-assisted anchoring of ultra-small Ru clusters onto TiO_2 with excellent catalytic activity and stability.* Journal of Materials Chemistry A, 2013. **1**(7): p. 2461-2467.

40. Wang, F., et al., *Catalytic behavior of supported Ru nanoparticles on the (101) and (001) facets of anatase TiO_2.* RSC Advances, 2014. **4**(21): p. 10834-10840.

41. Karelovic, A. and P. Ruiz, *Mechanistic study of low temperature CO_2 methanation over Rh/TiO_2 catalysts.* Journal of Catalysis, 2013. **301**: p. 141-153.

42. Porosoff, M.D. and J.G. Chen, *Trends in the catalytic reduction of CO_2 by hydrogen over supported monometallic and bimetallic catalysts.* Journal of Catalysis, 2013. **301**(0): p. 30-37.

43. Novák, É., et al., *CO_2 Hydrogenation on Rh/TiO_2 Previously Reduced at Different Temperatures.* Topics in Catalysis, 2002. **20**(1-4): p. 107-117.

44. Westermann, A., et al., *The promoting effect of Ce in the CO_2 methanation performances on NiUSY zeolite: A FTIR In Situ/Operando study.* Catalysis Today, 2017. **283**: p. 74-81.

45. de Leitenburg, C., A. Trovarelli, and J. Kašpar, *A Temperature-Programmed and Transient Kinetic Study of CO_2 Activation and Methanation over CeO_2-Supported Noble Metals.* Journal of Catalysis, 1997. **166**(1): p. 98-107.

46. Yashima, M., et al., *High-temperature neutron powder diffraction study of cerium dioxide CeO_2 up to 1770 K.* Chemical Physics Letters, 2003. **372**(5): p. 784-787.

47. Yashima, M. and S. Kobayashi, *Positional disorder of oxygen ions in ceria at high temperatures.* Applied Physics Letters, 2004. **84**(4): p. 526-528.

48. Knappe, P. and L. Eyring, *Preparation and electron microscopy of intermediate phases in the interval Ce_7O_{12}-$Ce_{11}O_{20}$.* Journal of Solid State Chemistry, 1985. **58**(3): p. 312-324.

49. Zinkevich, M., D. Djurovic, and F. Aldinger, *Thermodynamic modelling of the cerium–oxygen system.* Solid State Ionics, 2006. **177**(11): p. 989-1001.

50. Sørensen, O.T., *Thermodynamic studies of the phase relationships of nonstoichiometric cerium oxides at higher temperatures.* Journal of Solid State Chemistry, 1976. **18**(3): p. 217-233.

51. Kümmerle, E.A. and G. Heger, *The Structures of C–$Ce_2O_{3+\delta}$, Ce_7O_{12}, and $Ce_{11}O_{20}$.* Journal of Solid State Chemistry, 1999. **147**(2): p. 485-500.

52. Zou, H., X. Dong, and W. Lin, *Selective CO oxidation in hydrogen-rich gas over CuO/CeO_2 catalysts.* Applied Surface Science, 2006. **253**(5): p. 2893-2898.

53. Soler, L., et al., *CO oxidation and $COPrO_x$ over preformed Au nanoparticles supported over nanoshaped CeO_2.* Applied Catalysis B: Environmental, 2016. **197**: p. 47-55.

54. Saqer, S.M., D.I. Kondarides, and X.E. Verykios, *Catalytic Activity of Supported Platinum and Metal Oxide Catalysts for Toluene Oxidation.* Topics in Catalysis, 2009. **52**(5): p. 517-527.

55. Gonzalez-DelaCruz, V.M., et al., *Morphology changes induced by strong metal–support interaction on a Ni–ceria catalytic system.* Journal of Catalysis, 2008. **257**(2): p. 307-314.

56. Kim, K.-H. and S.-K. Ihm, *Heterogeneous catalytic wet air oxidation of refractory organic pollutants in industrial wastewaters: A review.* Journal of Hazardous Materials, 2011. **186**(1): p. 16-34.

57. Liu, S., et al., *Soot oxidation over CeO_2 and Ag/CeO_2: Factors determining the catalyst activity and stability during reaction.* Journal of Catalysis, 2016. **337**: p. 188-198.

58. Bueno-López, A., *Diesel soot combustion ceria catalysts.* Applied Catalysis B: Environmental, 2014. **146**: p. 1-11.

59. Liu, S., et al., *Ceria-based catalysts for soot oxidation: a review.* Journal of Rare Earths, 2015. **33**(6): p. 567-590.

60. Kovacevic, M., et al., *The effects of morphology of cerium oxide catalysts for dehydrogenation of ethylbenzene to styrene.* Applied Catalysis A: General, 2015. **505**: p. 354-364.

61. Bunluesin, T., R.J. Gorte, and G.W. Graham, *Studies of the water-gas-shift reaction on ceria-supported Pt, Pd, and Rh: Implications for oxygen-storage properties.* Applied Catalysis B: Environmental, 1998. **15**(1): p. 107-114.

62. Löfberg, A., et al., *Ni/CeO_2 based catalysts as oxygen vectors for the chemical looping dry reforming of methane for syngas production.* Applied Catalysis B: Environmental, 2017. **212**: p. 159-174.

63. Craciun, R., B. Shereck, and R.J. Gorte, *Kinetic studies of methane steam reforming on ceria-supported Pd.* Catalysis Letters, 1998. **51**(3): p. 149-153.

64. Wang, X. and R.J. Gorte, *Steam reforming of n-butane on Pd/ceria.* Catalysis Letters, 2001. **73**(1): p. 15-19.

65. Mudiyanselage, K., et al., *Reactions of ethanol over CeO2 and Ru/CeO2 catalysts.* Applied Catalysis B: Environmental, 2016. **197**: p. 198-205.

66. Gandhi, H.S., et al., *Laboratory Evaluation of Three-Way Catalysts*. 1976, SAE International.

67. Trovarelli, A., *Catalytic Properties of Ceria and CeO_2-Containing Materials.* Catalysis Reviews, 1996. **38**(4): p. 439-520.

68. Herz, R.K., *Dynamic behavior of automotive catalysts. 1. Catalyst oxidation and reduction.* Industrial & Engineering Chemistry Product Research and Development, 1981. **20**(3): p. 451-457.

69. Herz, R.K., *Dynamic Behavior of Automotive Three-Way Emission Control Systems*, in *Studies in Surface Science and Catalysis*, A. Crucq and A. Frennet, Editors. 1987, Elsevier. p. 427-444.

70. Yao, H.C. and Y.F.Y. Yao, *Ceria in automotive exhaust catalysts.* Journal of Catalysis, 1984. **86**(2): p. 254-265.

71. Su, E.C., C.N. Montreuil, and W.G. Rothschild, *Oxygen storage capacity of monolith three-way catalysts.* Applied Catalysis, 1985. **17**(1): p. 75-86.

72. Kummer, J.T., *Catalysts for automobile emission control.* Progress in Energy and Combustion Science, 1980. **6**(2): p. 177-199.

73. Perrichon, V., et al., *Thermal stability of a high surface area ceria under reducing atmosphere.* Applied Catalysis A: General, 1995. **129**(1): p. 69-82.

74. Li, H.-Y., et al., *Multiple configurations of the two excess 4f electrons on defective CeO_2(111): Origin and implications.* Physical Review B, 2009. **79**(19): p. 193401.

75. Chueh, W.C., et al., *High-Flux Solar-Driven Thermochemical Dissociation of CO_2 and H_2O Using Nonstoichiometric Ceria.* Science, 2010. **330**(6012): p. 1797-1801.

76. Furler, P., J.R. Scheffe, and A. Steinfeld, *Syngas production by simultaneous splitting of H_2O and CO_2 via ceria redox reactions in a high-temperature solar reactor.* Energy & Environmental Science, 2012. **5**(3): p. 6098-6103.

77. Scheffe, J.R., M. Welte, and A. Steinfeld, *Thermal Reduction of Ceria within an Aerosol Reactor for H_2O and CO_2 Splitting.* Industrial & Engineering Chemistry Research, 2014. **53**(6): p. 2175-2182.

78. Kašpar, J., P. Fornasiero, and N. Hickey, *Automotive catalytic converters: current status and some perspectives.* Catalysis Today, 2003. **77**(4): p. 419-449.

79. Fornasiero, P., et al., *Rh-Loaded CeO_2-ZrO_2 Solid-Solutions as Highly Efficient Oxygen Exchangers: Dependence of the Reduction Behavior and the Oxygen Storage Capacity on the Structural-Properties.* Journal of Catalysis, 1995. **151**(1): p. 168-177.

80. Shannon, R., *Revised effective ionic radii and systematic studies of interatomic distances in halides and chalcogenides.* Acta Crystallographica Section A, 1976. **32**(5): p. 751-767.

81. Raju, V., S. Jaenicke, and G.-K. Chuah, *Effect of hydrothermal treatment and silica on thermal stability and oxygen storage capacity of ceria–zirconia.* Applied Catalysis B: Environmental, 2009. **91**(1–2): p. 92-100.

82. Si, R., et al., *Enhanced Thermal Stability and Oxygen Storage Capacity for $Ce_xZr_{1-x}O_2$ (x = 0.4−0.6) Solid Solutions by Hydrothermally Homogenous Doping of Trivalent Rare Earths.* The Journal of Physical Chemistry C, 2007. **111**(2): p. 787-794.

83. Daturi, M., et al., *Reduction of High Surface Area CeO_2−ZrO_2 Mixed Oxides.* The Journal of Physical Chemistry B, 2000. **104**(39): p. 9186-9194.

84. Monte, R.D. and J. Kaspar, *Nanostructured CeO_2-ZrO_2 mixed oxides.* Journal of Materials Chemistry, 2005. **15**(6): p. 633-648.

85. Vlaic, G., et al., *Relationship between the Zirconia-Promoted Reduction in the Rh-Loaded $Ce_{0.5}Zr_{0.5}O_2$ Mixed Oxide and the Zr–O Local Structure.* Journal of Catalysis, 1997. **168**(2): p. 386-392.

86. Fornasiero, P., et al., *Relationships between Structural/Textural Properties and Redox Behavior in $Ce_{0.6}Zr_{0.4}O_2$ Mixed Oxides.* Journal of Catalysis, 1999. **187**(1): p. 177-185.

87. Shah, P.R., et al., *Evidence for Entropy Effects in the Reduction of Ceria−Zirconia Solutions.* Chemistry of Materials, 2006. **18**(22): p. 5363-5369.

88. Aneggi, E., et al., *Insights into the redox properties of ceria-based oxides and their implications in catalysis.* Journal of Alloys and Compounds, 2006. **408–412**: p. 1096-1102.

89. Li, P., I.W. Chen, and J.E. Penner-Hahn, *Effect of Dopants on Zirconia Stabilization—An X-ray Absorption Study: I, Trivalent Dopants.* Journal of the American Ceramic Society, 1994. **77**(1): p. 118-128.

90. Madier, Y., et al., *Oxygen Mobility in CeO_2 and $Ce_xZr_{(1-x)}O_2$ Compounds: Study by CO Transient Oxidation and $^{18}O/^{16}O$ Isotopic Exchange.* The Journal of Physical Chemistry B, 1999. **103**(50): p. 10999-11006.

91. Murota, T., et al., *Production method of cerium oxide with high storage capacity of oxygen and its mechanism.* Journal of Alloys and Compounds, 1993. **193**(1): p. 298-299.

92. Trovarelli, A., et al., *Nanophase Fluorite-Structured CeO_2–ZrO_2 Catalysts Prepared by High-Energy Mechanical Milling.* Journal of Catalysis, 1997. **169**(2): p. 490-502.

93. Yashima, M., et al., *Crystal Structure and Oxide-Ion Diffusion of Nanocrystalline, Compositionally Homogeneous Ceria–Zirconia $Ce_{0.5}Zr_{0.5}O_2$ up to 1176 K.* Crystal Growth & Design, 2013. **13**(2): p. 829-837.

94. Rao, G.R., et al., *NO decomposition over partially reduced metallized CeO_2-ZrO_2 solid solutions.* Catalysis Letters, 1994. **24**(1): p. 107-112.

95. Boaro, M., et al., *The Dynamics of Oxygen Storage in Ceria–Zirconia Model Catalysts Measured by CO Oxidation under Stationary and Cycling Feedstream Compositions.* Journal of Catalysis, 2000. **193**(2): p. 338-347.

96. Ocampo, F., B. Louis, and A.-C. Roger, *Methanation of carbon dioxide over nickel-based $Ce_{0.72}Zr_{0.28}O_2$ mixed oxide catalysts prepared by sol–gel method.* Applied Catalysis A: General, 2009. **369**(1–2): p. 90-96.

97. Gorte, R.J., *Ceria in catalysis: From automotive applications to the water–gas shift reaction.* AIChE Journal, 2010. **56**(5): p. 1126-1135.

98. Aneggi, E., C. de Leitenburg, and A. Trovarelli, *Ceria-based formulation for catalysts for diesel soot combustion*, in *Catalysis by Ceria and Related Materials*, A. Trovarelli and P. Fornasiero, Editors. 2013, Imperial College Press: London. p. 565-621.

99. Can, F., et al., *Composition-Dependent Performance of $Ce_xZr_{1-x}O_2$ Mixed-Oxide-Supported WO_3 Catalysts for the NO_x Storage Reduction–Selective Catalytic Reduction Coupled Process.* ACS Catalysis, 2013. **3**(6): p. 1120-1132.

100. Zhou, K. and Y. Li, *Catalysis Based on Nanocrystals with Well-Defined Facets.* Angewandte Chemie International Edition, 2012. **51**(3): p. 602-613.

101. Yuan, Q., et al., *Controlled synthesis and assembly of ceria-based nanomaterials.* Journal of Colloid and Interface Science, 2009. **335**(2): p. 151-167.

102. Mai, H.-X., et al., *Shape-Selective Synthesis and Oxygen Storage Behavior of Ceria Nanopolyhedra, Nanorods, and Nanocubes.* The Journal of Physical Chemistry B, 2005. **109**(51): p. 24380-24385.

103. Yan, L., et al., *Template-Free Hydrothermal Synthesis of CeO_2 Nano-octahedrons and Nanorods: Investigation of the Morphology Evolution.* Crystal Growth & Design, 2008. **8**(5): p. 1474-1477.

104. Yu, R., et al., *Controlled Synthesis of CeO_2 Flower-Like and Well-Aligned Nanorod Hierarchical Architectures by a Phosphate-Assisted Hydrothermal Route.* The Journal of Physical Chemistry C, 2008. **112**(50): p. 19896-19900.

105. Berestok, T., et al., *Tuning Branching in Ceria Nanocrystals.* Chemistry of Materials, 2017. **29**(10): p. 4418-4424.

106. Zhou, K., et al., *Enhanced catalytic activity of ceria nanorods from well-defined reactive crystal planes.* Journal of Catalysis, 2005. **229**(1): p. 206-212.

107. Conesa, J., *Computer modeling of surfaces and defects on cerium dioxide.* Surface Science, 1995. **339**(3): p. 337-352.

108. Skorodumova, N.V., M. Baudin, and K. Hermansson, *Surface properties of CeO_2 from first principles.* Physical Review B, 2004. **69**(7): p. 075401.

109. Herschend, B., M. Baudin, and K. Hermansson, *Electronic structure of the CeO_2(1 1 0) surface oxygen vacancy.* Surface Science, 2005. **599**(1–3): p. 173-186.

110. Herschend, B., M. Baudin, and K. Hermansson, *CO adsorption on CeO_2 (1 1 0) using hybrid-DFT embedded-cluster calculations.* Chemical Physics, 2006. **328**(1–3): p. 345-353.

111. Zhou, X.-D. and W. Huebner, *Size-induced lattice relaxation in CeO_2 nanoparticles.* Applied Physics Letters, 2001. **79**(21): p. 3512-3514.

112. Nolan, M., et al., *Density functional theory studies of the structure and electronic structure of pure and defective low index surfaces of ceria.* Surface Science, 2005. **576**(1–3): p. 217-229.

113. Nolan, M., S.C. Parker, and G.W. Watson, *The electronic structure of oxygen vacancy defects at the low index surfaces of ceria.* Surface Science, 2005. **595**(1–3): p. 223-232.

114. Ganduglia-Pirovano, M.V., J.L.F. Da Silva, and J. Sauer, *Density-Functional Calculations of the Structure of Near-Surface Oxygen Vacancies and Electron Localization on CeO_2 (111).* Physical Review Letters, 2009. **102**(2): p. 026101.

115. Yang, Z., et al., *Oxygen vacancy pairs on CeO_2 (110): A DFT + U study.* Physics Letters A, 2009. **373**(31): p. 2786-2792.

116. Fabris, S., et al., *Electronic and Atomistic Structures of Clean and Reduced Ceria Surfaces.* The Journal of Physical Chemistry B, 2005. **109**(48): p. 22860-22867.

117. Sayle, D.C., S.A. Maicaneanu, and G.W. Watson, *Atomistic Models for CeO_2 (111), (110), and (100) Nanoparticles, Supported on Yttrium-Stabilized Zirconia.* Journal of the American Chemical Society, 2002. **124**(38): p. 11429-11439.

118. Huang, M. and S. Fabris, *CO Adsorption and Oxidation on Ceria Surfaces from DFT+U Calculations.* The Journal of Physical Chemistry C, 2008. **112**(23): p. 8643-8648.

119. Wu, Z., M. Li, and S.H. Overbury, *On the structure dependence of CO oxidation over CeO_2 nanocrystals with well-defined surface planes.* Journal of Catalysis, 2012. **285**(1): p. 61-73.

120. Tana, et al., *Morphology-dependent redox and catalytic properties of CeO_2 nanostructures: Nanowires, nanorods and nanoparticles.* Catalysis Today, 2009. **148**(1–2): p. 179-183.

121. Lv, J., et al., *Exclusively selective oxidation of toluene to benzaldehyde on ceria nanocubes by molecular oxygen.* Chemical Communications, 2010. **46**(32): p. 5909-5911.

122. Aneggi, E., et al., *Shape-Dependent Activity of Ceria in Soot Combustion.* ACS Catalysis, 2014. **4**(1): p. 172-181.

123. Vilé, G., et al., *Ceria in Hydrogenation Catalysis: High Selectivity in the Conversion of Alkynes to Olefins.* Angewandte Chemie International Edition, 2012. **51**(34): p. 8620-8623.

124. Vilé, G., et al., *Opposite Face Sensitivity of CeO_2 in Hydrogenation and Oxidation Catalysis.* Angewandte Chemie International Edition, 2014. **53**(45): p. 12069-12072.

125. Liu, Y., et al., *Reverse water–gas shift reaction over ceria nanocube synthesized by hydrothermal method.* Catalysis Communications, 2016. **76**: p. 1-6.

126. Torrente-Murciano, L. and F.R. Garcia-Garcia, *Effect of nanostructured support on the WGSR activity of Pt/CeO_2 catalysts.* Catalysis Communications, 2015. **71**: p. 1-6.

127. Divins, N.J., et al., *The influence of nano-architectured CeO_x supports in RhPd/CeO_2 for the catalytic ethanol steam reforming reaction.* Catalysis Today, 2015. **253**: p. 99-105.

128. Hsiao, W.-I., et al., *The effect of the morphology of nanocrystalline CeO_2 on ethanol reforming.* Chemical Physics Letters, 2007. **441**(4–6): p. 294-299.

129. Yi, G., et al., *Preferential CO oxidation in a H_2-rich gas by Au/CeO_2 catalysts: Nanoscale CeO_2 shape effect and mechanism aspect.* Catalysis Today, 2010. **157**(1–4): p. 83-88.

130. Huang, X.-S., et al., *Morphology effects of nanoscale ceria on the activity of Au/CeO_2 catalysts for low-temperature CO oxidation.* Applied Catalysis B: Environmental, 2009. **90**(1–2): p. 224-232.

131. Torrente-Murciano, L., et al., *Effect of nanostructured ceria as support for the iron catalysed hydrogenation of CO_2 into hydrocarbons.* Physical Chemistry Chemical Physics, 2016. **18**(23): p. 15496-15500.

132. Wang, F., et al., *Catalytic behavior of supported Ru nanoparticles on the {1 0 0}, {1 1 0}, and {1 1 1} facet of CeO_2.* Journal of Catalysis, 2015. **329**(0): p. 177-186.

133. Trovarelli, A., et al., *Rh-CeO_2 interaction induced by high-temperature reduction. Characterization and catalytic behaviour in transient and continuous conditions.* Journal of the Chemical Society, Faraday Transactions, 1992. **88**(9): p. 1311-1319.

134. de Leitenburg, C. and A. Trovarelli, *Metal-Support Interactions in Rh/CeO_2, Rh/TiO_2, and Rh/Nb_2O_5 Catalysts as Inferred from CO_2 Methanation Activity.* Journal of Catalysis, 1995. **156**(1): p. 171-174.

135. Tauster, S.J., S.C. Fung, and R.L. Garten, *Strong metal-support interactions. Group 8 noble metals supported on titanium dioxide.* Journal of the American Chemical Society, 1978. **100**(1): p. 170-175.

136. Bernal, S., et al., *Some contributions of electron microscopy to the characterisation of the strong metal–support interaction effect.* Catalysis Today, 2003. **77**(4): p. 385-406.

137. Choi, E.J., et al., *Hydrogenation of CO_2 to methanol over Pd–Cu/CeO_2 catalysts.* Molecular Catalysis, 2017. **434**: p. 146-153.

138. Wang, Z., et al., *Strong metal-support interaction in novel core-shell Au-CeO_2 nanostructures induced by different pretreatment atmospheres and its influence on CO oxidation.* Nanoscale, 2016. **8**(11): p. 5865-5872.

139. Ay, H. and D. Üner, *Dry reforming of methane over CeO_2 supported Ni, Co and Ni–Co catalysts.* Applied Catalysis B: Environmental, 2015. **179**: p. 128-138.

140. Du, X., et al., *Morphology Dependence of Catalytic Properties of Ni/CeO_2 Nanostructures for Carbon Dioxide Reforming of Methane.* The Journal of Physical Chemistry C, 2012. **116**(18): p. 10009-10016.

141. Abid, M., V. Paul-Boncour, and R. Touroude, *Pt/CeO2 catalysts in crotonaldehyde hydrogenation: Selectivity, metal particle size and SMSI states.* Applied Catalysis A: General, 2006. **297**(1): p. 48-59.

142. Trovarelli, A., et al., *CO_2 Methanation Under Transient and Steady-State Conditions over Rh/CeO_2 and CeO_2-Promoted Rh/SiO_2: The Role of Surface and Bulk Ceria.* Journal of Catalysis, 1995. **151**(1): p. 111-124.

143. Zamar, F., et al., *CeO_2-based solid solutions with the fluorite structure as novel and effective catalysts for methane combustion.* Journal of the Chemical Society, Chemical Communications, 1995(9): p. 965-966.

144. Moser, M., et al., *Structure and reactivity of ceria–zirconia catalysts for bromine and chlorine production via the oxidation of hydrogen halides.* Journal of Catalysis, 2015. **331**: p. 128-137.

145. Heck, R.M., R.J. Farrauto, and S.T. Gulati, *Catalytic Air Pollution Control: Commercial Technology*. 2012: Wiley.

146. Agarwal, S., L. Lefferts, and B.L. Mojet, *Ceria Nanocatalysts: Shape Dependent Reactivity and Formation of OH.* ChemCatChem, 2013. **5**(2): p. 479-489.

147. Qiao, Z.-A., Z. Wu, and S. Dai, *Shape-Controlled Ceria-based Nanostructures for Catalysis Applications.* ChemSusChem, 2013. **6**(10): p. 1821-1833.

148. Agarwal, S., et al., *Surface-Dependence of Defect Chemistry of Nanostructured Ceria.* The Journal of Physical Chemistry C, 2015. **119**(22): p. 12423-12433.

149. Aneggi, E., et al., *Higher activity of Diesel soot oxidation over polycrystalline ceria and ceria–zirconia solid solutions from more reactive surface planes.* Catalysis Today, 2012. **197**(1): p. 119-126.

150. Piumetti, M., et al., *Nanostructured ceria-based catalysts for soot combustion: Investigations on the surface sensitivity.* Applied Catalysis B: Environmental, 2015. **165**: p. 742-751.

151. Trovarelli, A. and J. Llorca, *Ceria Catalysts at Nanoscale: How Do Crystal Shapes Shape Catalysis?* ACS Catalysis, 2017. **7**(7): p. 4716-4735.

152. Yang, C., et al., *Surface Faceting and Reconstruction of Ceria Nanoparticles.* Angewandte Chemie International Edition, 2017. **56**(1): p. 375-379.

153. López, J.M., et al., *The prevalence of surface oxygen vacancies over the mobility of bulk oxygen in nanostructured ceria for the total toluene oxidation.* Applied Catalysis B: Environmental, 2015. **174–175**: p. 403-412.

154. Bernal, S., et al., *Reversibility of hydrogen chemisorption on a ceria-supported rhodium catalyst.* Journal of Catalysis, 1992. **137**(1): p. 1-11.

155. Salasc, S., et al., *Oxygen Titration of Spill-Over Hydrogen in Ceria and Ceria–Alumina Supported Platinum–Rhodium Catalysts: Application to the Determination of the Ceria Surface in Contact with Metal.* Journal of Catalysis, 2000. **189**(2): p. 401-409.

156. Teschner, D., et al., *Ceria as a new support of noble metal catalysts for hydrocarbon reactions: chemisorption and catalytic studies.* Solid State Ionics, 2001. **141–142**: p. 709-713.

157. Boaro, M., et al., *The use of temperature-programmed and dynamic/transient methods in catalysis: characterization of ceria-based, model three-way catalysts.* Catalysis Today, 2003. **77**(4): p. 407-417.

158. Ahmed, F., et al., *Adsorption and dissociation of molecular hydrogen on Pt/CeO2 catalyst in the hydrogen spillover process: A quantum chemical molecular dynamics study.* Applied Surface Science, 2010. **256**(24): p. 7643-7652.

159. Yang, Z., et al., *Atomic and electronic structure of unreduced and reduced CeO2 surfaces: A first-principles study.* The Journal of Chemical Physics, 2004. **120**(16): p. 7741-7749.

160. Trovarelli, A., C. de Leitenburg, and G. Dolcetti, *CO and CO_2 hydrogenation under transient conditions over Rh-CeO_2: novel positive effects of metal-support interaction on catalytic activity and selectivity.* Journal of the Chemical Society, Chemical Communications, 1991(7): p. 472-473.

161. Wang, F., et al., *Active Site Dependent Reaction Mechanism over Ru/CeO_2 Catalyst toward CO_2 Methanation.* Journal of the American Chemical Society, 2016. **138**(19): p. 6298-6305.

162. Wu, Z., et al., *Probing Defect Sites on CeO_2 Nanocrystals with Well-Defined Surface Planes by Raman Spectroscopy and O_2 Adsorption.* Langmuir, 2010. **26**(21): p. 16595-16606.

163. Bunluesin, T., R.J. Gorte, and G.W. Graham, *CO oxidation for the characterization of reducibility in oxygen storage components of three-way automotive catalysts.* Applied Catalysis B: Environmental, 1997. **14**(1): p. 105-115.

164. Graham, G.W., et al., *Characterization of model automotive exhaust catalysts: Pd on Zr-rich ceria-zirconia supports.* Catalysis Letters, 2000. **67**(2-4): p. 99-105.

165. Sugiura, M., *Oxygen storage materials for automotive catalysts: Ceria-zirconia solid solutions.* Catalysis Surveys from Asia, 2003. **7**(1): p. 77-87.

166. Piumetti, M., et al., *Nanostructured ceria-zirconia catalysts for CO oxidation: Study on surface properties and reactivity.* Applied Catalysis B: Environmental, 2016. **197**: p. 35-46.

167. Kašpar, J., P. Fornasiero, and M. Graziani, *Use of CeO_2-based oxides in the three-way catalysis.* Catalysis Today, 1999. **50**(2): p. 285-298.

168. Wang, J.A., et al., *Phase composition, reducibility and catalytic activity of Rh/zirconia and Rh/zirconia-ceria catalysts.* Journal of Molecular Catalysis A: Chemical, 2005. **239**(1–2): p. 249-256.

169. Henderson, M.A. and S.D. Worley, *An infrared study of the hydrogenation of carbon dioxide on supported rhodium catalysts.* The Journal of Physical Chemistry, 1985. **89**(8): p. 1417-1423.

170. Szailer, T., et al., *Effect of H_2S on the hydrogenation of carbon dioxide over supported Rh catalysts.* Topics in Catalysis, 2007. **46**(1): p. 79-86.

171. Fornasiero, P., et al., *Thermal stability and oxygen storage capacity of noble metal/ceria-zirconia catalysts for the automotive converters with the on-board-diagnostics (OBD).* Studies in Surface Science and Catalysis, 2000. **130**: p. 1355-1360.

172. Mamontov, E., et al., *Lattice Defects and Oxygen Storage Capacity of Nanocrystalline Ceria and Ceria-Zirconia.* The Journal of Physical Chemistry B, 2000. **104**(47): p. 11110-11116.

173. Neto, R.C.R. and M. Schmal, *Synthesis of CeO_2 and $CeZrO_2$ mixed oxide nanostructured catalysts for the iso-syntheses reaction.* Applied Catalysis A: General, 2013. **450**(0): p. 131-142.

174. Wambach, J., A. Baiker, and A. Wokaun, *CO_2 hydrogenation over metal/zirconia catalysts.* Physical Chemistry Chemical Physics, 1999. **1**(22): p. 5071-5080.

175. Janvier, C., et al., *Thermodynamic description of the nonstoichiometric defect structure in $Ce_{1-x}Zr_xO_2$ solid solution powders.* Solid State Ionics, 2000. **127**(3–4): p. 207-222.

176. Bedrane, S., C. Descorme, and D. Duprez, *$^{16}O/^{18}O$ isotopic exchange: A powerful tool to investigate oxygen activation on $M/Ce_xZr_{1-x}O_2$ catalysts.* Applied Catalysis A: General, 2005. **289**(1): p. 90-96.

177. Kurnatowska, M. and L. Kepinski, *Structure and thermal stability of nanocrystalline $Ce_{1-x}Rh_xO_{2-y}$ in reducing and oxidizing atmosphere.* Materials Research Bulletin, 2013. **48**(2): p. 852-862.

178. Alikin, E.A. and A.A. Vedyagin, *High Temperature Interaction of Rhodium with Oxygen Storage Component in Three-Way Catalysts.* Topics in Catalysis, 2016. **59**(10): p. 1033-1038.

179. Ševčíková, K., et al., *Experimental and Theoretical Study on the Electronic Interaction between Rh Adatoms and CeO_x Substrate in Dependence on a Degree of Cerium Oxide Reduction.* The Journal of Physical Chemistry C, 2016. **120**(10): p. 5468-5476.

180. Tanaka, Y., T. Iizuka, and K. Tanabe, *Infrared spectroscopic study of CO and CO_2 adsorption on Rh-ZrO_2, Rh-Al_2O_3 and Rh-MgO.* Journal of the Chemical Society, Faraday Transactions 1: Physical Chemistry in Condensed Phases, 1982. **78**(7): p. 2215-2225.

181. Jacquemin, M., A. Beuls, and P. Ruiz, *Catalytic production of methane from CO_2 and H_2 at low temperature: Insight on the reaction mechanism.* Catalysis Today, 2010. **157**(1–4): p. 462-466.

182. Balducci, G., et al., *Computer Simulation Studies of Bulk Reduction and Oxygen Migration in CeO_2−ZrO_2 Solid Solutions.* The Journal of Physical Chemistry B, 1997. **101**(10): p. 1750-1753.